AD NUMBER

AD874374

LIMITATION CHANGES

TO:

Approved for public release; distribution is unlimited.

FROM:

Distribution authorized to U.S. Gov't. agencies and their contractors; Critical Technology; MAR 1970. Other requests shall be referred to Army Aviation Materiel Labortory, Fort Eustis, VA 23604. This document contains export-controlled technical data.

AUTHORITY

usaamrdl ltr, 18 jun 1971

AD

USAAVLABS TECHNICAL REPORT 70-4A

WIND TUNNEL INVESTIGATION OF AIRFOILS OSCILLATING IN REVERSE FLOW

VOLUME I

SUMMARY AND EVALUATION OF RESULTS

By
Lewis Gray
Leo U. Dadone
David W. Gross
Richard F. Child

March 1970

U. S. ARMY AVIATION MATERIEL LABORATORIES
FORT EUSTIS, VIRGINIA

CONTRACT DAAJ02-68-C-0064
THE BOEING COMPANY
VERTOL DIVISION
PHILADELPHIA, PENNSYLVANIA

Disclaimers

The findings in this report are not to be construed as an official Department of the Army position unless so designated by other authorized documents.

When Government drawings, specifications, or other data are used for any purpose other than in connection with a definitely related Government procurement operation, the United States Government thereby incurs no responsibility nor any obligation whatsoever; and the fact that the Government may have formulated, furnished, or in any way supplied the said drawings, specifications, or other data is not to be regarded by implication or otherwise as in any manner licensing the holder or any other person or corporation, or conveying any rights or permission, to manufacture, use, or sell any patented invention that may in any way be related thereto.

Disposition Instructions

Destroy this report when no longer needed. Do not return it to the originator.

DEPARTMENT OF THE ARMY
HEADQUARTERS US ARMY AVIATION MATERIEL LABORATORIES
FORT EUSTIS, VIRGINIA 23604

This report has been reviewed by the U. S. Army Aviation Materiel Laboratories and is considered to be technically sound. The report is published for the exchange of information and the stimulation of ideas.

Task 1F162204A14231
Contract DAAJ02-68-C-0064
USAAVLABS Technical Report 70-4A
March 1970

WIND TUNNEL INVESTIGATION OF AIRFOILS OSCILLATING IN REVERSE FLOW

Final Report

VOLUME I

SUMMARY AND EVALUATION OF RESULTS

D8-2474-1

By
Lewis Gray
Leo U. Dadone
David W. Gross
Richard F. Child

Prepared by

THE BOEING COMPANY
VERTOL DIVISION
Philadelphia, Pennsylvania

for

U.S. ARMY AVIATION MATERIEL LABORATORIES
FORT EUSTIS, VIRGINIA

SUMMARY

This report presents the results of an experimental investigation of the dynamic airloads on an airfoil immersed in reverse flow such as occurs on the retreating side of a helicopter rotor disc in forward flight. Forces and moments in two-dimensional flow were determined from airfoil differential pressures measured during pitching oscillation. Mach number, Reynolds number, and mean angle-of-attack ranges corresponded to those typically encountered under full-scale flight conditions. Frequencies of oscillation were varied between values corresponding to the 1/rev and typical first elastic torsional frequencies of rotor blades.

Pitching oscillation was shown to postpone normal force and pitching moment stall to angles of attack well beyond static values. Large increases in dynamic C_N and C_M maxima due to reduced frequency and pitch rate effects were observed, while variations due to Mach number were found to be relatively small and corresponded to those occurring under static conditions. Pitching moment hysteresis effects produced regions of negative damping for all test Mach numbers in oscillations at mean angles of attack near and greater than the static stall value.

Variation of trailing-edge tab angle 3 degrees up and 3 degrees down from the X-axis at angles of attack from approximately 160 degrees to 200 degrees in reverse flow was observed to produce only small changes in dynamic C_N and C_M magnitudes without appreciable changes in stall postponement or hysteresis patterns. The changes in C_N and C_M observed under dynamic conditions are similar to those observed under steady flow (static) conditions.

With the Vertol 23010-1.58 airfoil, the dynamic $C_{N_{MAX}}$ values achieved in reverse flow are considerably less than those achieved in forward flight for oscillation at a frequency corresponding to the rotor 1/rev rate. At such low frequencies, the Vertol 23010-1.58 airfoil demonstrates a leading-edge type of stall in forward flight for Mach numbers up to 0.5, and a thin airfoil type of stall in reverse flow. This results in stall at lower angles of attack with lower dynamic $C_{N_{MAX}}$ values. At the higher oscillation rates, for reduced frequencies greater than 0.25, dynamic C_N maxima are similar in magnitude under both forward and reverse flow.

FOREWORD

The results of a wind tunnel test program to investigate the dynamic airloads acting on an airfoil oscillating in reverse flow are summarized in this report. The work was performed for the United States Army Aviation Materiel Laboratories under Contract DAAJ02-68-C-0064 (Task IF162204A14231) and under the technical cognizance of Patrick Cancro of the Aeromechanics Division of USAAVLABS.

The report consists of two volumes:

Volume I, Summary and Evaluation of Results

Volume II, Data Report

The tests were conducted at the Commercial Airplane Division of The Boeing Company in the Supersonic Wind Tunnel. The assistance and cooperation of the Model Design, Instrumentation, and Supersonic Wind Tunnel Testing Groups are gratefully acknowledged. The assistance of Messrs. I. Walton and M. Brill of the Vertol Division in running the tests is greatly appreciated.

TABLE OF CONTENTS

LIST OF ILLUSTRATIONS

LIST OF SYMBOLS

$A(k)$	real part of Theodorsen's complex function for unsteady flow
b	airfoil semichord, feet
$B(k)$	imaginary part of Theodorsen's complex function for unsteady flow
C_D	airfoil drag coefficient
$\bar{C}_D$	mean value of drag coefficient over an oscillation cycle
$C(k)$	Theodorsen's complex function for unsteady flow ($A(k) + j\,B(k)$)
C_M	airfoil pitching moment coefficient about geometric quarter-chord, positive nose up
C_N	airfoil normal force coefficient, positive up
$C_{N_{MAX}}$	maximum magnitude of normal force coefficient attained in oscillation cycle
C_P	pressure coefficient, $(P - P_S)/\frac{1}{2}\rho V^2$
c	airfoil chord, feet
f	drive frequency of airfoil motion in pitch, Hertz
H	tunnel height, feet
h	instantaneous translation position, positive up, feet
$\dot{h}$	first differential of h with respect to time
$\ddot{h}$	second differential of h with respect to time
j	imaginary part of complex number, value equal to square root of -1
k	reduced frequency, $\pi fc/V$
M	tunnel free-stream Mach number
n	number of harmonic

P	static pressure, pounds per square inch absolute
P_S	tunnel test section static pressure, pounds per square inch absolute
P_T	tunnel test section total pressure, pounds per square inch absolute
RN	Reynolds number based on airfoil chord
TD	value of theoretical aerodynamic cycle damping
TP	wind tunnel test point identification
T_T	tunnel test section total temperature, degrees Rankine
V	tunnel velocity, feet per second
W	work function, foot-pounds
x	airfoil chordwise location, measured from leading edge, positive rearward, feet
xm	airfoil chordwise location of pitching moment reference center, measured from the streamwise leading edge, feet
xp	airfoil chordwise location of pitch axis, measured from the streamwise leading edge, feet
y	airfoil surface location measured perpendicular to chord line, positive upward, feet
α	instantaneous airfoil angle of attack, positive nose up
$\dot{\alpha}$	first differential of α with respect to time
$\ddot{\alpha}$	second differential of α with respect to time
α_o	mean angle of attack, positive nose up, degrees
$\Delta\alpha$	amplitude of pitching motion
ΔC_p	differential pressure coefficient, $\Delta P/\frac{1}{2}\rho V^2$
$\Delta C_p/C_N$	differential pressure coefficient divided by the instantaneous normal force coefficient
ΔP	differential pressure, pounds per square foot

θ	pitching motion cyclic reference angle, degrees
$\dot{\theta}$	first differential of θ with respect to time
ρ	density of air, slugs per cubic foot
ϕ_M	phase lead of first harmonic pitching moment response with respect to airfoil motion, degrees
ϕ_N	phase lead of first harmonic normal force response with respect to airfoil motion, degrees
1/rev, 3/rev, etc.	one per revolution, three per revolution, etc., corresponding to ratio of airfoil drive frequency to equivalent rotor drive frequency
$\oint$	contour integral

INTRODUCTION

The speed and lifting capability of present high-speed helicopter rotor systems are limited, not only by power requirements, but also by critical aerodynamic considerations. Avoidance of high-transonic drag levels and compliance with rotor noise "Mach bang" restrictions usually limit blade tip Mach numbers on the advancing side to high subsonic values near 0.9. Consequently, at high forward speeds, a region of reverse flow exists on the retreating side of the rotor disc (i.e., flow over the rotor blade from the trailing edge to the leading edge).

The boundary of this reverse-flow region is nominally a circle of diameter equivalent to the rotor advance ratio expressed as a fraction of blade radius. It is centered on the 270-degree rotor azimuth and extends outward from the hub. The presence of reduced dynamic pressure on the retreating blade, combined with the requirement for roll equilibrium, thus implies the need to develop relatively high positive sectional lift coefficients outboard of the reverse-flow region. For this reason, retreating-blade stall is a limiting factor on rotor performance. Any enlargement of the reverse-flow region enhances its importance, since the outer segment of the blade must overcome any down loads on the inboard portion subjected to reverse flow.

Blade operation in the reverse-flow region represents an area of helicopter rotor technology which has been largely ignored. The dynamic environment in reverse flow is highly nonlinear in nature due to the combination of the relatively low in-plane velocity and the nonuniform induced-downwash flow field. Thus, the reverse-flow region effective pitch rates include frequency components above the 1/rev rate associated with the blade cycle. Since dynamic blade motions in forward flow are known to have strong effects on airloads and on stall postponement,[1] it is expected that appreciable effects also exist in reverse flow. While the presence of a sharp, streamwise leading edge is known to reduce maximum lift and angle of attack for static stall, the behavior under a dynamic environment had heretofore not been determined.

The objective of the program of wind tunnel tests on oscillating airfoils is to acquire a comprehensive set of two-dimensional airfoil aerodynamic data in a dynamic environment representative of the reverse-flow region of a rotor disc. This matrix of test data forms a basis from which mathematical formulations and an understanding of dynamic stall phenomena in reverse flow can be developed.

TEST FACILITIES, MODELS, AND DATA SYSTEM

This section presents a description of the basic test facilities, apparatus, and data recording and reduction system. This equipment has been documented in a report on earlier oscillatory testing[1] and includes refinements to the data recording and reduction techniques as reported for later tests[2].

TEST FACILITIES

The subsonic, variable-density, two-dimensional, 1-by-3-foot test section of the Boeing 4-by-4-foot supersonic wind tunnel was used to test a 6.38-inch-chord airfoil section model. The test section total pressure and airfoil drive frequencies were chosen to simulate the Reynolds numbers and reduced frequencies corresponding to a 2-foot-chord, full-scale rotor blade oscillating at frequencies from 1/rev to 6/rev.

The pitch oscillating mechanism is shown in Figure 1. A hydraulic motor is used to drive a flywheel with an eccentrically mounted cam. The cam slides in a slotted crank which is rigidly attached to the airfoil model on the pitch axis. Four fixed nominal amplitudes of oscillation, from 2.5 to 10 degrees in 2.5-degree increments, are provided by cam locations of differing radial eccentricity.

AIRFOIL MODEL AND INSTRUMENTATION

The airfoil section chosen for testing under reverse-flow conditions was the Vertol 23010-1.58, which is currently used on production CH-46 and CH-47 helicopters. This section is representative of the state of the art in airfoil design and provides a good compromise between the high lift characteristics and transonic drag rise behavior of the leading-edge camber airfoil designs required for helicopter rotors. The Vertol 23010-1.58 airfoil has a camber line similar to the NACA 230 series, a thickness ratio of approximately 10 percent, and a cusped trailing edge which consists of a flat sheet extension of about 5-percent chord. The section contour and coordinates are shown in Figure 2; a statement of the basic model parameters and instrumentation features is given in the table on page 5.

Extensive oscillatory testing under forward-flow conditions was performed on this airfoil during 1966 and 1967 and is reported in Reference 1.

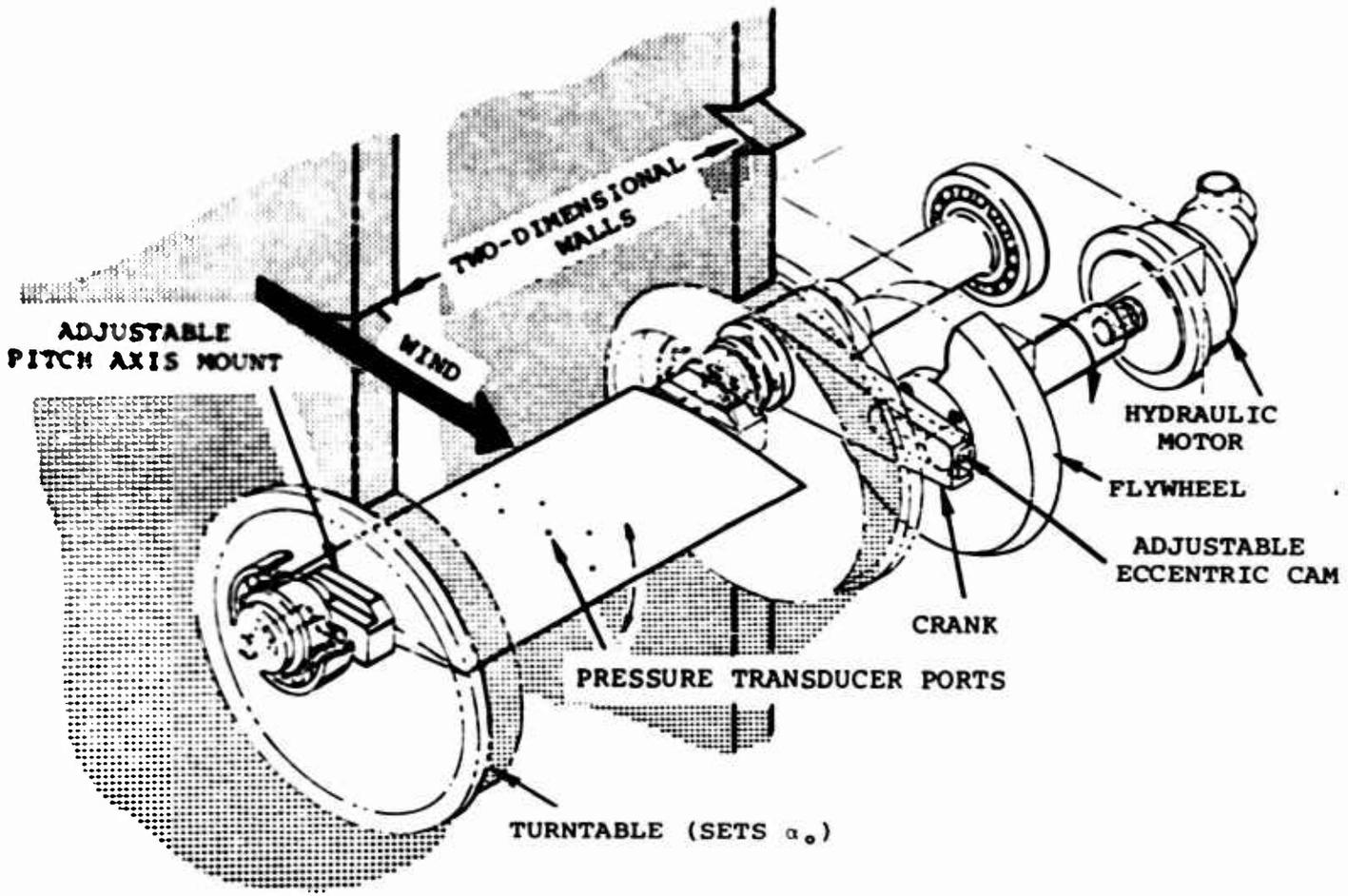

Figure 1. Pitch Oscillating Mechanism.

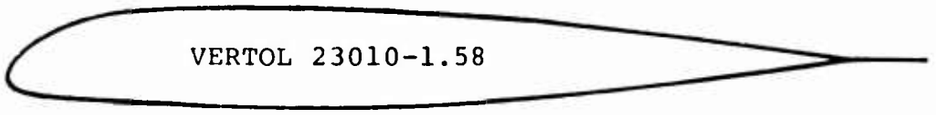

x/c	y/c UPPER	y/c LOWER
0	-0.0251	0.0215
0.0056	-0.0070	0.0336
0.0096	-0.0028	0.0361
0.0135	0.0008	0.0374
0.0254	0.0097	0.0394
0.0333	0.0145	0.0401
0.0571	0.0253	0.0419
0.0967	0.0369	0.0443
0.1462	0.0451	0.0471
0.1957	0.0489	0.0497
0.2452	0.0499	0.0517
0.2848	0.0499	0.0523
0.3937	0.0479	0.0503
0.4729	0.0444	0.0464
0.5521	0.0396	0.0412
0.6313	0.0335	0.0346
0.7502	0.0223	0.0228
0.8293	0.0137	0.0139
0.9086	0.0046	0.0047
0.9440	0.0010	0.0011
1.000	0.0010	0.0011

LEADING EDGE RADIUS = 0.0158

CENTER $\begin{cases} x/c = 0.0158 \\ y/c = 0.0215 \end{cases}$

Figure 2. Test Airfoil Coordinates.

AIRFOIL MODEL AND INSTRUMENTATION DATA	
Item	Description
Airfoil Section	Vertol 23010-1.58
Model Span	12 inches nominal
Model Scale	1/4, based on 2-foot-chord rotor blade
Model Chord	6.38 inches
Thickness Ratio	10.2 percent
Construction	Machined from maraging steel
Transducer Type	Kulite XPLH1-125-50D, -25D
Number Installed	16
Location in Percent Chord	0.5, 2.3, 5.0, 9.3, 20, 30, 40, 50, 60, 70, 83, 88, 92, 95, 97.5, 99.5
Pressure Range	$\pm$50 psi located at 0.5, 2.3, 5.0, 9.3, 83, 92, 97.5, 99.5 $\pm$25 psi located at remaining positions

DATA RECORDING AND REDUCTION SYSTEM

The complete data recording and reduction system is shown schematically in Figure 3. Data recording, on-line oscillograph, and X-Y plotter presentation were controlled automatically during the test through the tunnel operating console. After analysis and editing of the oscillograph records, all further data reduction was performed off-line at the Vertol Division.

Data Recording

All test data, including airfoil pressures and tunnel operating conditions, were recorded simultaneously by a pair of Sangamo Model 3500 FM, wideband, 14-channel tape recorders. A time code signal and a flywheel 1/rev pulse were recorded on both tapes to provide data synchronization. In addition, an Electronic Associates Model TR48 analog computer was used to integrate the differential pressures to provide preliminary on-line values of C_N and C_M.

All test parameters, including C_N and C_M, were displayed simultaneously on oscillograph stripouts for direct data monitoring. In addition, an X-Y pen plotter was used on-line to record scaled aerodynamic damping versus mean angle of attack during oscillatory testing and C_N versus angle of attack during static testing.

Data Reduction

Six-hundred-and-thirty-nine different test conditions were recorded and digitally processed. Each oscillatory test point was constructed from an average of at least 10 individual consecutive data cycles (20 cycles at drive frequencies of 48 Hertz and higher), with approximately 50 points read for each data cycle.

To process this information, the off-line data reduction system described in Reference 1 was used to convert the analog signals to digital form and to provide all final data output. Additional calibrations were made to allow for the nonlinear sensitivity characteristics of the transducer units.

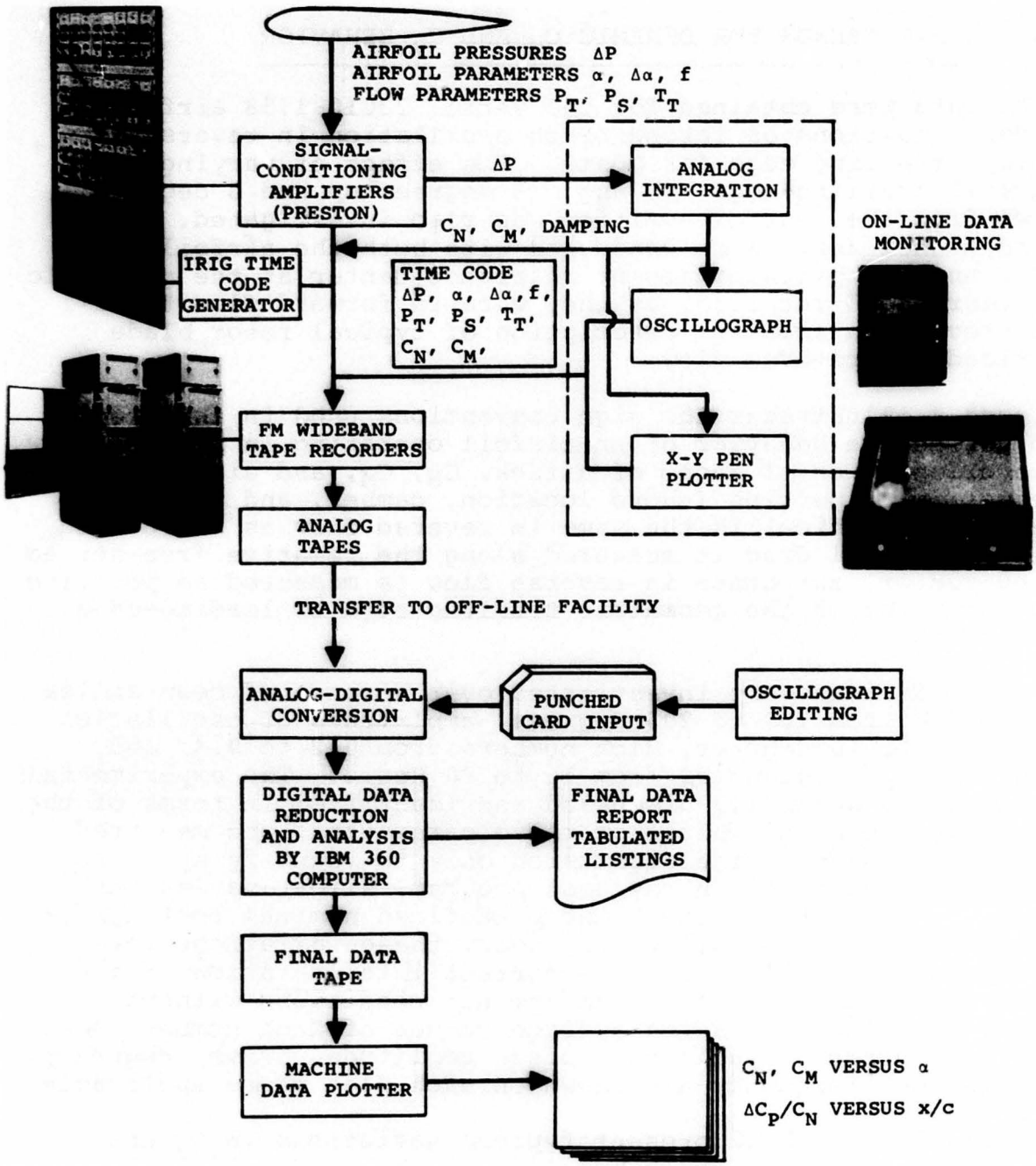

Figure 3. Data Recording and Reduction System.

EXPERIMENTAL RESULTS

PARAMETRIC TRENDS FOR DYNAMIC C_N AND C_M BEHAVIOR

Test data were obtained for the Vertol 23010-1.58 airfoil under conditions of forced pitch oscillation in reverse flow (i.e., trailing edge foremost). The effect of varying the airfoil trailing-edge tab angle 3 degrees up and 3 degrees down from the neutral position was also investigated. The wind tunnel tests were conducted with both the airfoil pitch axis and the pitching moment reference center at the geometric quarter-chord location, as they were in forward flow tests[1], to provide an accurate description of typical rotor blade airloads in reverse flow.

Figure 4 illustrates the sign conventions used in this report to define the behavior of an airfoil operating in reverse flow. The orientation of angle of attack, C_N, C_M, and airfoil geometric properties (chord location, camber, and trailing-edge tab position) is the same in reverse flow as in forward flow. Airfoil drag is measured along the relative free-stream wind vector, and hence in reverse flow is measured as positive in the sense of the geometric trailing-edge to leading-edge direction.

Test conditions were investigated over a range of mean angles of attack from 160 to 205 degrees, amplitudes of oscillation from 2.5 to 10 degrees, Mach numbers from 0.2 to 0.4, and oscillatory frequencies from 16 to 80 Hertz. The experimental results are generally discussed and identified in terms of the predefined nominal values of these parameters, and measured values are used in the discussion only to identify specific items. As expected in any test program, slight variations occurred between the exact and predefined nominal test conditions for each test point. However, these variations were sufficiently small to allow a correct interpretation of the data trends and levels at the nominal conditions without cross-plotting. Measured average values of Mach number, mean angle of attack, oscillatory pitch amplitude, drive frequency, and reduced frequency are shown on each plot where applicable.

Figures 5 through 12 present typical variations in C_N and C_M versus angle-of-attack behavior on the Vertol 23010-1.58 airfoil in reverse flow due to the effects of mean angle of attack, oscillatory amplitude, drive frequency, Mach number, and trailing-edge tab angle. The following sections discuss and illustrate the characteristic data trends attributable to the various parameters. Unless otherwise noted, the discussions refer to the trailing-edge tab in the neutral position.

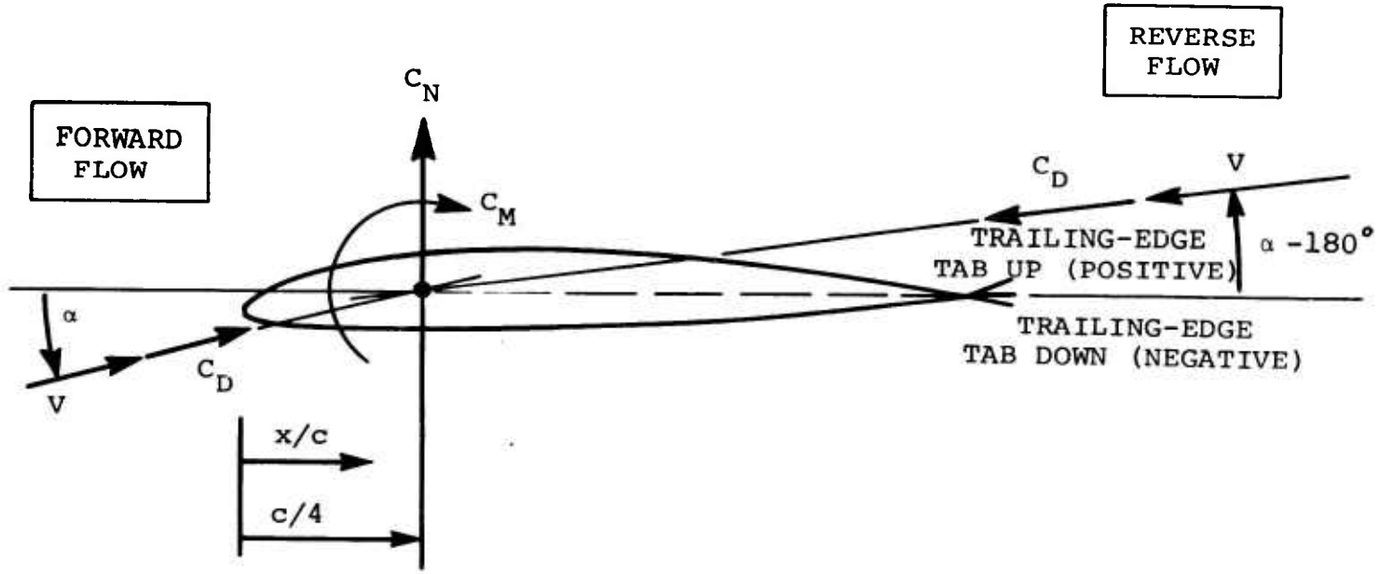

Figure 4. Aerodynamic Sign Convention Used in Reverse Flow.

The aerodynamic characteristics for this airfoil in reverse flow are generally similar to those obtained under forward-flow conditions for thin airfoils, as previously reported[2].

Effect of Mean Angle of Attack

Figure 5 presents C_N and C_M versus angle-of-attack traces for a 5-degree amplitude, 16-Hertz oscillation of the Vertol 23010-1.58 airfoil at M = 0.2 and k = 0.12. A sequence of traces at mean angles of attack from 182.48 to 199.88 degrees shows the development of dynamic C_N and C_M from fully attached to fully stalled flow conditions. Static, nonoscillatory data are included on the plots for reference.

The first C_N and C_M traces, at α_o = 182.48 degrees, show typical unstalled behavior. The near-elliptical shapes of the data loops are similar to those predicted by the potential flow theory.* It is noted that the pitching moment magnitude is approximately half that of the normal force and is of opposite sign. This results from the location of the moment reference center at the geometric quarter chord, which is actually the three-quarter chord in reverse flow.

The second pair of traces, at α_o = 187.38 degrees, shows signs of incipient stall at the maximum angle of attack in the cycle. The typical increases and delay in maximum C_N and C_M magnitudes that have been observed to accompany dynamic stall[1,2] are again present. In addition, as previously observed in forward flow, the pitching moment shows an earlier initial reduction than does the normal force.

As the mean angle of attack increases further, the stall angle also increases, but it occurs progressively earlier in the cycle. Peak maximum C_N and C_M values are shown to occur at α_o = 192.41 degrees. At α_o = 199.88 degrees, the last pair of traces shows fully developed stall throughout oscillation.

Figure 6 compares C_N and C_M versus angle of attack for f = 16 Hertz and M = 0.4 (similar data at M = 0.2 were not available) at two mean angles of attack equidistant from 180 degrees. The trailing-edge tab is in the neutral position to give trailing-edge symmetry. The dashed lines for the lower mean angle-of-attack range (α_o = 175 degrees) are shown with an inverted sign convention to provide as direct a comparison as

*Comparisons of experimental and theoretical C_N and C_M behavior are discussed in a later section.

possible. Although the static data in Appendix I show a slightly earlier stall for angles of attack less than 180 degrees, this is not evident in the oscillatory data. The small shifts in mean C_N and C_M levels are consistent with those experienced under static conditions.

The effect on C_N and C_M due to a variation of mean angle of attack through stall over ranges both greater and less than 180 degrees should not show changes in flow behavior caused by leading-edge geometry, since the Vertol 23010-1.58 airfoil is near symmetrical aft of about 75-percent chord, assuming a neutral trailing-edge tab position. The resulting variations in C_N and C_M are therefore due to changes in the rear flow-separation points which are sensitive to camber effects and to the high surface curvatures in this region close to the airfoil nose.

Effect of Pitching Frequency

Figure 7 shows a sequence of C_N and C_M loops illustrating the effect of increasing frequency for a 5-degree amplitude oscillation at M = 0.2 and α_o approximately 192.5 degrees.

The most noticeable effect of increasing frequency is the progressive delay of the C_N and C_M breaks at stall. At the lowest frequency, approximately 16 Hertz, the C_M break occurs during the increasing-angle-of-attack portion of the cycle at an angle of attack substantially beyond that for static stall. The next C_M trace, at approximately f = 32 Hertz, breaks just before the maximum angle of attack is reached. The traces at all higher frequencies show a C_M break during the decreasing-angle-of-attack portion of the oscillation. This is accompanied by a reversal in the direction of the C_M loop.

Effect of Amplitude of Oscillation at Fixed Maximum Angle of Attack

Figure 8 shows the variation of C_N and C_M stall behavior at four different amplitudes of oscillation for a constant maximum angle of attack at f = 16 Hertz and M = 0.2. Since the nominal frequency remains unchanged, differences in the C_N and C_M stall behavior are attributed to pitch rate effects, $d\alpha/dt$ being proportional to $f\Delta\alpha$.

The principal effects of increasing amplitude are to increase both the stall delay and $C_{N_{MAX}}$. However, the data loops at $\Delta\alpha$ = 10 degrees show dynamic stall to be delayed to a position very close to the maximum angle-of-attack condition, thus limiting $C_{N_{MAX}}$.

As may be expected, these characteristics are similar to those previously noted to correspond to frequency increases. Both effects are equivalent to pitch-rate increases.

Effect of Mach Number

A comparison of C_N and C_M versus angle-of-attack traces at constant reduced frequency (k = 0.24) is presented in Figure 9 to illustrate the differences in dynamic characteristics that are dependent on Mach number variation. Three curves for Mach numbers from 0.2 to 0.4 are shown for a 5-degree oscillation at α_o = 192.5 degrees. All three traces show a remarkable similarity both in the position of the stall breaks and the peak magnitudes of C_N and C_M. The most significant variation between the traces occurs during the period between stall and stall recovery. However, the separated flow conditions which exist over the uppermost wing surface at this time would be expected to produce irregular C_N and C_M stall recovery patterns such as those commonly observed under static conditions.

It appears that Mach number effects on dynamic stall in reverse flow are of minor significance, at least up to M = 0.4. This is in general agreement with thin airfoil behavior[2], which shows only small variations in stall angle of attack over the range of test Mach numbers.

Effect of Airfoil Geometry

Angle of attack for dynamic stall and maximum attainable normal force coefficient are sensitive to leading-edge flow behavior. Thus, geometric variations in the angle of the trailing-edge tab are likely to affect airfoil performance in the reverse-flow regime.

Figure 10 shows the effect of varying the trailing-edge tab deflection on C_N and C_M for a 5-degree amplitude of oscillation at M = 0.2, f = 16 Hertz, and α_o = 192.5 degrees. All three pairs of traces are generally similar except for differences in the steady C_N and C_M levels. Figure 11 gives a similar comparison at a high frequency, f = 80 Hertz, and substantiates those features noted at low frequency. An illustration of trailing-edge, tab-angle variation at a higher Mach number is limited by available test data to M = 0.3 and f = 16 Hertz, as shown in Figure 12. The features noted here in the C_N and C_M behavior do not show any significant differences from those seen at M = 0.2. It is thus concluded that small variations in the trailing-edge tab position have only a small influence on the inception of dynamic stall at Mach numbers up to 0.3.

DYNAMIC $C_{N_{MAX}}$ AND DAMPING DATA

Figure 13 presents the maximum attained C_N versus reduced frequency at $\Delta\alpha$ = 5 degrees. The reduced-frequency parameter, k, which relates the effects of pitch frequency to free stream speed, shows a particularly strong influence, whereas only weak Mach number effects are indicated. Mach number effects change the maximum value of C_N by a small margin similar to the differences existing under static conditions (see Appendix I). This relatively small influence of Mach number on C_{NMAX}, unlike the strong suppressive effect reported for this airfoil oscillating under forward flow conditions[1], is attributed to the presence of a sharp, streamwise leading edge. This effect is characteristic of thin airfoil stall behavior[2,3].

The area enclosed by any C_M trace versus angle of attack is proportional to the net work per cycle done by the airfoil on the surrounding air. This area is known as "cycle damping" and is proportional to the contour integral,

$$W = -\oint C_M \cdot d\alpha$$

The damping is positive for a counterclockwise loop. Areas enclosed by a clockwise loop indicate an energy input to the airfoil system from the surrounding air and represent, by definition, negative damping.

The effect of oscillation frequency on pitch damping is presented in Figure 14. At angles of attack close to α = 180 degrees the damping shows an approximate correspondence to the theoretical magnitude, indicated by unity. The inception of stall is accompanied by a destabilizing downtrend in the damping value. Increases in frequency delay the onset of negative damping. Note that this is preceded by a positive trend in the damping at the higher test frequencies. Negative damping, once obtained, persists over all higher angles of attack shown.

In application to helicopter rotors, aerodynamic pitch damping is most important at the frequency corresponding to that of the blade first elastic torsional mode[5,6,7]. Figure 15 shows the effect of Mach number on pitch damping for a 2.5-degree amplitude of oscillation at f = 80 Hertz. Increases in Mach number between 0.2 and 0.4 reduce the stall delay and consequently produce an earlier onset of negative damping. This behavior is consistent with the degree to which the dynamic stall delay is dependent on the reduced frequency, as noted in the earlier discussion on the C_N and C_M versus α behavior.

To show the effect of oscillatory amplitude, Figure 16 compares pitch damping at $\Delta\alpha$ = 2.5 and 5.0 degrees for a 64 Hertz oscillation at M = 0.2. Increasing amplitude increases pitch rate effects and delays stall to produce a stabilizing effect, provided that the airfoil is not operating in the totally stalled condition.

DISCUSSION OF STALL AND REATTACHMENT PROCESSES

Examination of the detail variations in the aerodynamic loading during pitch oscillation provides an informative basis for understanding the flow processes governing the dynamic C_N, C_M, and damping behavior. A study of the variations in chordwise loading experienced under nonoscillatory conditions precedes the main discussion in order to provide a background for comparison with the dynamic results.

Note that the multiple chordwise pressure distribution plots presented in Figures 19, 21 and 23 have been normalized by dividing ΔC_p by C_N for clarity.

Chordwise Loadings Under Static Conditions

Figure 17 compares chordwise pressure distributions for M = 0.2 and 0.4 at angles of attack above and below the point where deviation from the linear portion of the lift curve occurs for the Vertol 23010-1.58 airfoil operating in reverse flow.* At M = 0.2, the loading given for approximately α = 185 degrees shows a high suction peak close to the streamwise leading edge and is typical of moderate angle-of-attack conditions below stall. This suction peak is followed by a rapid pressure recovery and is similar to that observed in thin airfoil stall[3]. The pressure distribution shown at approximately α = 192.5 typifies a fully developed stall condition. The leading-edge pressures show a lower suction level, and the pressure recovery is less rapid.

The pressure distribution comparison at M = 0.4 shows similar general characteristics to those noted at M = 0.2. However, the pressure recovery following the streamwise leading-edge suction peak is less rapid for the condition below stall. In addition, there is a distinctly sharper secondary pressure peak in the vicinity of the downstream flow separation points.

*Static test data in reverse flow are presented in Appendix I.

Dynamic Stall Loading Behavior

Figure 18 presents average-cycle time histories of stall for C_N, C_M, and five selected chordwise ΔC_p's at f = 16 Hertz and M = 0.2. Equivalent static C_N and C_M traces, corresponding to the instantaneous angle of attack, are shown for comparison. It is seen that at this low test frequency, which corresponds to the rotor 1/rev motion, a substantial stall delay occurs with a peak C_N margin of about 0.5 above the static value being reached.

Figure 19 shows a sequence of corresponding chordwise loadings at 20-degree increments throughout the cycle. The first loading, at θ = 0 degrees, is shown for a flow condition that precedes stall. The second loading corresponds to the initial stage of dynamic stall and shows a redistribution of the loading near the leading edge to a flatter profile. Fully developed stall has occurred for the loading at θ = 40 degrees, and the distribution is virtually flat for about 60 percent of the chord. Recovery from stall is first indicated by an increase in the leading-edge pressure at θ = 180 degrees and appears to be complete at θ = 220 degrees.

As discussed previously in the study of parametric effects on dynamic stall, Mach number effects can be isolated at constant reduced frequency and oscillation amplitude. Figures 20 and 21 show cycle time history data similar to those of Figures 18 and 19 at the same reduced frequency but at M = 0.4.

In Figure 20, the C_N and C_M traces show stall delay and peak excursions from the static data as was noted at M = 0.2. The ΔC_p time histories show similar traits during stall and recovery but do, however, show substantially lower pressures at the trailing edge than exist at M = 0.2. These data agree with the pressure distribution characteristics already noted for static conditions. In addition, the leading-edge suction is seen to be higher at stall.

The corresponding sequence of chordwise loadings presented in Figure 21 indicates a stall behavior similar to that at M = 0.2. However, the loading during stall is less flat, and that during stall recovery shows a more peaky distribution.

Effect of Frequency

Figures 22 and 23 present data similar to those of Figures 18 and 19 and show the effect of increasing the frequency of oscillation to 80 Hertz at M = 0.2. The most noticeable effects of increased frequency on C_N and C_M are the extended stall delay and the lack of a sharply defined stall. However, note that the true time scale here is five times larger than at the lower frequency. Allowing for this consideration, the C_N and

C_M stall histories occur at a comparable rate. The ΔC_p traces show significant fluctuations during stall. This behavior has previously been reported in oscillatory tests of thin airfoils and has been theorized to be due to a free vortex formed in the leading-edge region of the upper surface at the time that stalled flow separation is initiated[2]. This free vortex is then shed as full stall develops and drifts downstream at a lower speed than free stream. The sequential chordwise loading distributions at high frequency, shown in Figure 22, also evidence the wave-like loading variations during stall.

Effects of Trailing-Edge Tab Deflection

The effect of a variation of trailing-edge tab deflection through 3 degrees up, and down, from the neutral position is illustrated in Figures 24 and 25 respectively at high-frequency conditions similar to those of Figure 22. Note that the pitching moment excursions from the steady flow traces do not show any significant variations. A comparison of the ΔC_p time histories indicates that a positive tab-angle deflection produces a small reduction in leading-edge suction and an increase in the downstream pressure loadings. A negative tab deflection may be seen to produce effects opposite to those noted above and of a similar order of magnitude.

DRAG IN PITCHING OSCILLATION

Difficulties in measuring the instantaneous airfoil drag under unsteady-flow conditions, as previously reported in Reference 1, limit the availability of drag data to a determination of time-average values. Such data were obtained by using a pitot-static probe to survey the wake momentum profile while traversing at a sufficiently slow rate compared to the airfoil motion. (The drag was averaged over at least five cycles of oscillation.)

Figure 26 compares average drag in pitching oscillation for three different frequencies at M = 0.4 with the trailing-edge tab in the neutral position. The static drag is shown as a dashed line for reference. Increasing the oscillation frequency from 16 to 80 Hertz raises the average drag in pitch oscillation under all conditions tested, thus substantiating previous results obtained for airfoils oscillating in forward-flow conditions[1,2]. Further agreement, up to the angle of attack for static stall in reverse flow, is shown by the oscillation-induced increase in the average drag above the static level at the corresponding mean angle of attack. However, at higher mean angles of attack beyond the static stall level the data show that oscillation eventually reduces the average drag to a value below the steady level; the crossover point is delayed by increases in frequency. A comprehensive explanation of this phenomenon would require a

more detailed knowledge of the flow structure time history during oscillation with stall than is obtainable from the differential pressure measurements.

COMPARISON WITH RESULTS OBTAINED UNDER FORWARD FLOW

The existence of substantial test data[1] obtained for the Vertol 23010-1.58 airfoil under forward-flow conditions using the same basic test equipment and data retrieval methods as reported here provides the basis for a comparison of aerodynamic behavior under both forward- and reverse-flow conditions. For this section of the report only, a special sign convention has been adopted for the airfoil coordinate system and aerodynamic measurements to present an easily understood direct comparison of airfoil performance. This notation uses the freestream velocity vector as a common reference such that airfoil chord location is measured downstream from the streamwise leading edge and both angle of attack and normal force are defined positive for the streamwise leading-edge "up" in the conventional manner. Pitching moments are referred to the 1/4-chord location measured from the streamwise leading edge.

Static C_N and C_M versus angle-of-attack behavior are compared for forward and reverse flow at M = 0.2 in Figure 27. The reverse-flow configuration stalls at a reduced angle of attack and exhibits a lower maximum normal force value without an abrupt drop such as that occurring in forward flow. In addition, the unstalled lift curve slope is slightly lower in reverse flow.

A second comparison of static C_N and C_M is shown in Figure 28 for M = 0.4, which indicates similar traits with approximately the same differences in angle of attack for stall as those observed in M = 0.2. However, at M = 0.4, the C_N behavior in reverse flow shows a smooth transition at stall without any drop such as that existing at M = 0.2.

Figure 29 shows a sequence of three pairs of chordwise pressure-loading profiles comparing forward- and reverse-flow configurations at M = 0.2 and at angles of attack well below stall, just below the reverse-flow stall angle, and for well-developed stall. The first loading distributions at low angles of attack show a general similarity. The reverse-flow profile shows a well-defined but reduced leading-edge suction and a trailing-edge peak due to the bluff-body, flow-separation behavior. The next pair of profiles correspond to an angle of attack close to stall for the reverse-flow configuration, and show a substantial loss of the leading-edge suction in reverse flow. At an angle of attack corresponding to fully developed stall under both forward- and reverse-flow operation, there is a small region of attached flow at the geometric leading edge for forward flow and a continued presence of the downstream trailing-edge flow separation pressure peak in reverse flow.

Comparisons of dynamic behavior between forward- and reverse-flow conditions are summarized in Figures 30 through 33. The maximum C_N attained during 5-degree amplitude pitch oscillation at a frequency (16 Hertz) corresponding to the rotor 1/rev is shown in Figure 30 as a function of Mach number. The maximum C_N level in reverse flow is considerably lower but shows a similar reduction trend as Mach number rises. The latter behavior is, however, largely influenced by reduced frequency. Figure 31 shows the variation of dynamic $C_{N_{MAX}}$ with reduced frequency for M = 0.2 and 0.4 in forward and reverse flow. At values of reduced frequency above about 0.25, it is seen that the effects of dynamic stall behavior predominate over those arising from airfoil streamwise leading-edge contour differences for Mach numbers in the range of 0.2 to 0.4.

A comparison of pitch damping characteristics for oscillation at 2.5-degree amplitude is given in Figure 32 for a frequency of 96 Hertz at M = 0.2 and 0.4. At M = 0.2, a large positive damping advantage is shown for reversed flow while at M = 0.4, less favorable damping trends demonstrate a reduction of 1-1/2 degrees in mean angle of attack for the onset of negative damping. It should be noted, however, that pitch damping is expressed as a ratio to the theoretical value. Since pitch oscillation in reverse flow is actually about the 3/4-chord position measured from the streamwise leading edge, the theoretically damped energy extraction level for the airfoil differs from that corresponding to oscillation in forward flow. For example, at the f = 96 Hertz, M = 0.2 condition, the theoretical damping energy in reverse flow is approximately 1/3 of the forward flow value. (See Appendix II.)

Thus, the relative magnitude of actual damping forces at this condition is smaller in reversed flow, and substantially reduces both the advantageous and disadvantageous damping ratio trends. Damping comparisons at 5-degree oscillatory amplitude are limited by the availability of test data to a frequency of 80 Hertz at M = 0.4, as shown in Figure 33. At this Mach number, the reverse-versus-forward flow differential in mean angle of attack for the onset of negative damping at 2.5-degree amplitude is carried through to the larger amplitude.

COMPARISON WITH THEORETICAL PREDICTIONS

A full comparison of measured static chordwise pressure distributions in reverse flow at angles of attack below stall with values predicted by potential flow theory may not be made because of the practical consideration that the Kutta-Joukowski trailing-edge stagnation point condition does not exist for a bluff trailing-edge body. Presently available computer programs which calculate two-dimensional theoretical pressure distributions for arbitrary airfoil section contours by employing a vortex polygon method such as that developed by Davenport[8] are

capable of being run with open trailing-edge sections. However, the large gap which would be left for the reverse-flow configuration renders these predictions doubtful.

A theoretical basis for an approximate comparison of static pressure distributions in reverse flow is the standard "flat plate" thin airfoil theory[4]. Figure 34 presents such a comparison for test data at M = 0.2 and 0.4. As expected, only a fair agreement in both cases was obtained, and the measured data show appreciable deviations. Most notable are the marked loss of streamwise leading-edge suction which results from the leading-edge separation bubble phenomenon, and the uneven pressure recovery pattern caused by the early trailing-edge flow separation in the airfoil nose region such as that occurring on a bluff trailing-edge body.

In Figure 35, the measured dynamic force and moment derivatives due to pitch oscillation are compared with theoretical predictions for conditions where no stall is present (i.e., mean angles of attack close to 180 degrees). Theoretical values, derived from a thin airfoil representation with effects of compressibility and tunnel walls (method of images) included, were calculated by use of a computer program supplied by NASA[10].

Measured values of the normal force amplitude are slightly lower than predicted. This is consistent with the reduction of lift-curve slope due to viscous effects. However, the data do not clearly substantiate the expected increase in lift-curve slope caused by compressibility. This characteristic is clouded by the degree of scatter in the test data. The normal force phase lead measurements show good agreement with theory at low values of reduced frequency but show an appreciable deviation (up to 10 degrees) at the higher frequencies.

The experimental pitching moment magnitudes show a better agreement with theory than do the normal force data. However, this is a direct result of an upstream shift in the aerodynamic center relative to the theoretical point at 3/4 chord (derived from thin airfoil theory), as noted in Appendix I. Since pitching moments are referred to the 1/4-chord location and are principally related to normal force magnitude, larger-than-expected values are obtained and thus counteract the reduction induced by viscosity. The moment phase lead data show deviation trends which are similar to those noted for the normal force but have a reduced maximum deviation of approximately 4 degrees.

CONCLUSIONS

1. Oscillatory pitching motions in reverse flow at amplitudes and frequencies experienced by blade elements of helicopter rotors strongly influence the postponement of normal force and pitching moment stall to angles of attack beyond static values. These dynamic effects obey trends similar to those experienced under forward flight conditions.

2. Increases in maximum C_N and C_M magnitudes in reverse flow result from pitch oscillation. These C_N and C_M changes are strongly influenced by the reduced frequency parameter at constant oscillatory amplitude and thus imply a dependence on the pitch rate variation parameter, $b\dot{\alpha}/V$. The small effects of Mach number noted under static, nonoscillatory conditions also prevail in the dynamic environment.

3. At frequencies corresponding to the rotor 1/rev motion, the maximum dynamic $C_{N_{MAX}}$ magnitude obtained in reverse flow is substantially less than that observed under forward-flow operation for Mach numbers in the range 0.2 to 0.4. The $C_{N_{MAX}}$ differential is greatest at the lower Mach number and is similar to that obtained under static conditions.

4. The general aerodynamic stall behavior for the Vertol 23010-1.58 airfoil oscillating in reverse flow is similar to that observed for thin airfoils such as the Vertol 13006-.7 and NACA 0006.

   At small angles of attack in static nonoscillatory flow, a flow separation at the leading edge develops, followed by subsequent reattachment. This phenomenon promotes an early but moderate static stall development which persists for all test Mach numbers between 0.2 and 0.4. Dynamic stall, however, becomes less influenced by static stall behavior as pitch rate effects are increased. At the higher frequencies of oscillation (k greater than 0.25), the dynamic $C_{N_{MAX}}$ is similar in magnitude to that experienced under forward-flow conditions. This similarity implies that the dependence of dynamic stall behavior on leading-edge contour effects is minimized at higher pitch rates.

5. The variation of trailing-edge tab deflection in reverse flow produces only minor changes in C_N and C_M levels without appreciably altering the angle of attack for stall.

6. Pitching oscillation at mean angles of attack in the range less than 180 degrees in reverse flow produces small changes in C_N and C_M magnitudes consistent with static behavior and with negligible differences in the oscillatory variations. Note here that the Vertol 23010-1.58 airfoil has an essentially symmetrical geometric trailing-edge contour aft of about 75-percent chord.

RECOMMENDATIONS

1. The representation of dynamic stall in reverse flow should be included in rotor high speed performance studies.

2. The data presented in this report should be further analyzed to obtain a mathematical description of dynamic stall. As a first step, an empirical formulation, of a type such as developed by Gross and Harris[7], provides a useful tool for the application of these data to rotor dynamic and aerodynamic computer analyses.

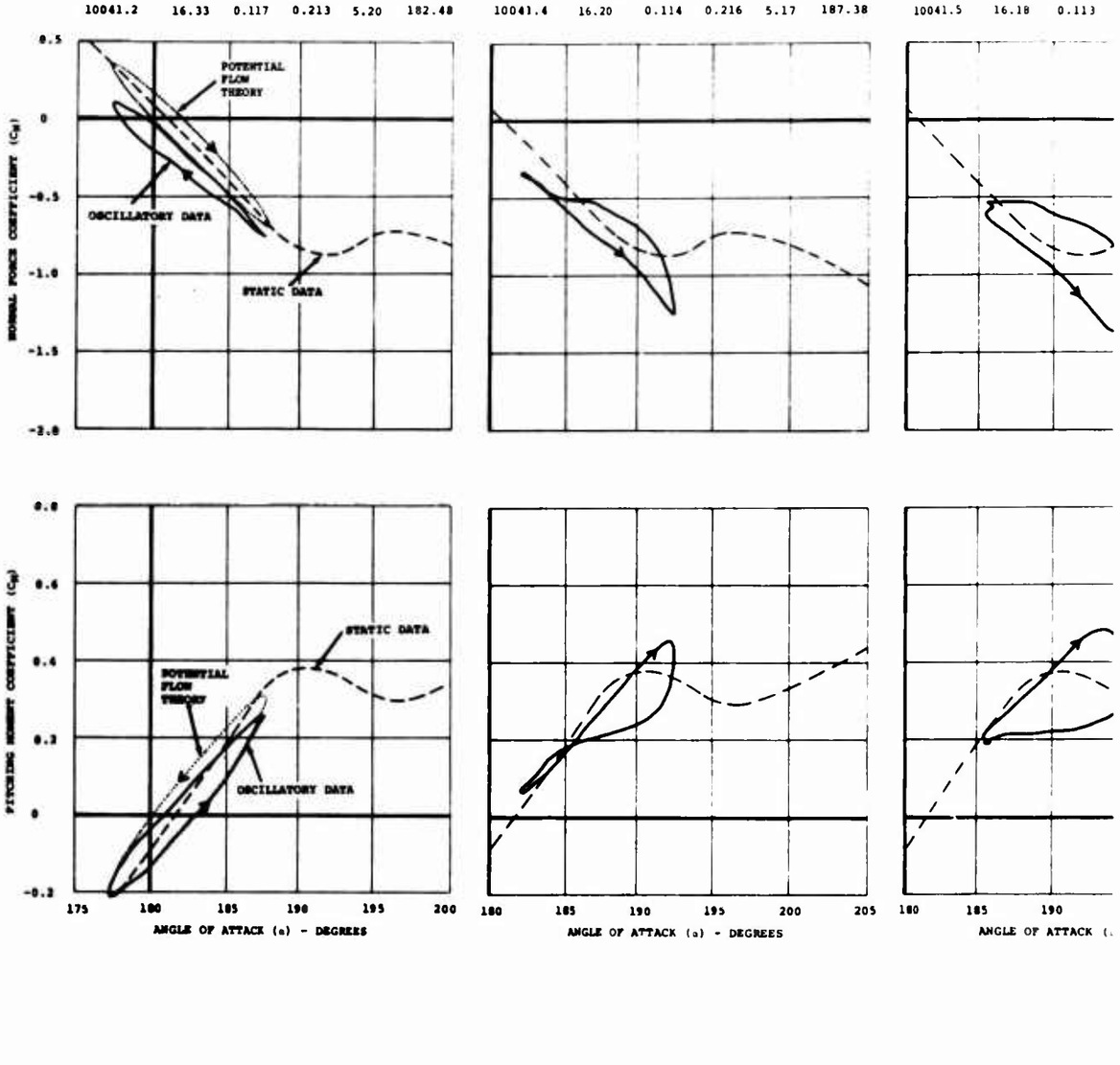

Figure 5. Effect of Mean Angle of Attack on Dynamic C_N and C_M for Pitch Oscillation at f = 16 Hertz, M = 0.2, and $\Delta\alpha$ = 5 Degrees.

TP	f (Hz)	k	M	Δα	α_o
10041.7	16.17	0.112	0.220	5.21	194.91
10041.8	16.23	0.112	0.221	5.16	199.88

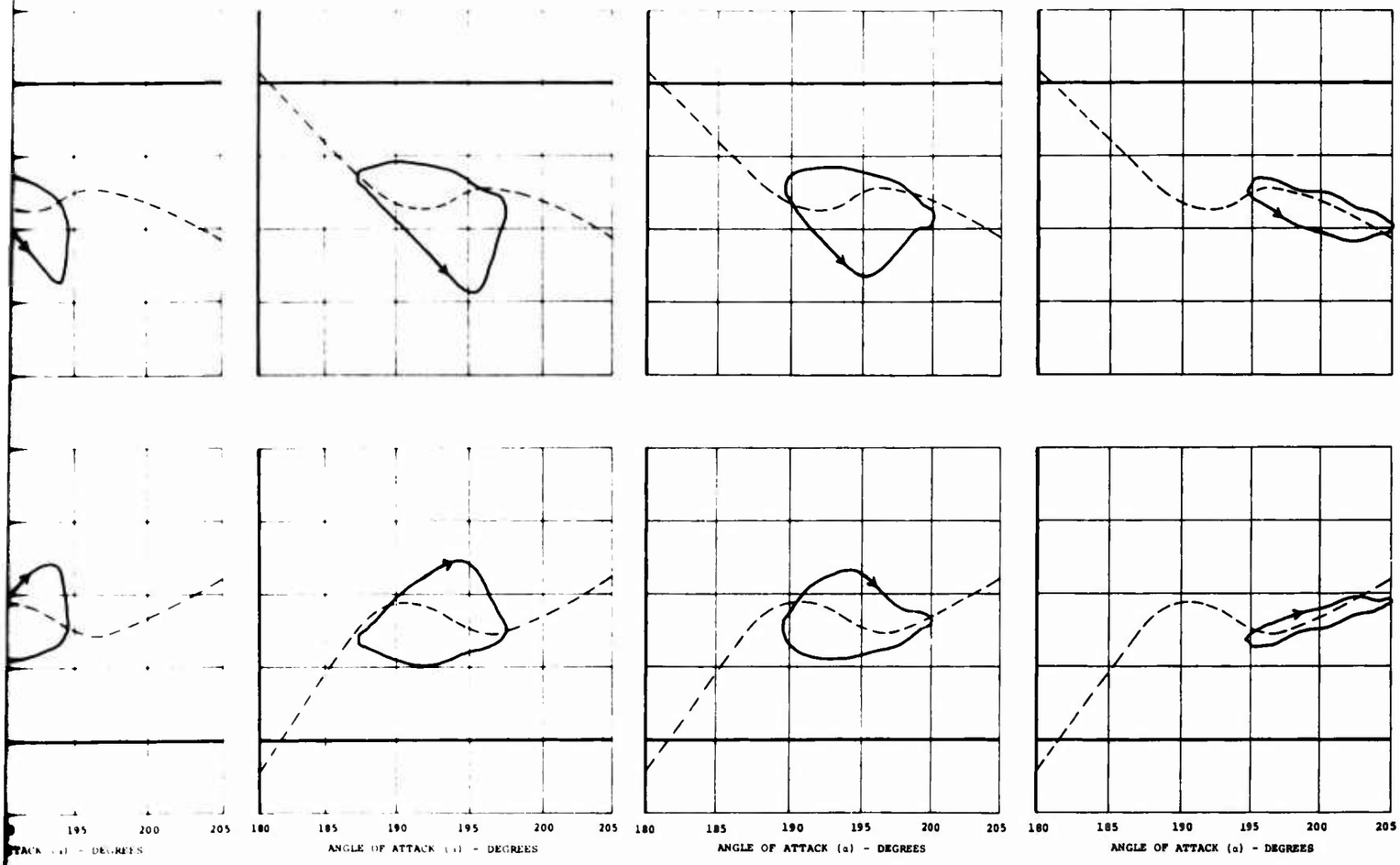

C_M

B

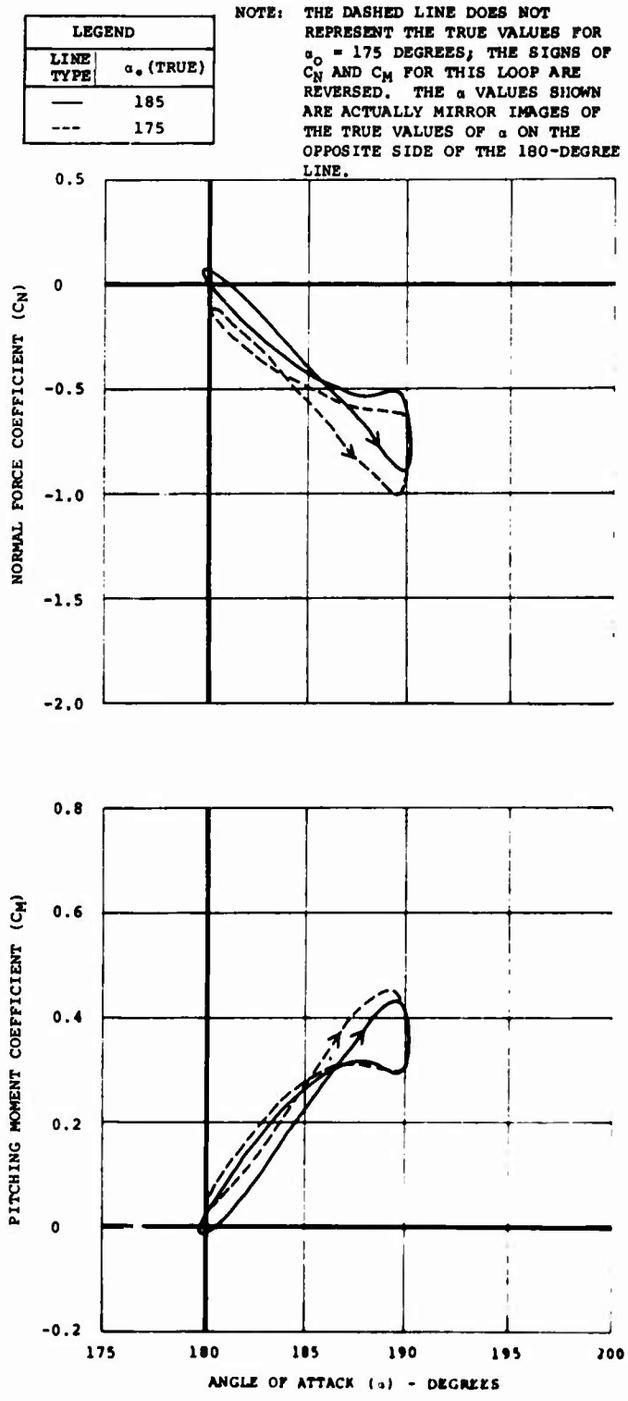

Figure 6. Comparison of Dynamic C_N and C_M Versus α for Pitch Oscillation at f = 16 Hertz, M = 0.2, $\Delta\alpha$ = 5 Degrees, and for Mean Angles of Attack Greater Than and Less Than 180 Degrees.

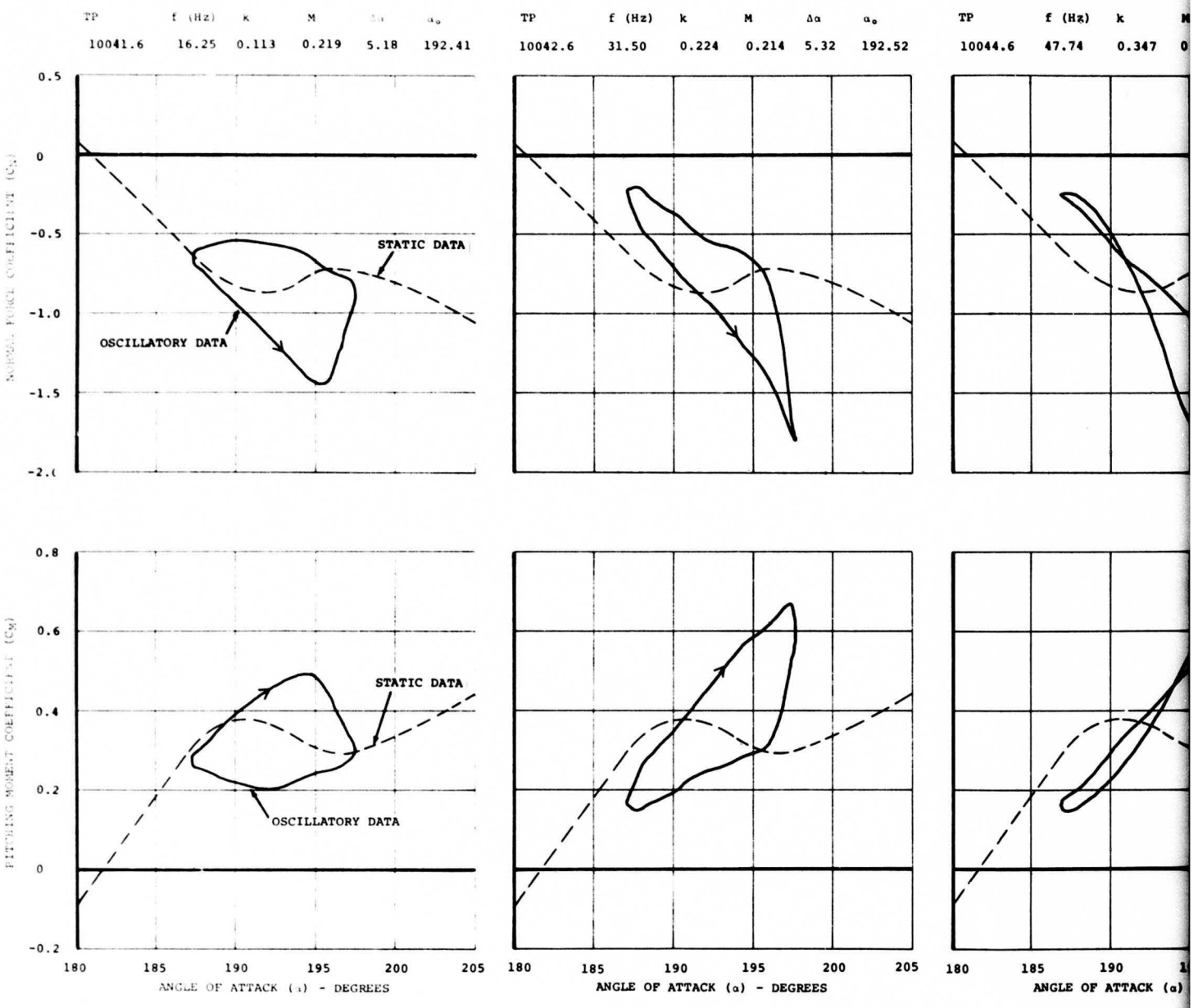

Figure 7. Effect of Drive Frequency on Dynamic C_N and C_M for Pitch Oscillation at M=0.2, $\Delta\alpha$ = 5 Degrees, and α_o = 192.5 Degrees.

f (Hz)	k	M	Δα	α_o
37.74	0.347	0.209	5.41	192.40

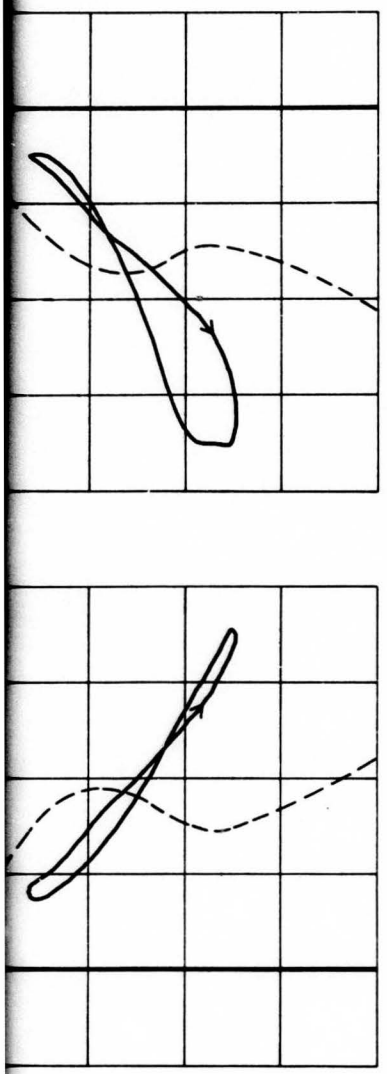

ANGLE OF ATTACK (α) - DEGREES

TP	f (Hz)	k	M	Δα	α_o
10046.6	64.44	0.455	0.214	5.43	192.42

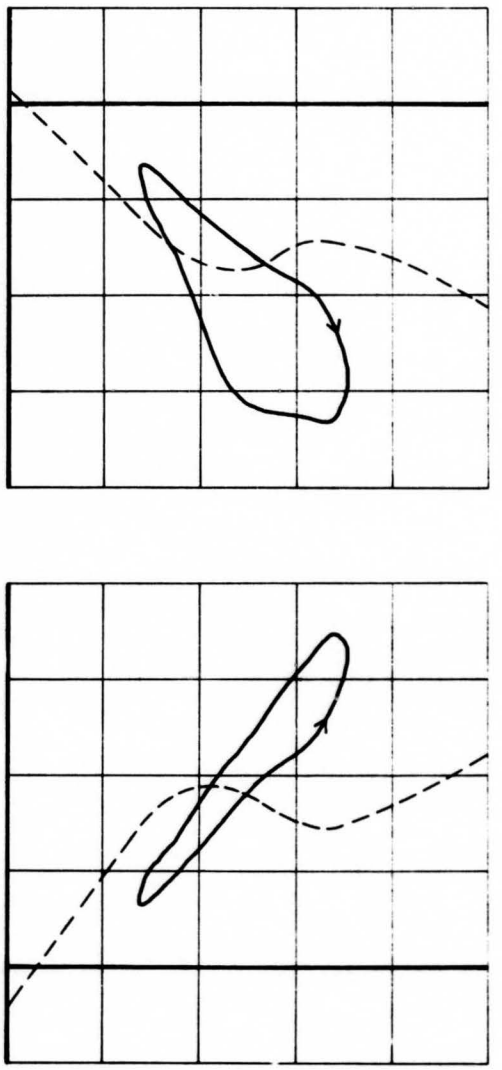

ANGLE OF ATTACK (α) - DEGREES

TP	f (Hz)	k	M	Δα	α_o
10065.6	79.36	0.568	0.210	5.44	192.50

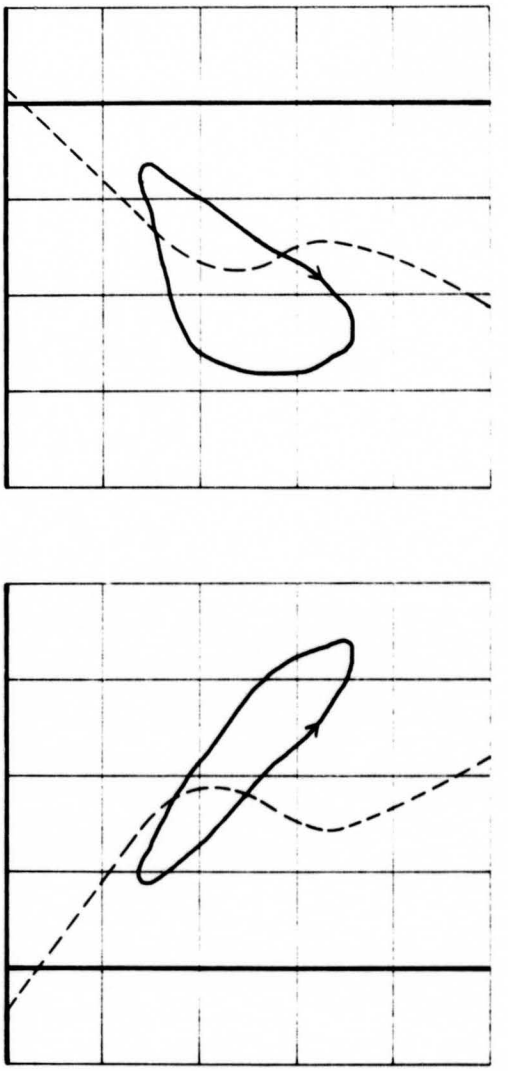

ANGLE OF ATTACK (α) - DEGREES

13

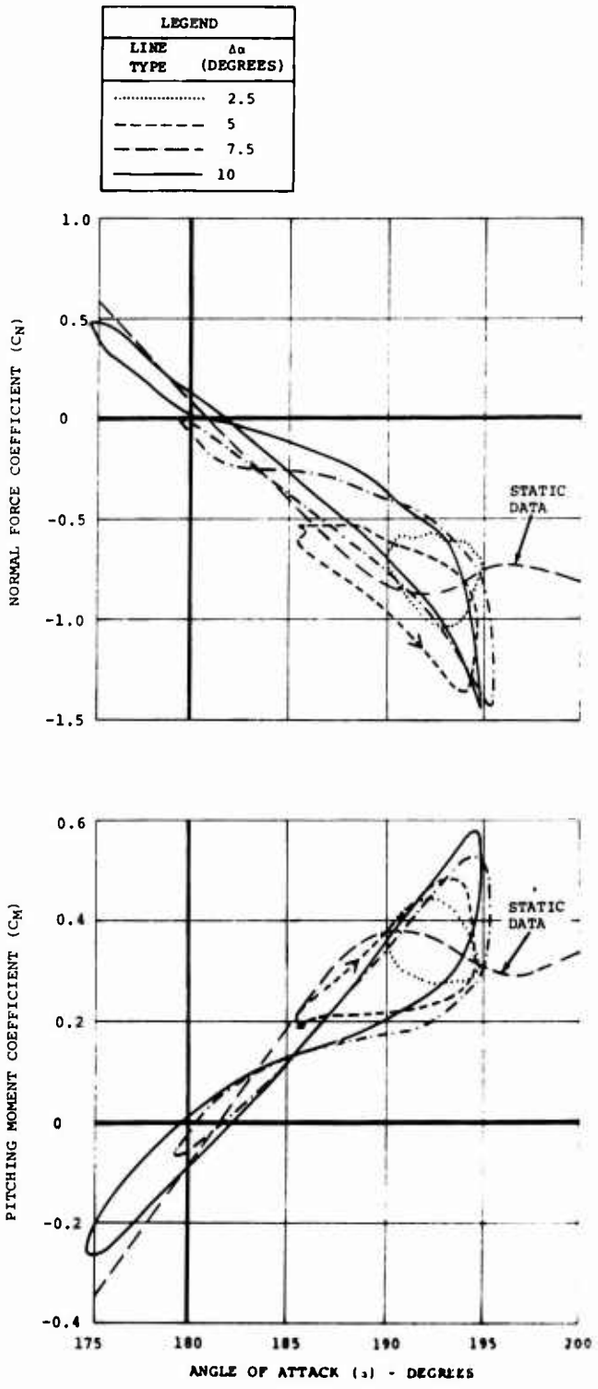

Figure 8. Effect of Oscillation Amplitude on Dynamic C_N and C_M Versus α for Pitch Oscillation at f = 16 Hertz, M = 0.2, and Constant Maximum α.

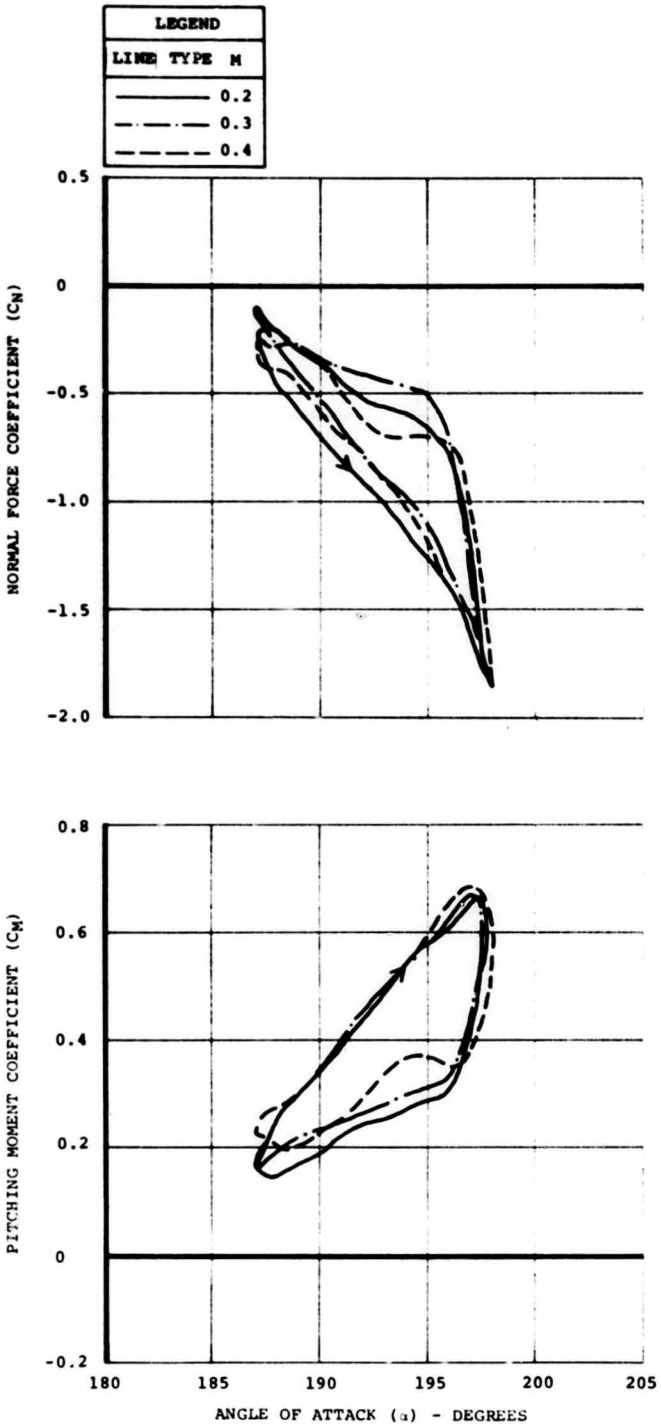

Figure 9. Effect of Mach Number on Dynamic C_N and C_M Versus α at $k = 0.24$, $\Delta\alpha = 5$ Degrees, and $\alpha_o = 192.5$ Degrees.

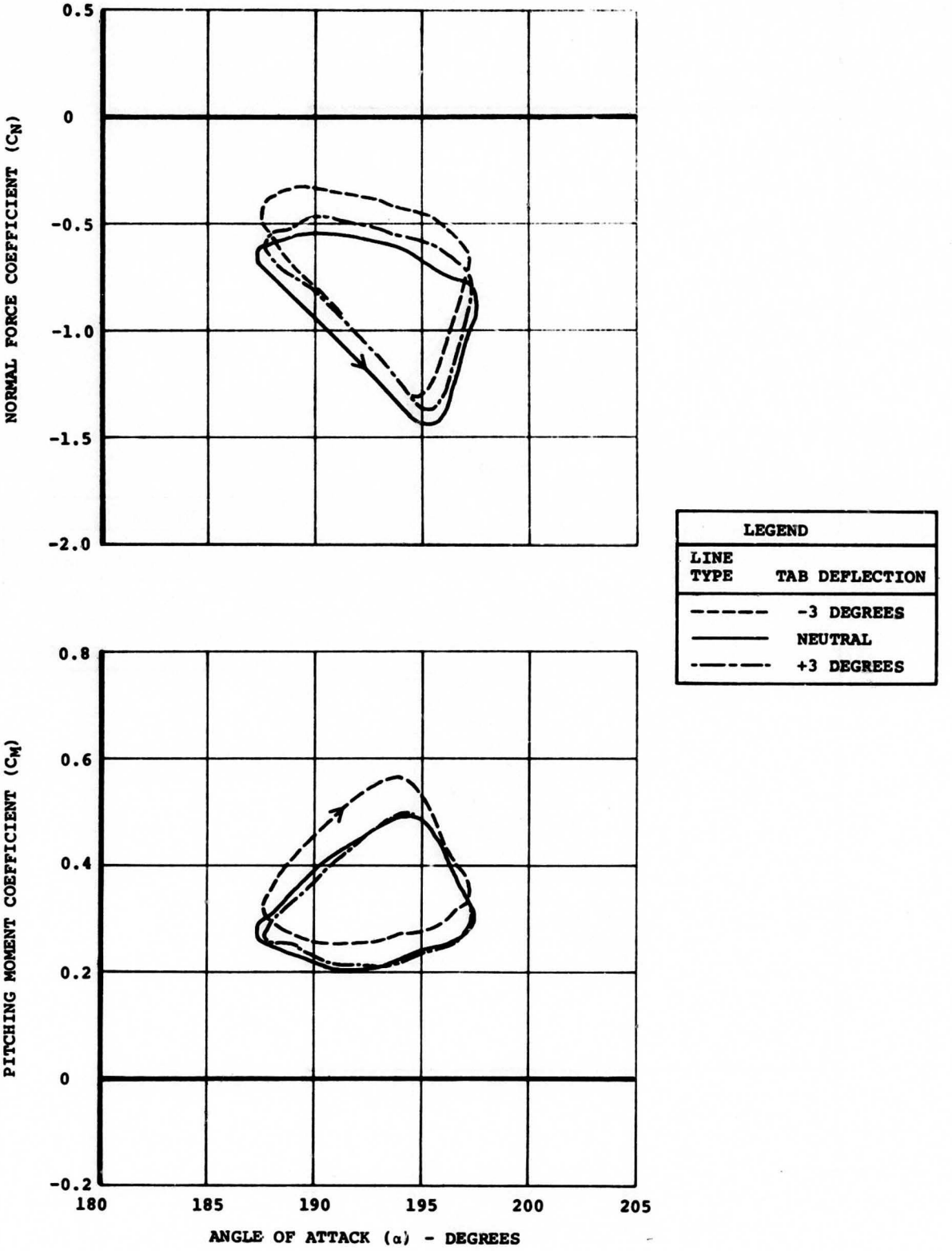

Figure 10. Effect of Trailing-Edge Tab Deflection on C_N and C_M Versus α at M = 0.2, f = 16 Hertz, and α_o = 192.5 Degrees.

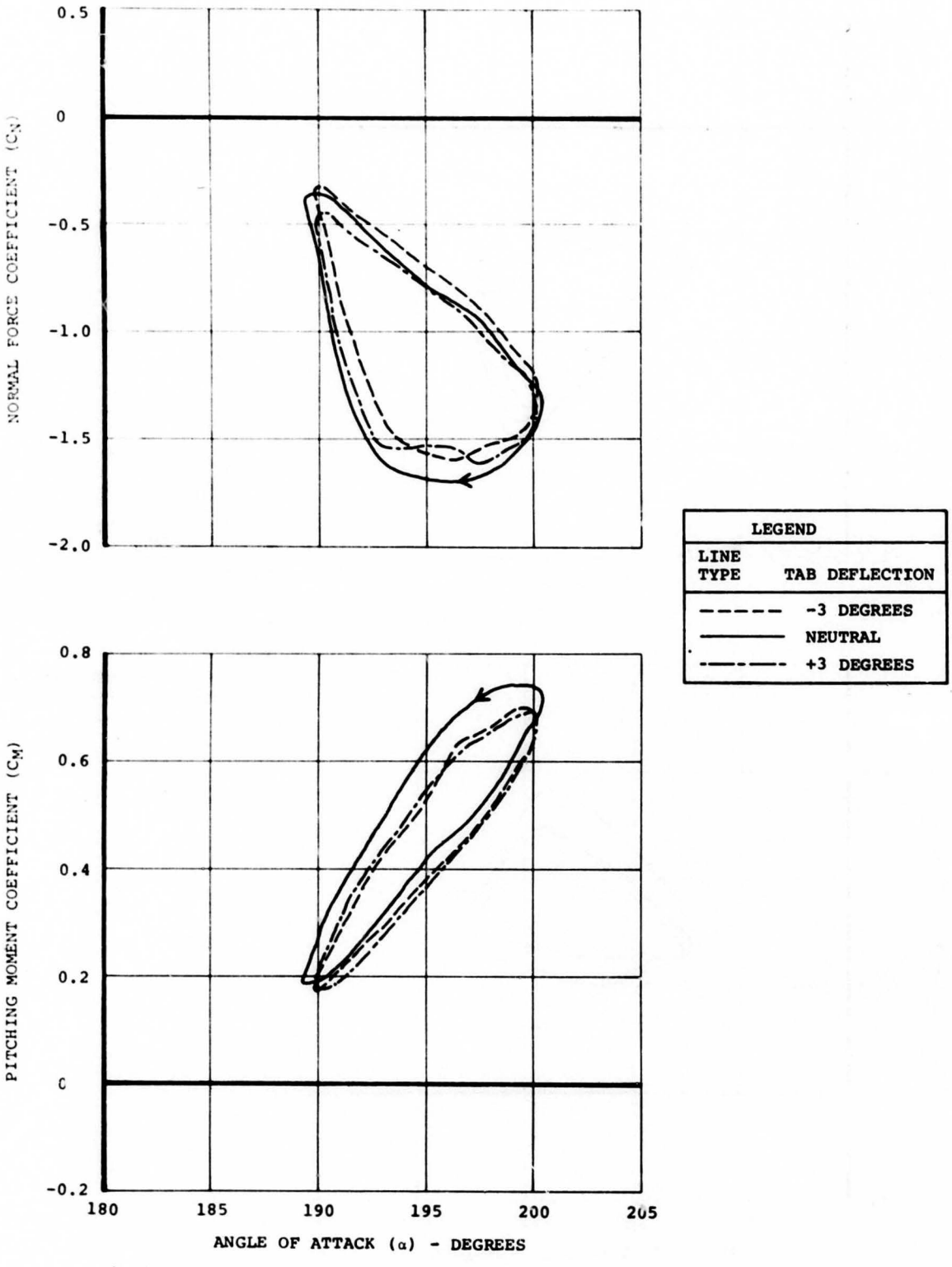

Figure 11. Effect of Trailing-Edge Tab Deflection on C_N and C_M Versus α at M = 0.2 and f = 80 Hertz.

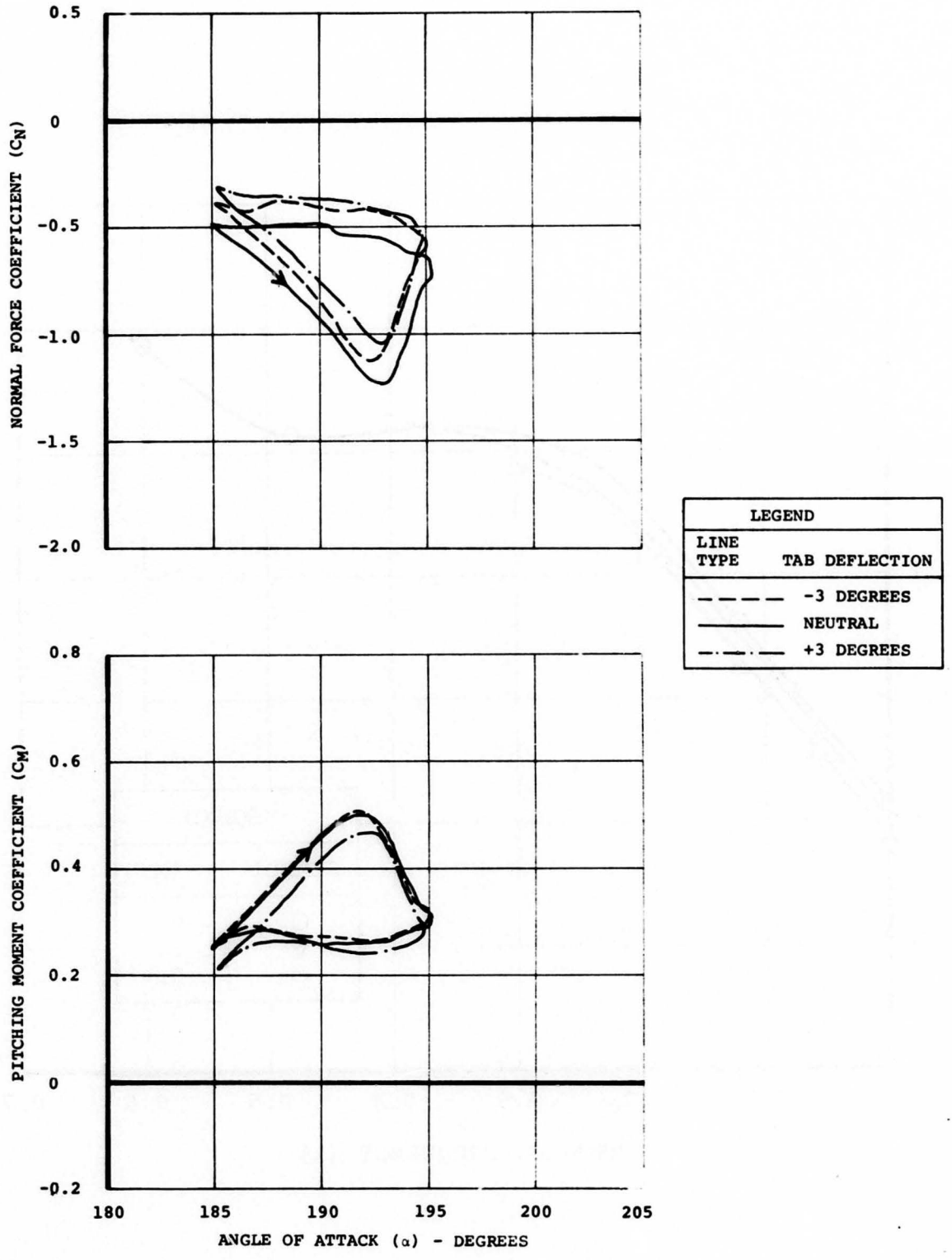

Figure 12. Effect of Trailing-Edge Tab Deflection on Dynamic C_N and C_M Versus α at M = 0.3 and f = 16 Hertz.

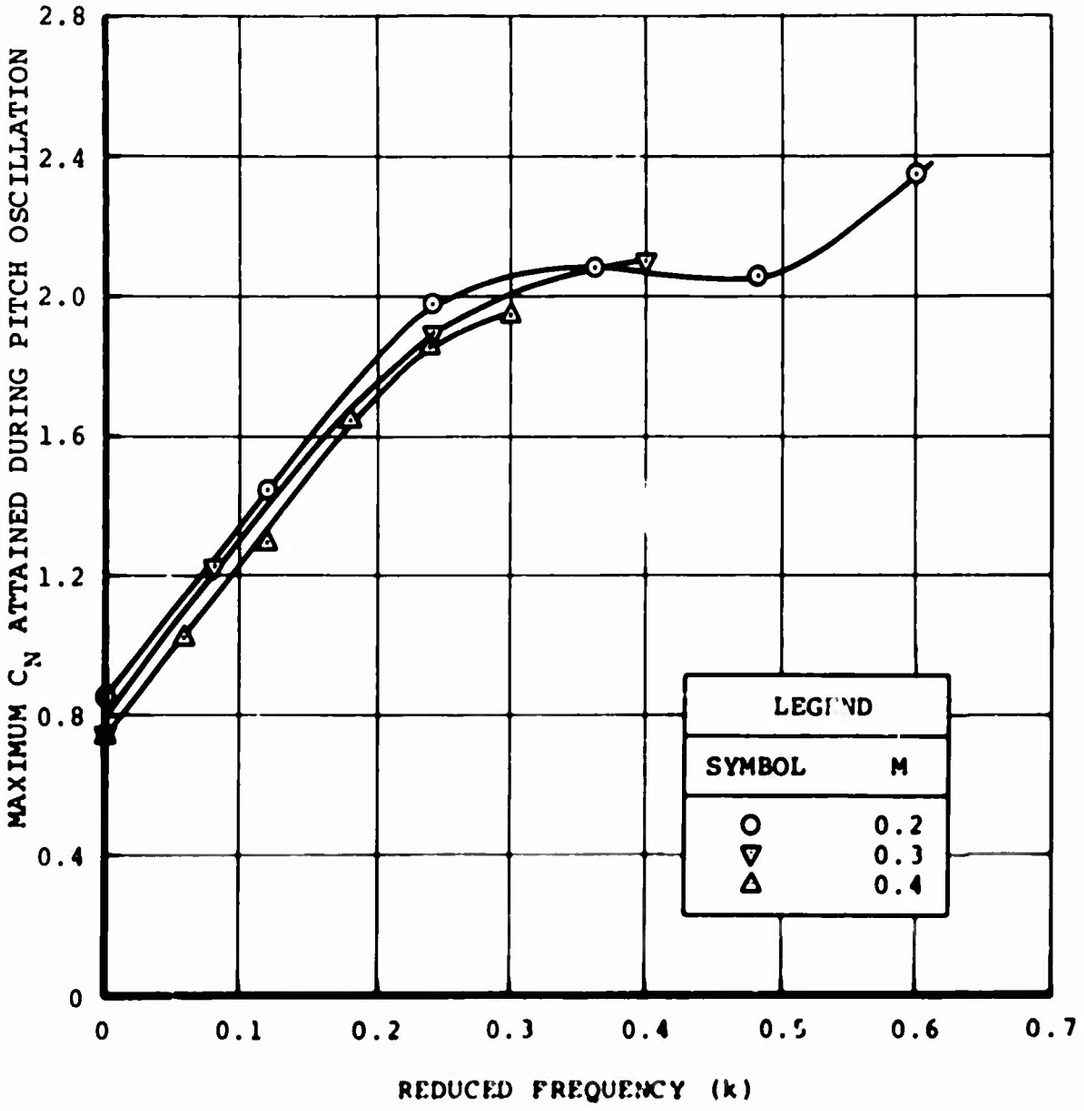

Figure 13. Maximum C_N Attained in Pitch Oscillation at $\Delta\alpha$ = 5 Degrees.

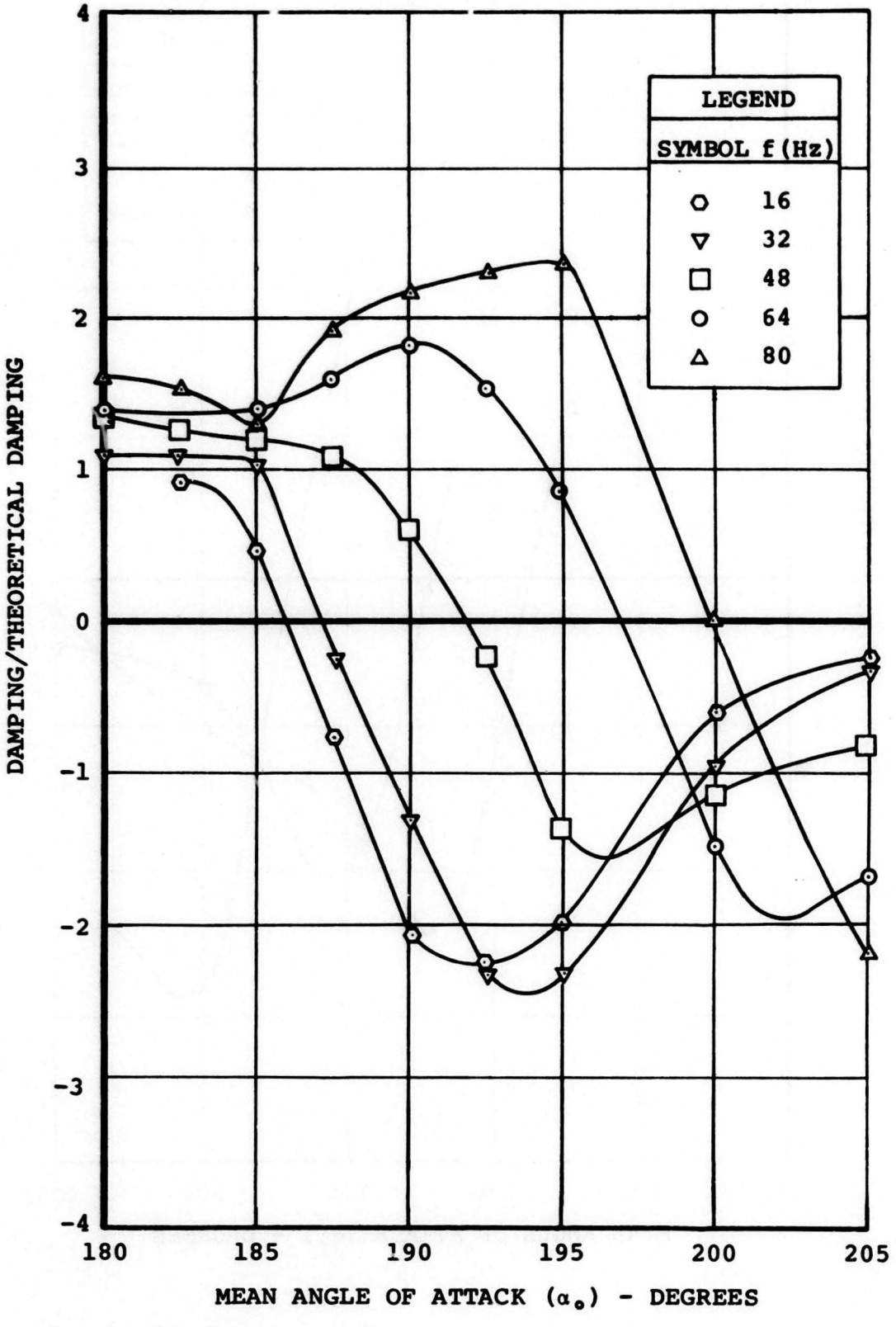

Figure 14. Effect of Drive Frequency on Pitch Damping Characteristics at M = 0.2 and $\Delta\alpha$ = 5 Degrees.

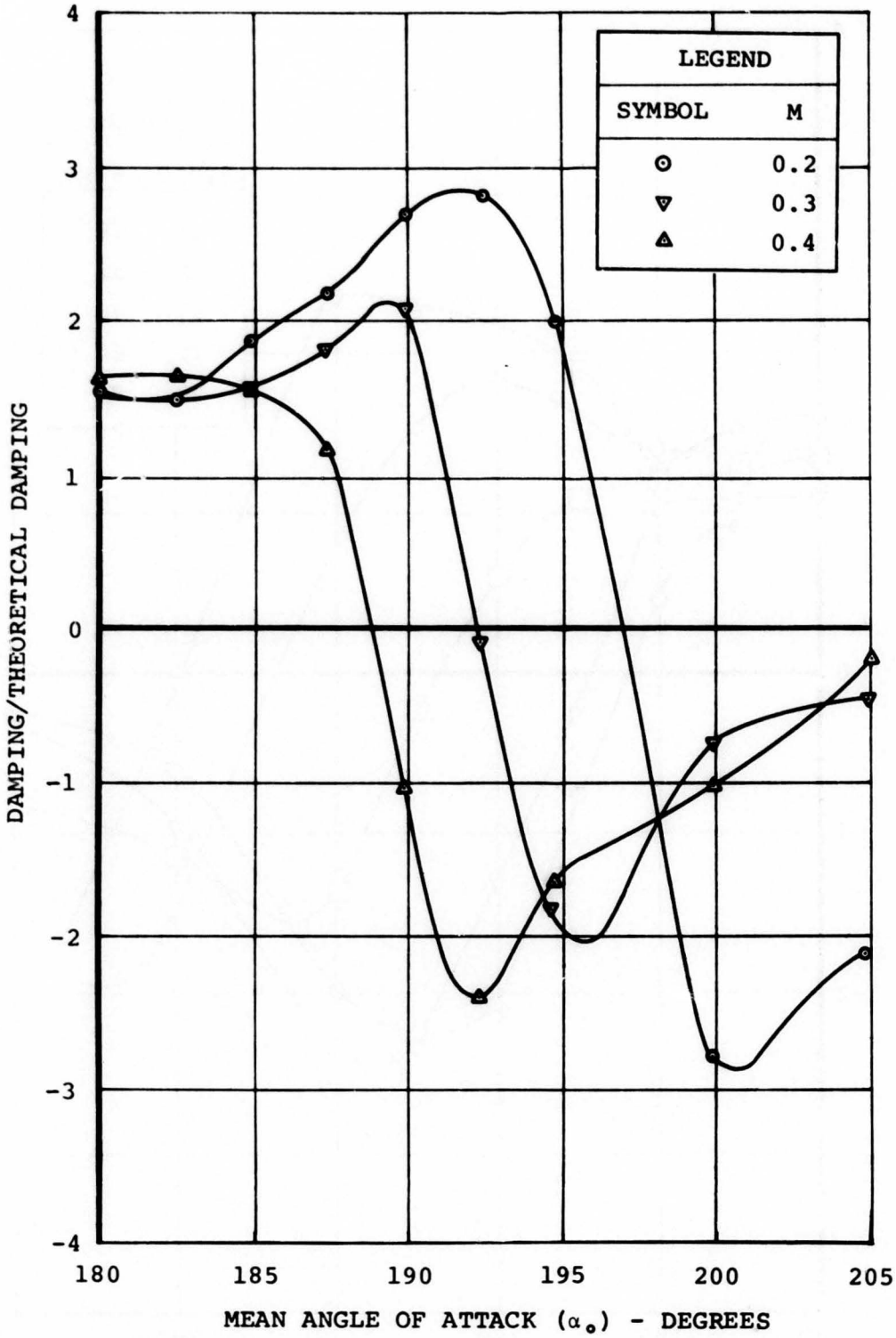

Figure 15. Effect of Mach Number on Pitch Damping Characteristics at f = 80 Hertz and $\Delta\alpha$ = 2.5 Degrees.

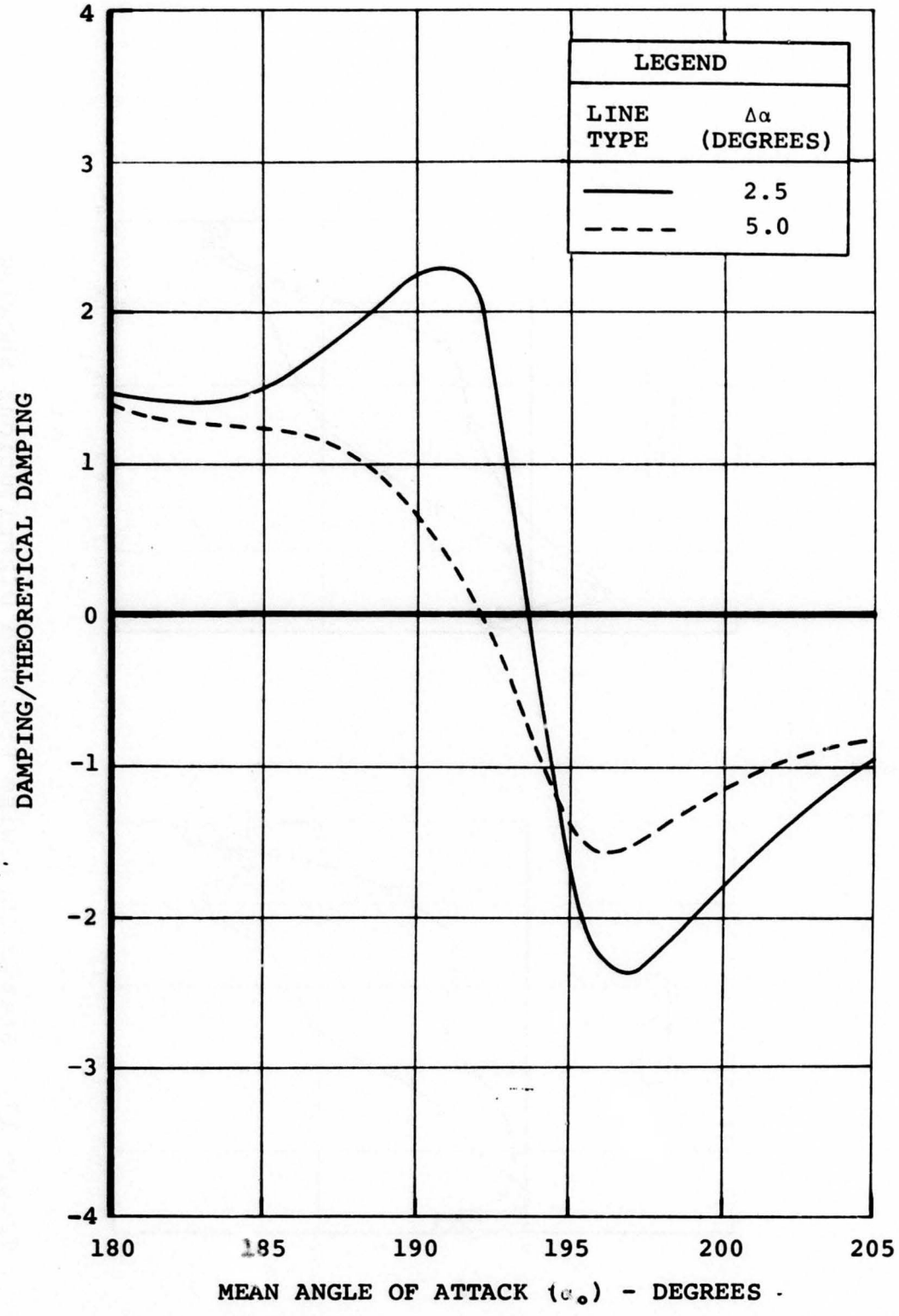

Figure 16. Effect of Oscillation Amplitude on Pitch Damping Characteristics at f = 64 Hertz and M = 0.2.

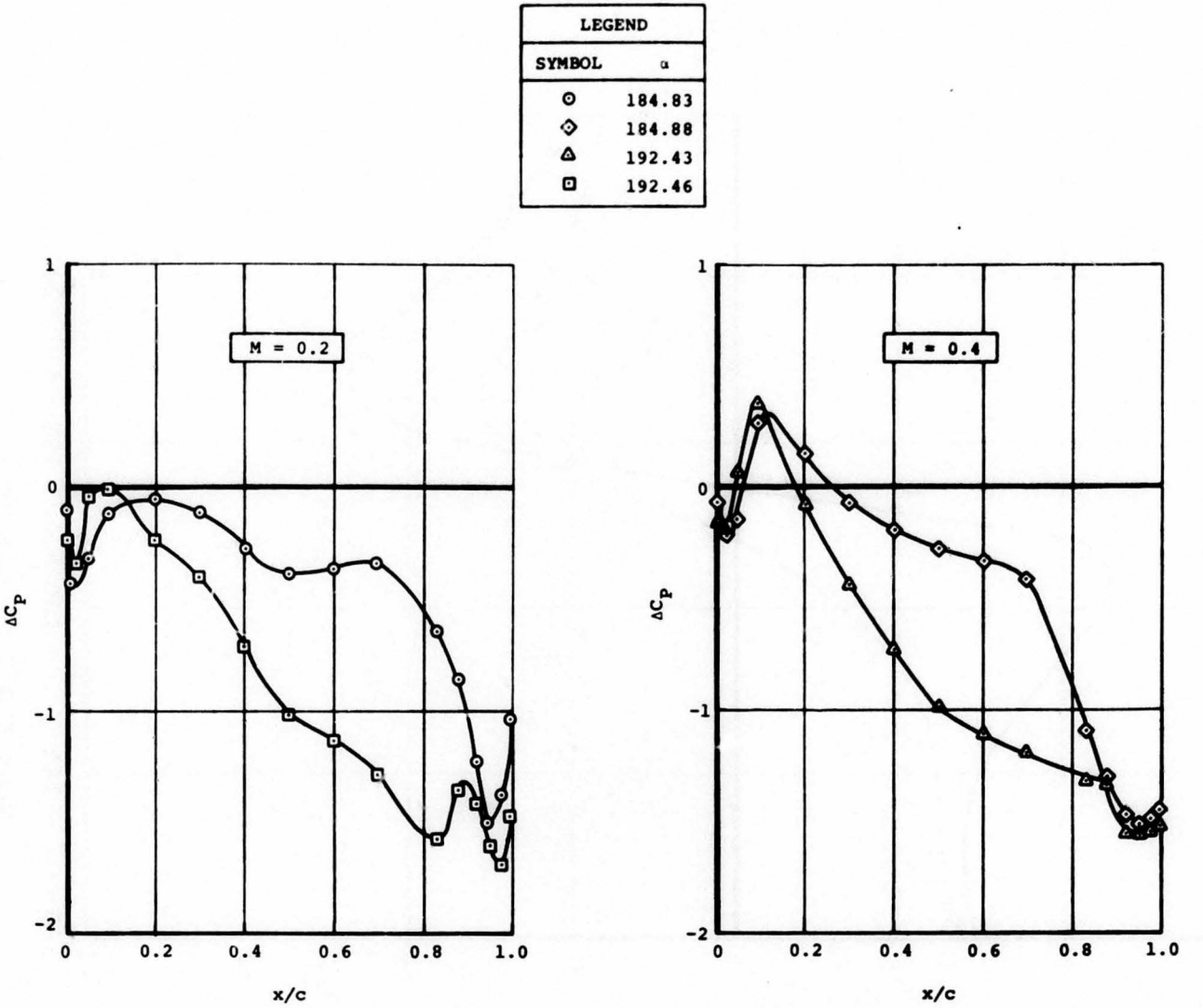

Figure 17. Static Chordwise Pressure Distributions Showing Stall Development in Reverse Flow at M = 0.2 and M = 0.4.

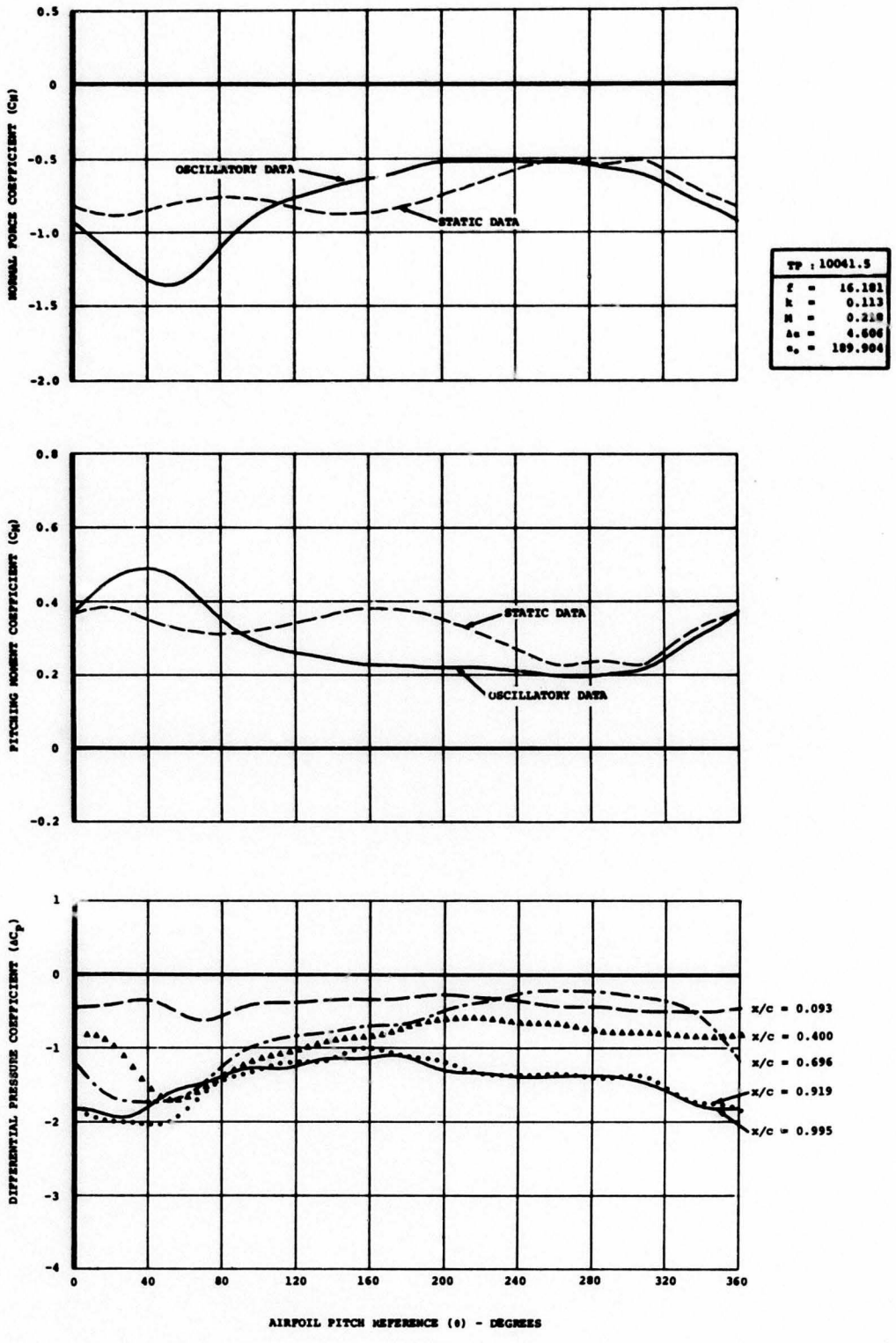

Figure 18. Cycle History of C_N, C_M, and ΔC_p for Pitch Oscillation at f = 16 Hertz, M = 0.2, and $\Delta\alpha$ = 5 Degrees.

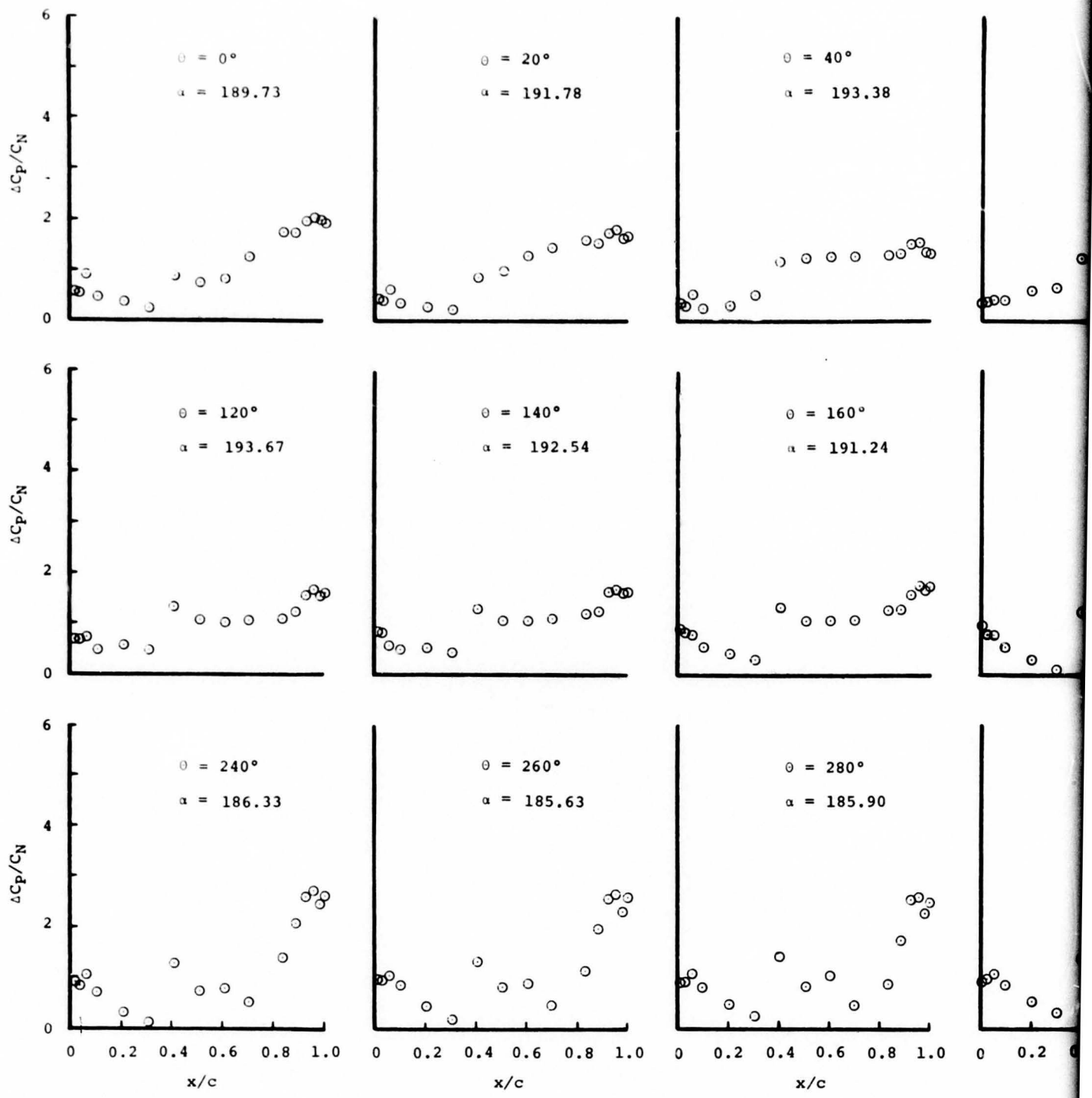

Figure 19. Sequential Chordwise Load Distributions for Pitch Oscillation at f = 16 Hertz, M = 0.2, and $\Delta\alpha$ = 5 Degrees.

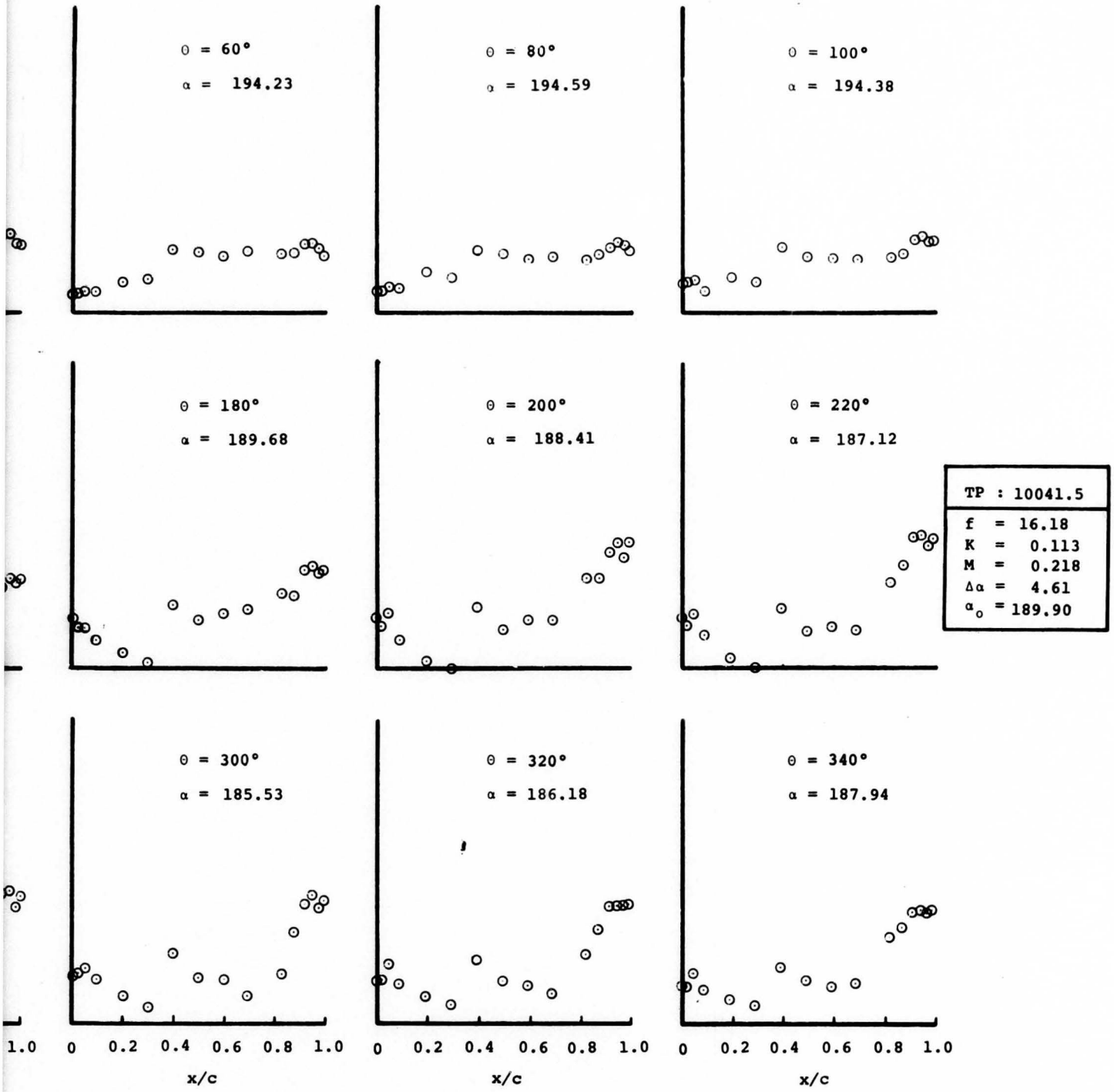
θ = 60°
α = 194.23
θ = 80°
α = 194.59
θ = 100°
α = 194.38
θ = 180°
α = 189.68
θ = 200°
α = 188.41
θ = 220°
α = 187.12
TP : 10041.5
f = 16.18
K = 0.113
M = 0.218
Δα = 4.61
α0 = 189.90
θ = 300°
α = 185.53
θ = 320°
α = 186.18
θ = 340°
α = 187.94
0 0.2 0.4 0.6 0.8 1.0
x/c
0 0.2 0.4 0.6 0.8 1.0
x/c
0 0.2 0.4 0.6 0.8 1.0
x/c

B

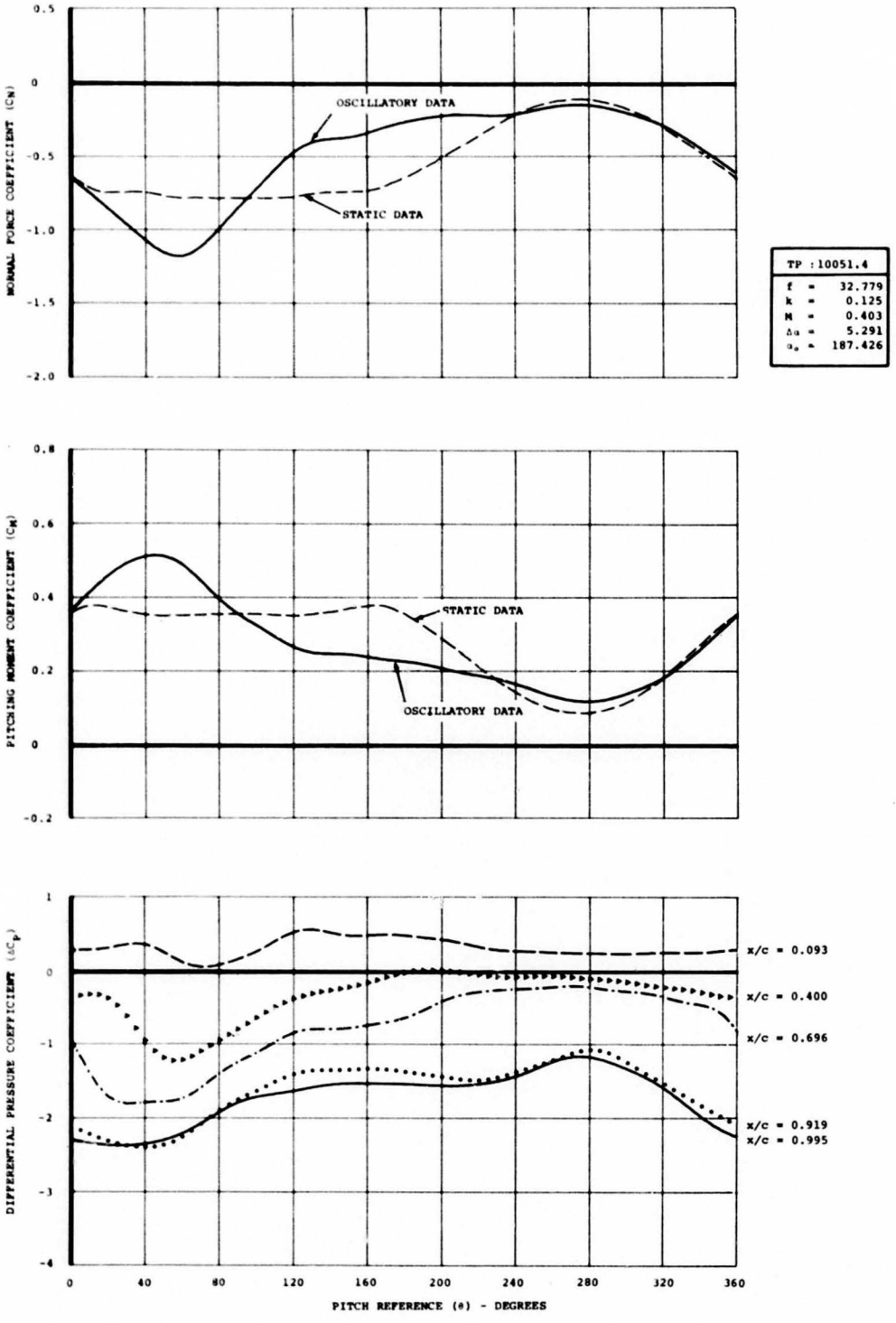

Figure 20. Cycle History of C_N, C_M, and ΔC_p for Pitch Oscillation at f = 32 Hertz, M = 0.4, and $\Delta\alpha$ = 5 Degrees.

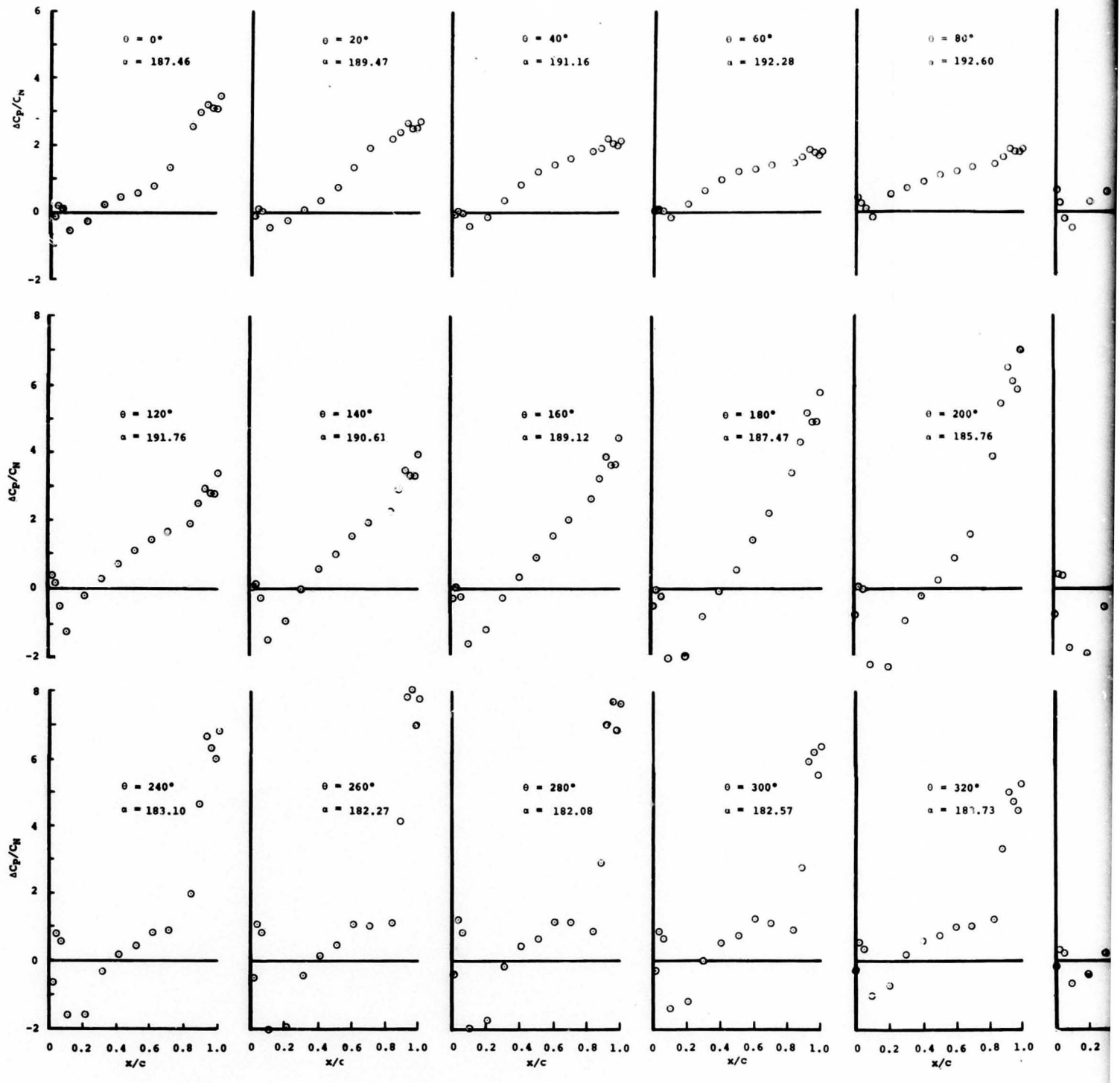

Figure 21. Sequential Chordwise Load Distributions for Pitch Oscillation at f = 32 Hertz, M = 0.4, and $\Delta\alpha$ = 5 Degrees.

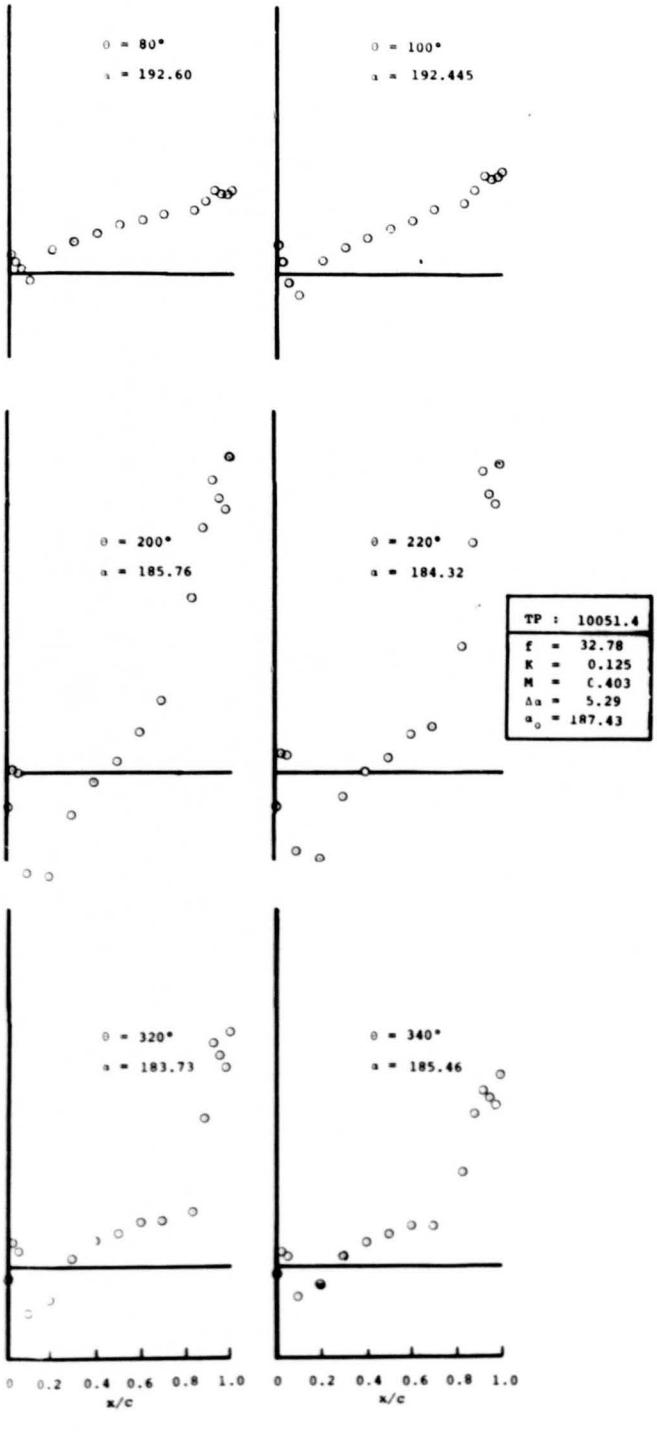
θ = 80°
α = 192.60
θ = 100°
α = 192.445
θ = 200°
α = 185.76
θ = 220°
α = 184.32
TP : 10051.4
f = 32.78
K = 0.125
M = 0.403
Δα = 5.29
α0 = 187.43
θ = 320°
α = 183.73
θ = 340°
α = 185.46
0 0.2 0.4 0.6 0.8 1.0
x/c
0 0.2 0.4 0.6 0.8 1.0
x/c

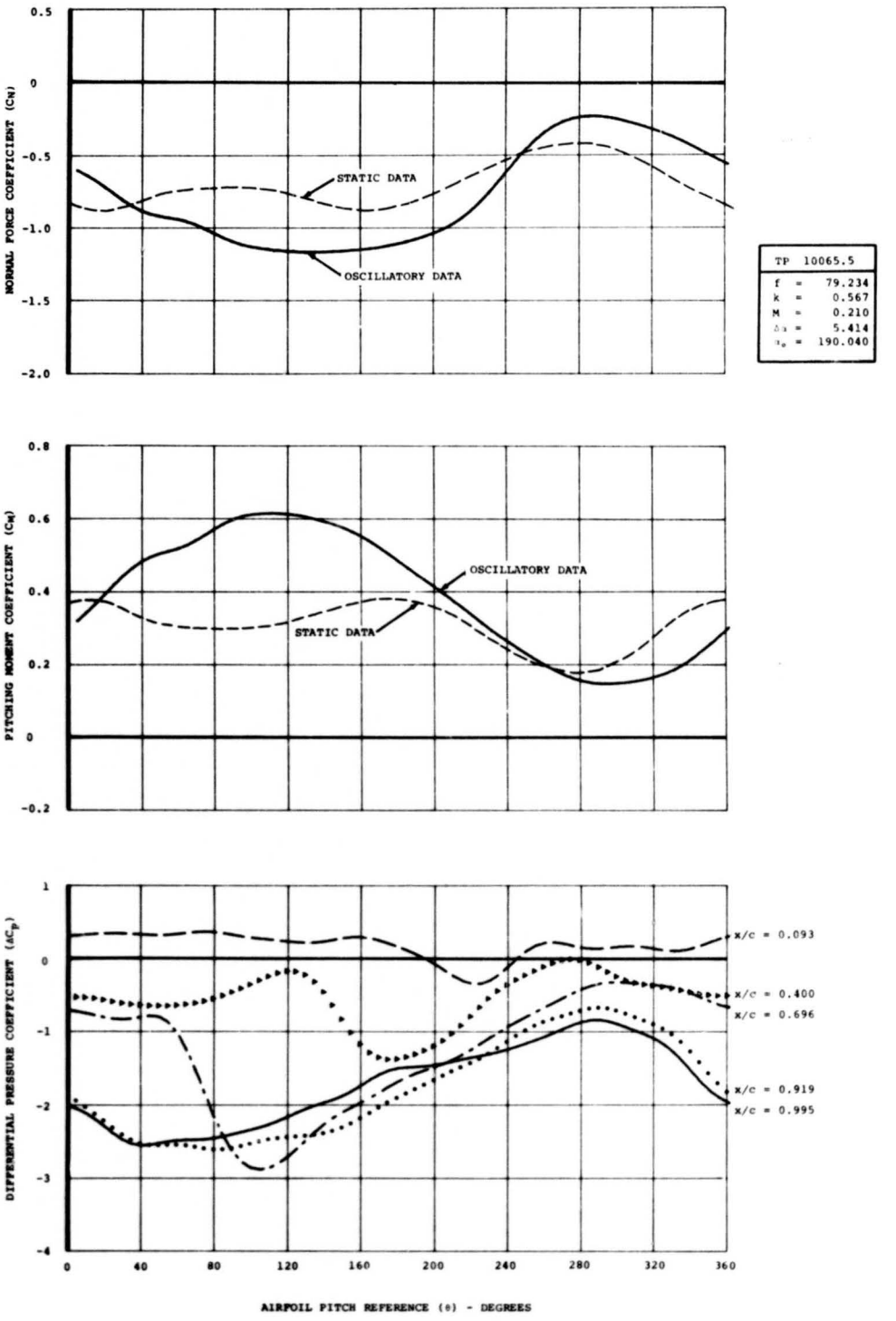

Figure 22. Cycle History of C_N, C_M, and ΔC_p for Pitch Oscillation at f = 80 Hertz, M = 0.2, and $\Delta\alpha$ = 5 Degrees.

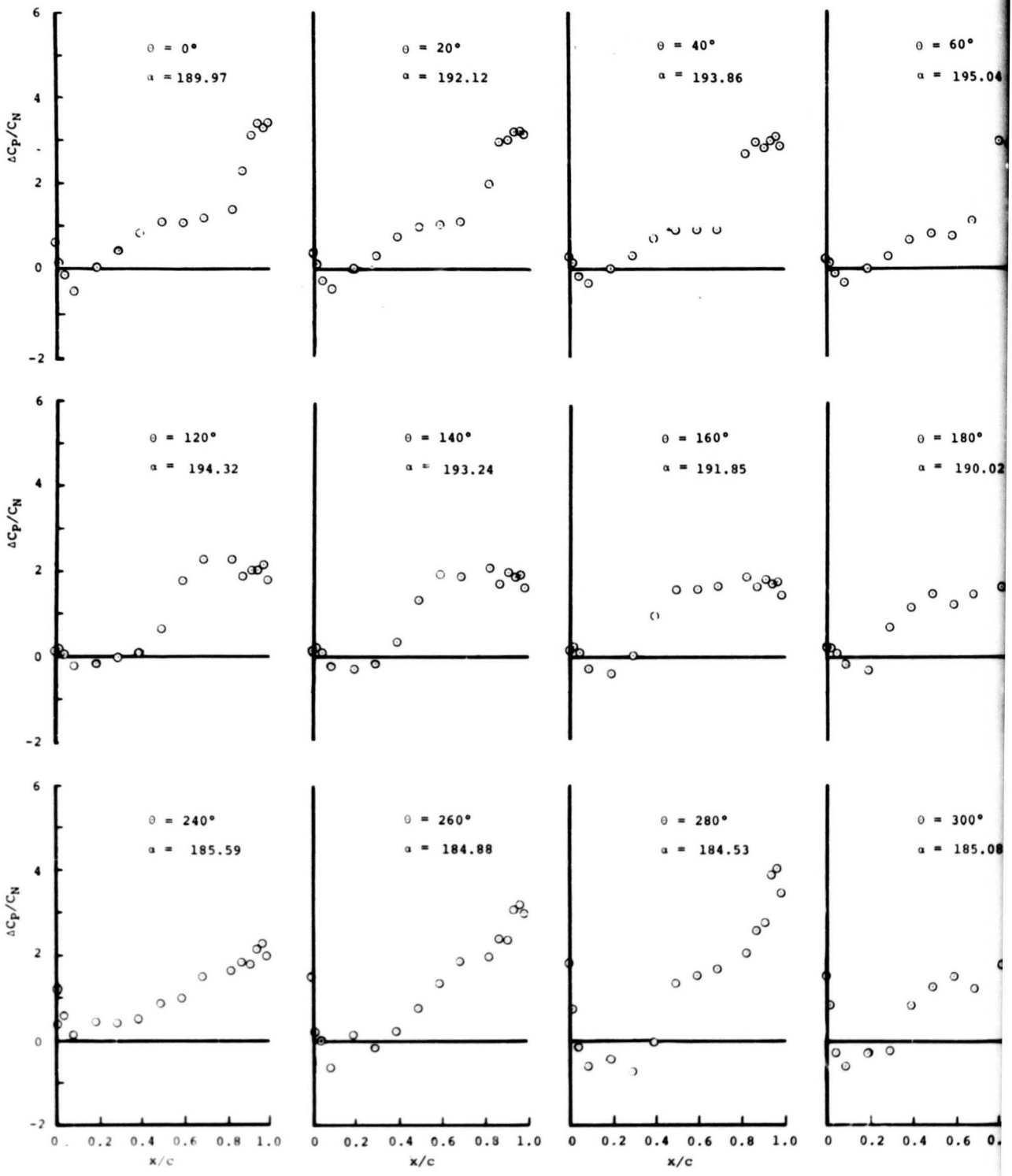

Figure 23. Sequential Chordwise Load Distributions for Pitch Oscillation at f = 80 Hertz, M = 0.2, and $\Delta\alpha$ = 5 Degrees.

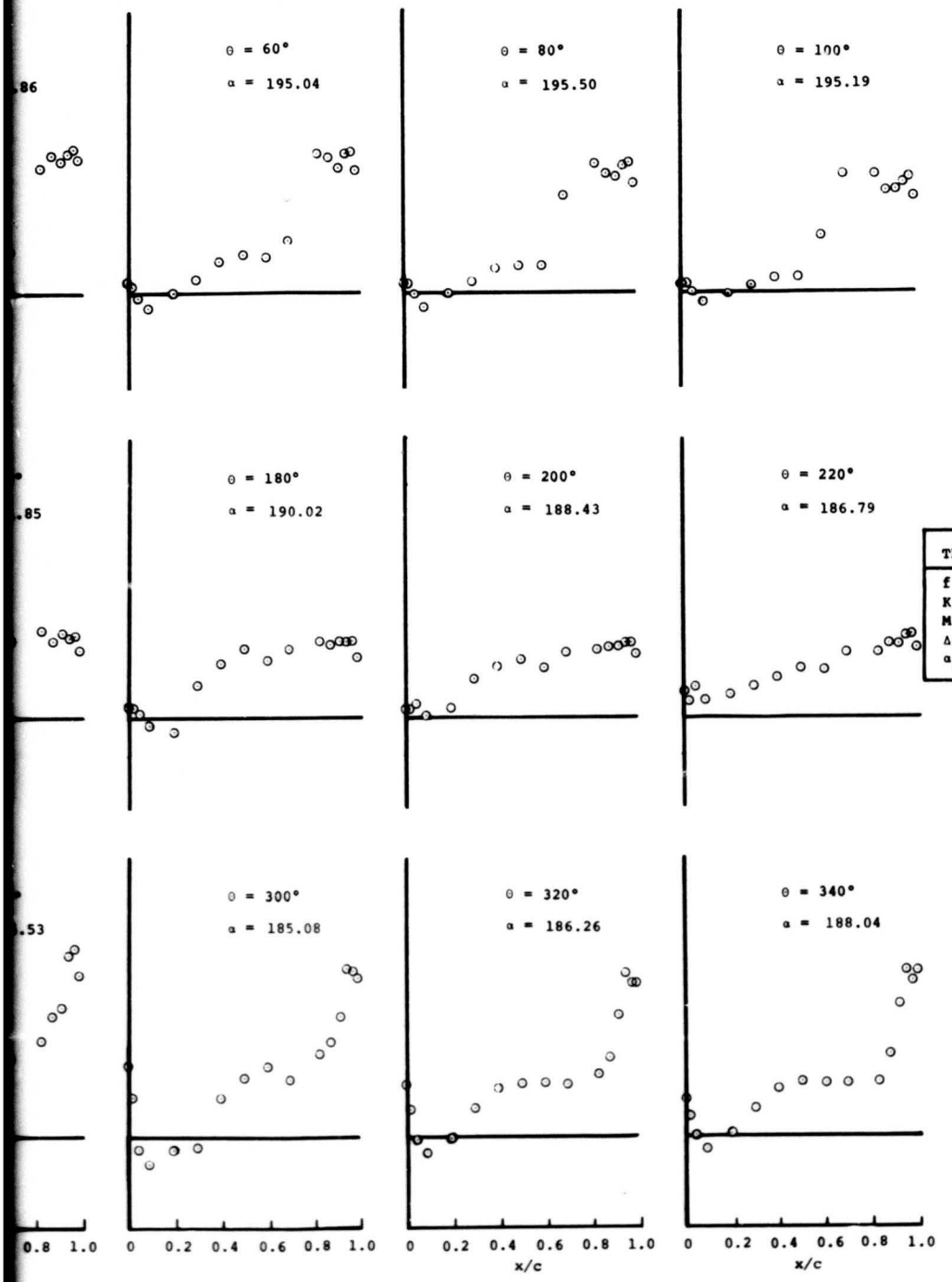

ributions for
rtz, M = 0.2,

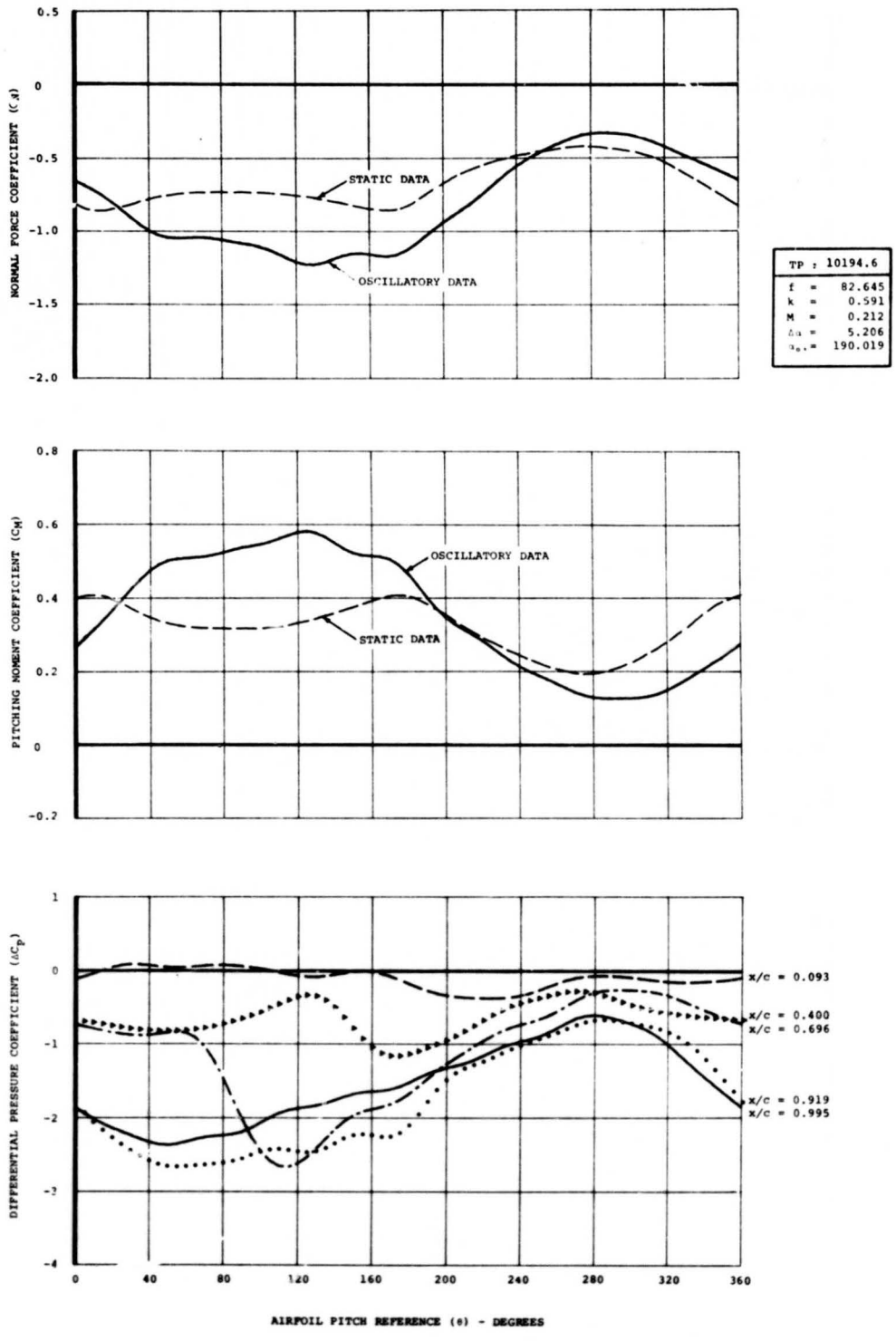

Figure 24. Cycle History of C_N, C_M, and ΔC_p for Pitch Oscillation at f = 80 Hertz, M = 0.2, and $\Delta\alpha$ = 5 Degrees With a 3-Degree Positive Trailing-Edge Tab Deflection.

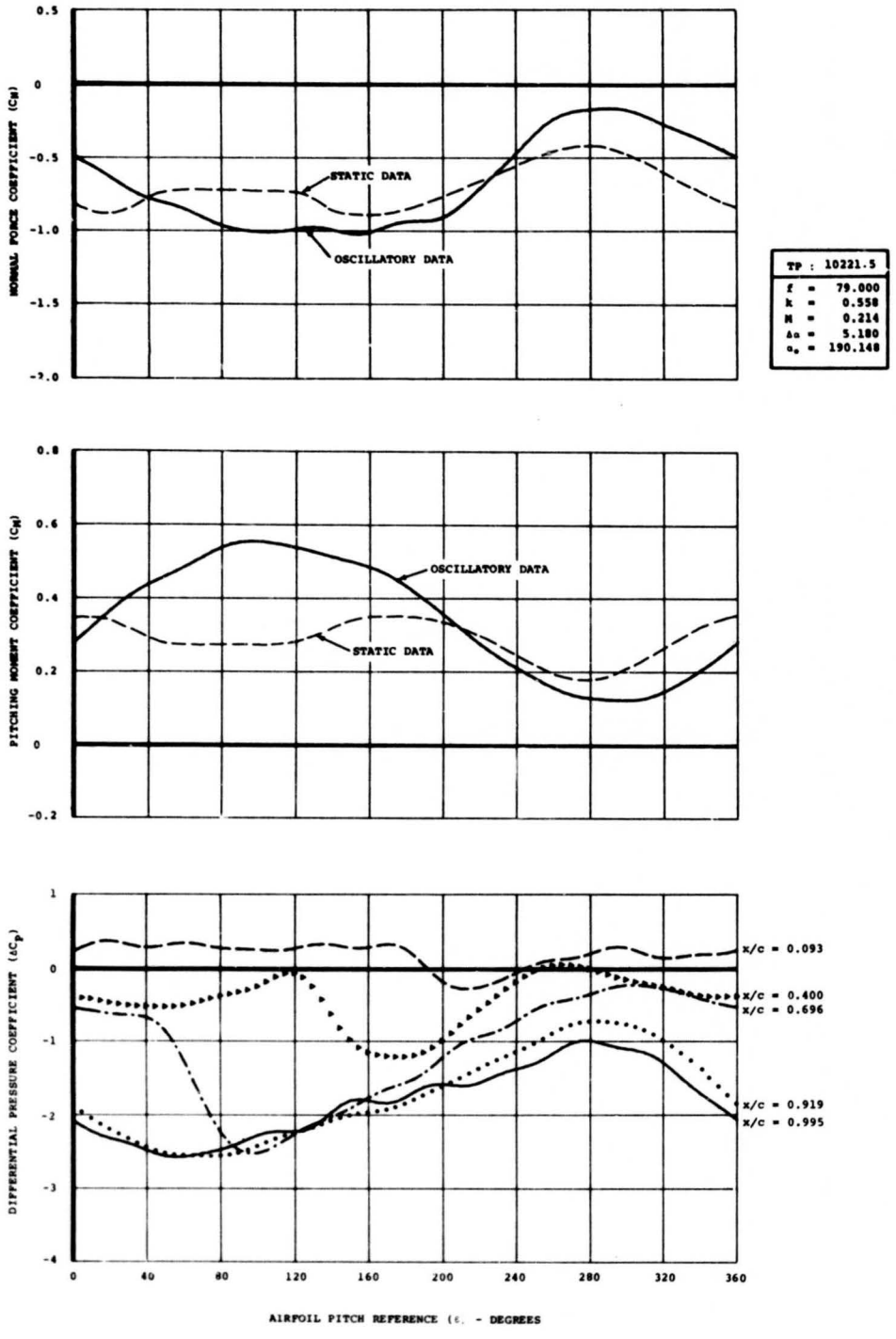

Figure 25. Cycle History of C_N, C_M, and ΔC_p for Pitch Oscillation at f = 80 Hertz, M = 0.2, and $\Delta\alpha$ = 5 Degrees With a 3-Degree Negative Trailing-Edge Tab Deflection.

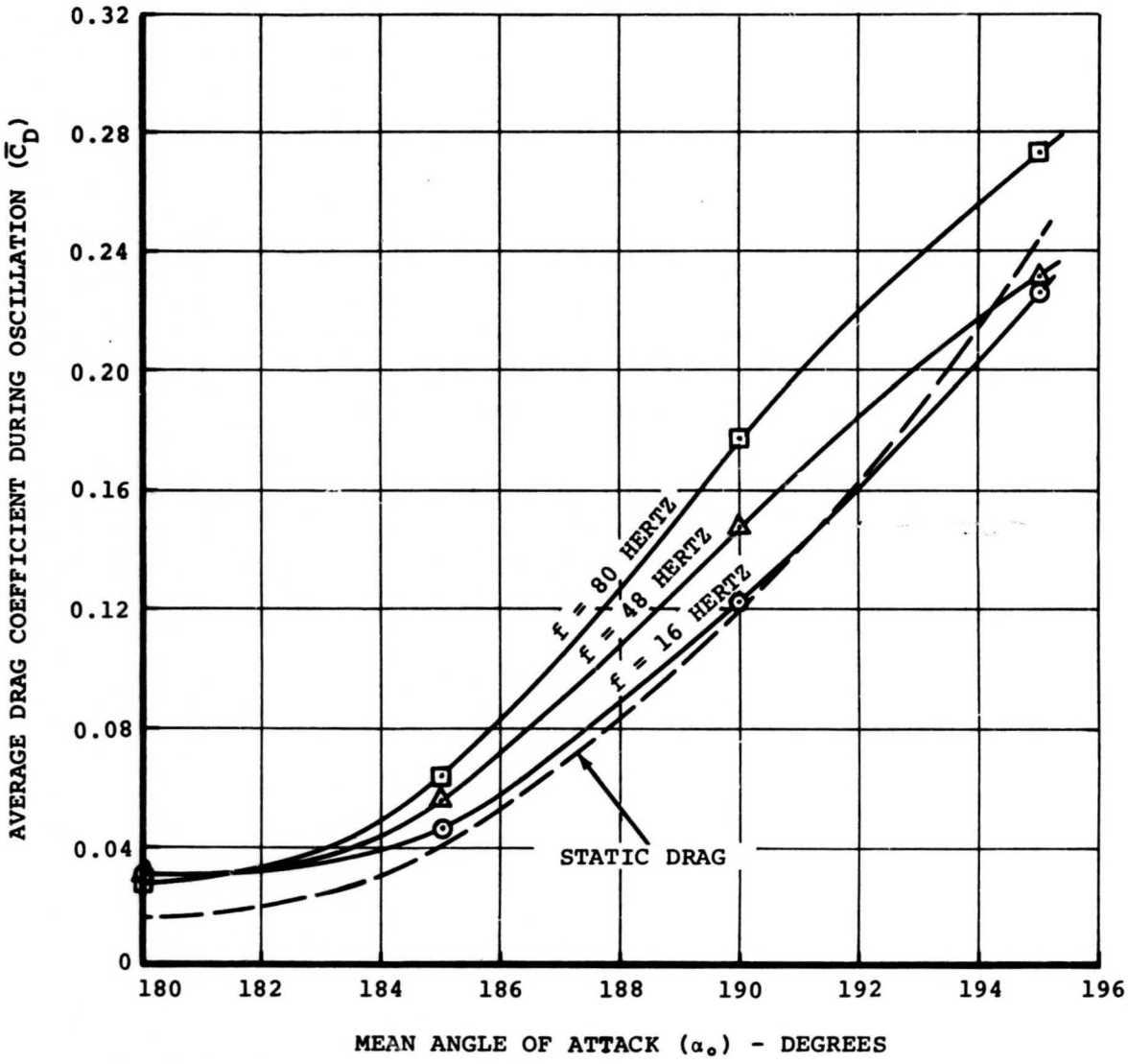

Figure 26. Effect of Drive Frequency on Oscillatory Drag for Pitch Oscillation at M = 0.4 and $\Delta\alpha$ = 5 Degrees.

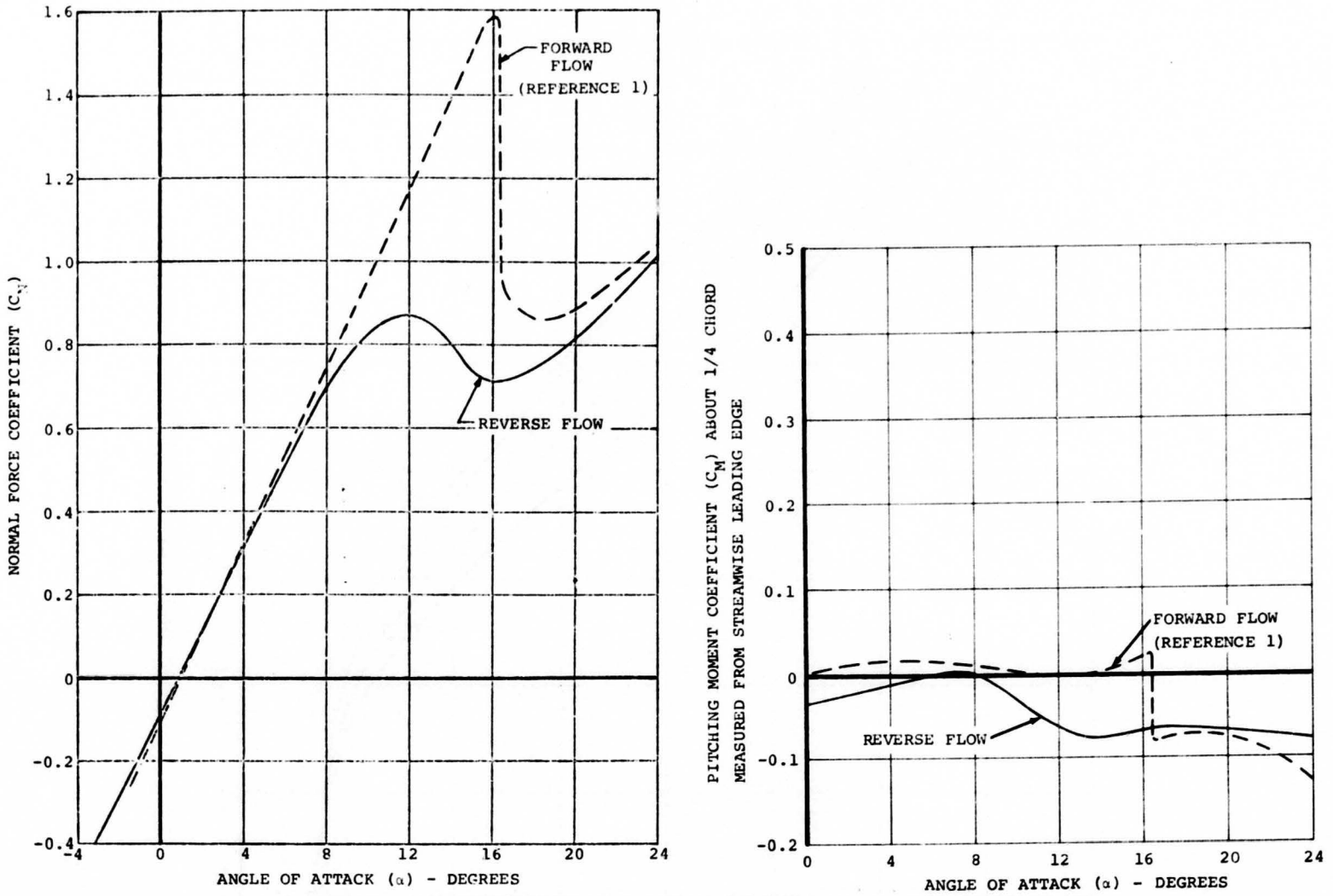

Figure 27. Comparison of Static C_N and C_M Versus α for the Vertol 23010-1.58 Airfoil in Forward and Reverse Flow at M = 0.2.

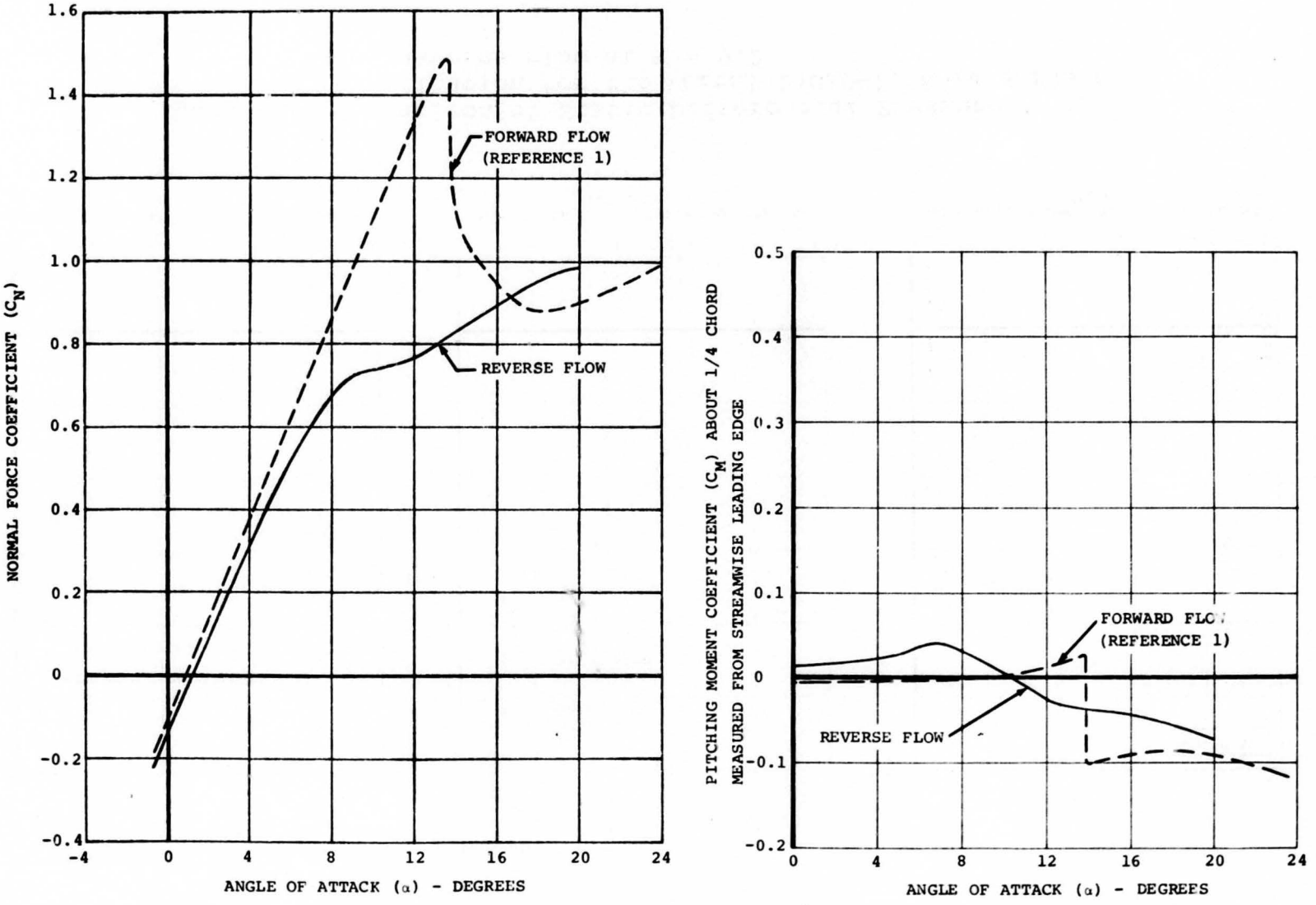

Figure 28. Comparison of Static C_N and C_M Versus α for the Vertol 23010-1.58 Airfoil in Forward and Reverse Flow at M = 0.4.

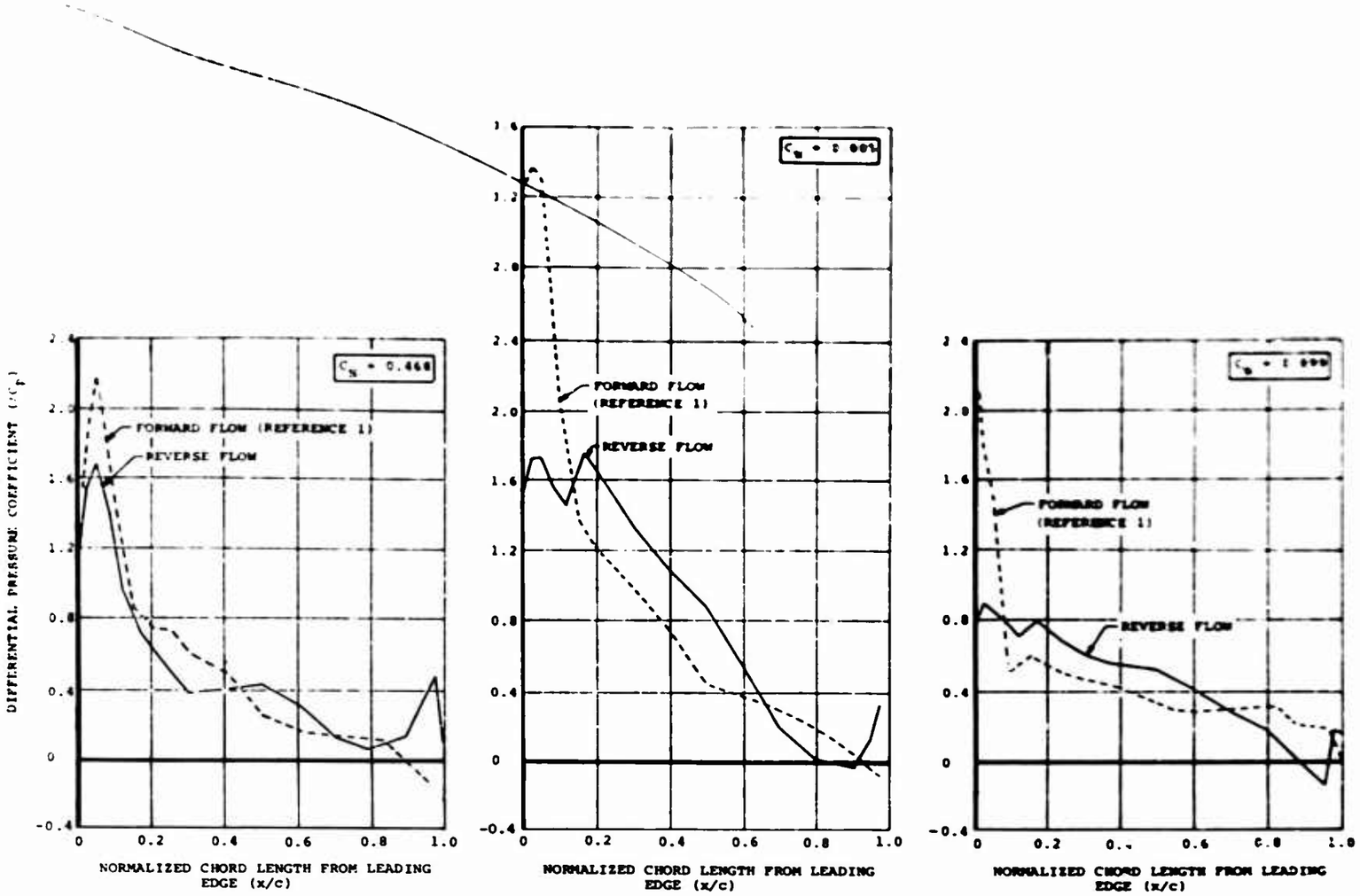

Figure 29. Comparison of Static Differential Pressure Distribution for the Vertol 23010-1.58 in Forward and Reverse Flow at M = 0.2.

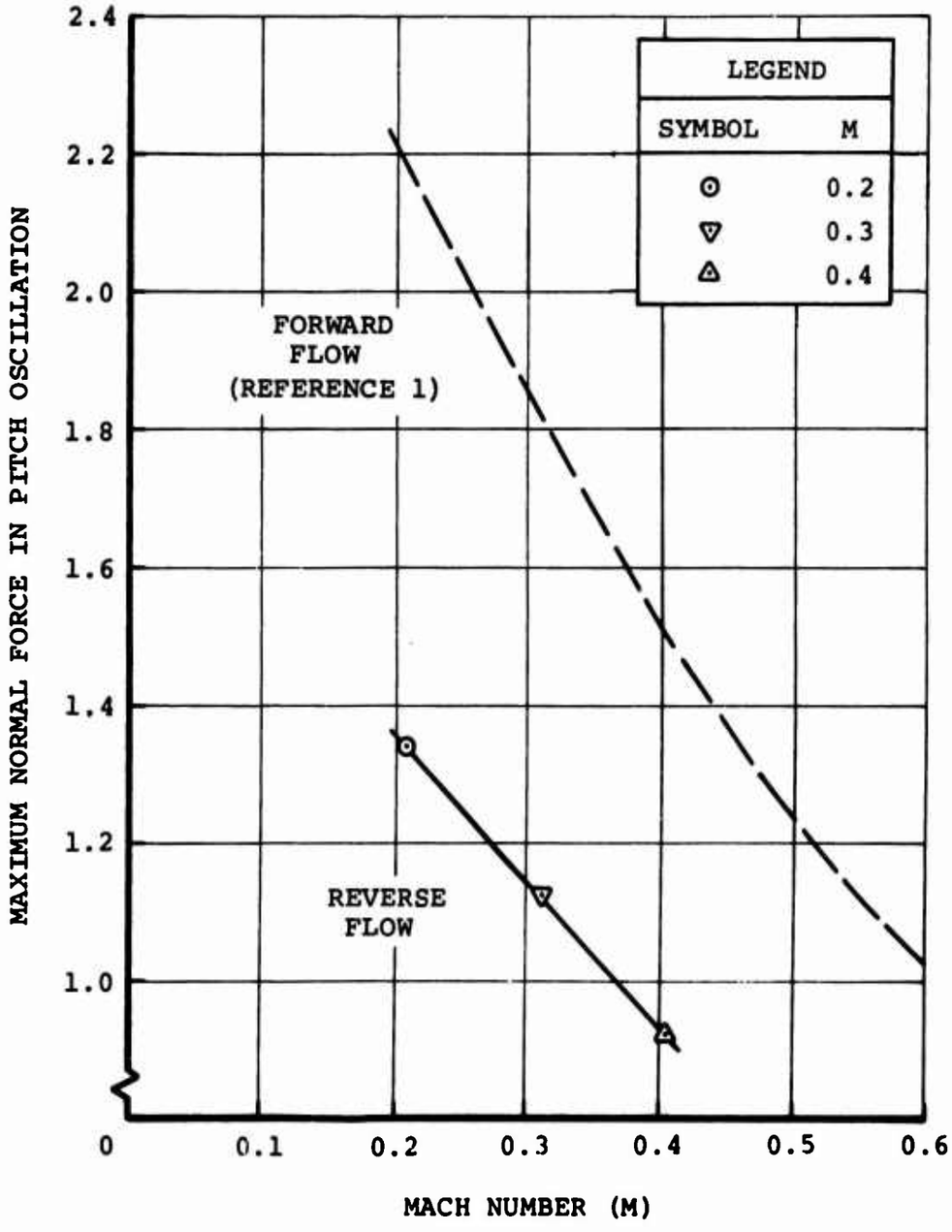

Figure 30. Comparison of Maximum Dynamic Normal Force Attained by the Vertol 23010-1.58 Airfoil During 5-Degree-Amplitude Pitch Oscillation in Forward and Reverse Flow at f = 16 Hertz.

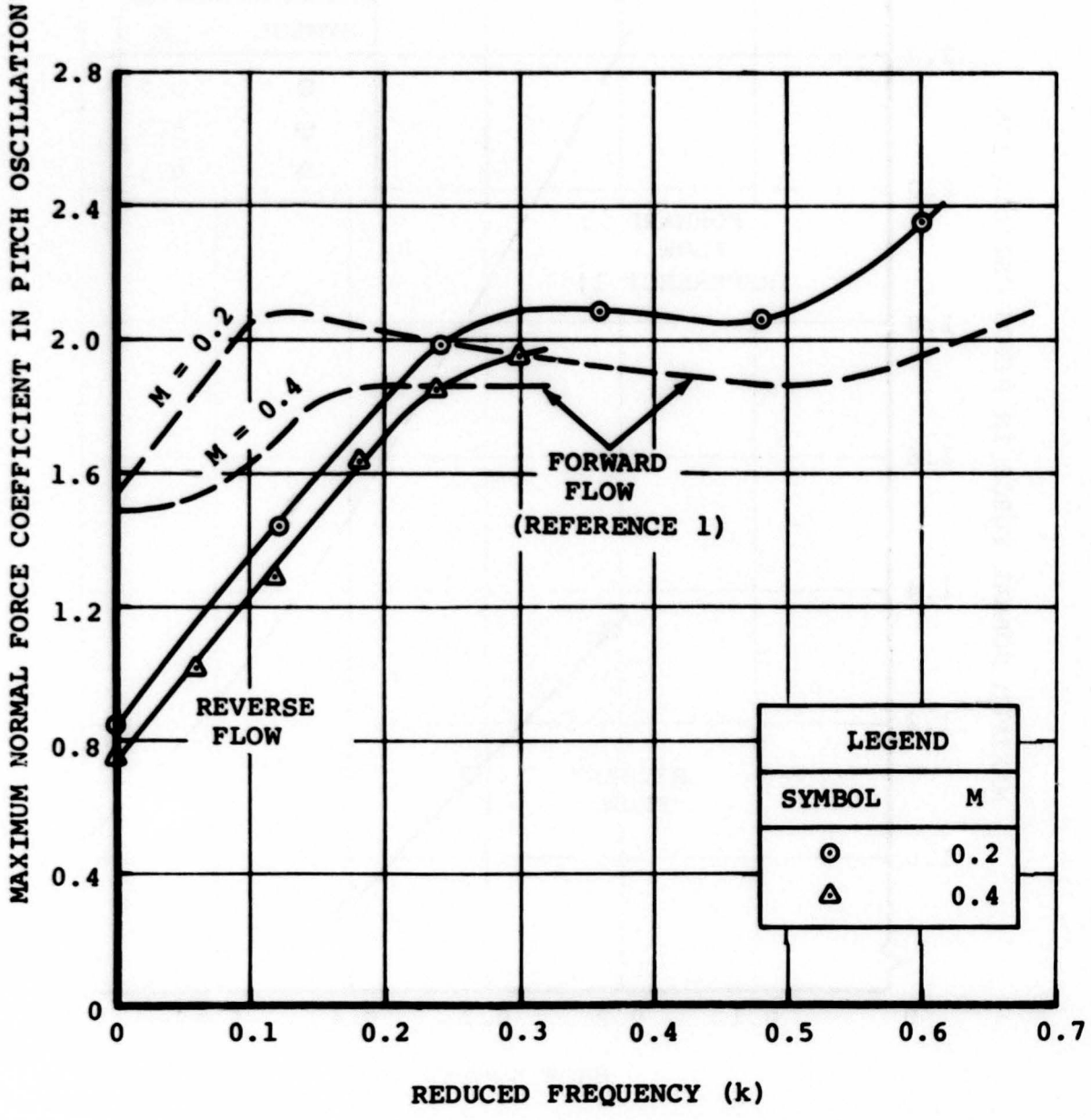

Figure 31. Comparison of Maximum Dynamic Normal Force Characteristics for the Vertol 23010-1.58 Airfoil in Forward and Reverse Flow at $\Delta\alpha$ = 5 Degrees.

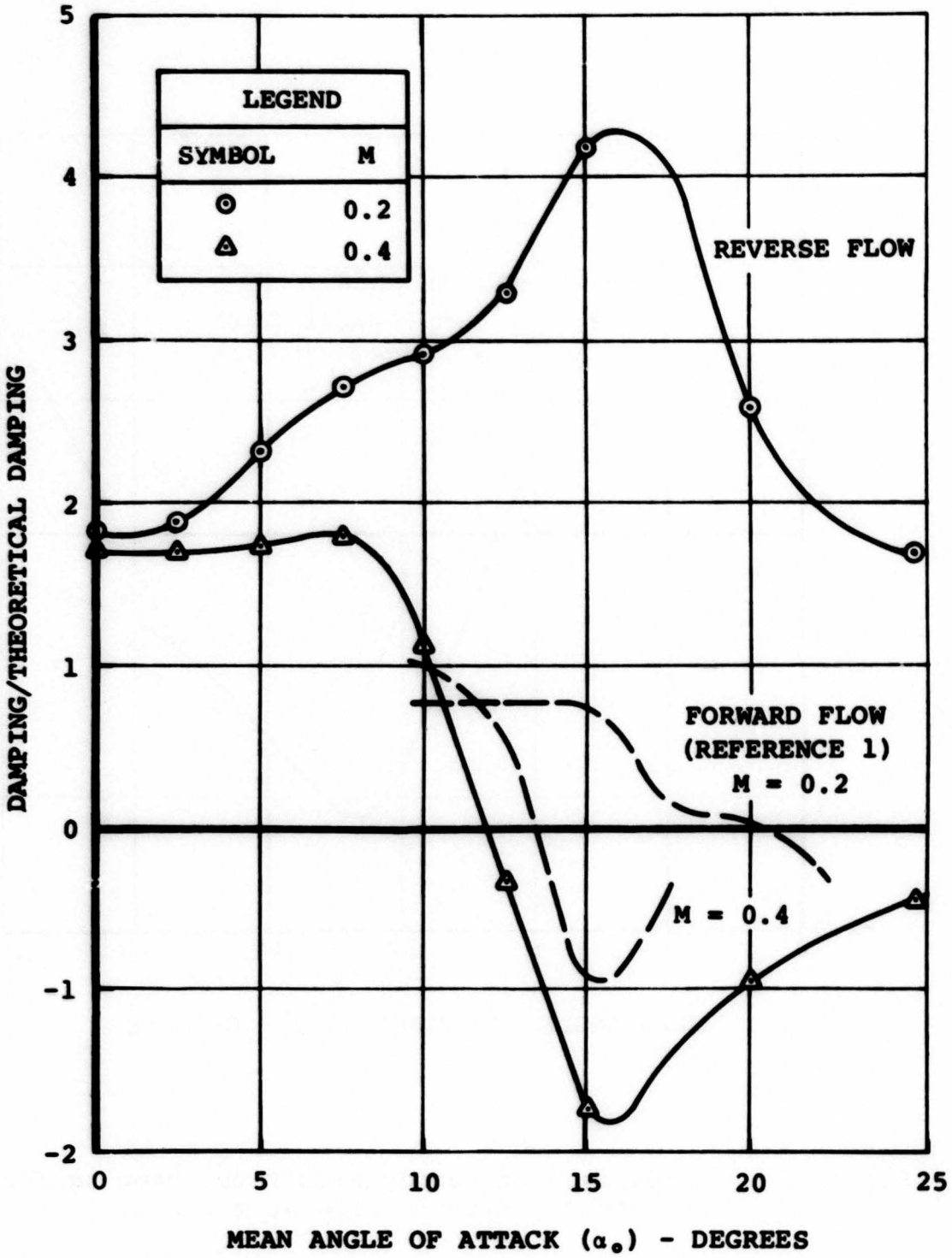

Figure 32. Comparison of Aerodynamic Pitch Damping for Forward and Reverse Flow at f = 96 Hertz, $\Delta\alpha$ = 2.5 Degrees.

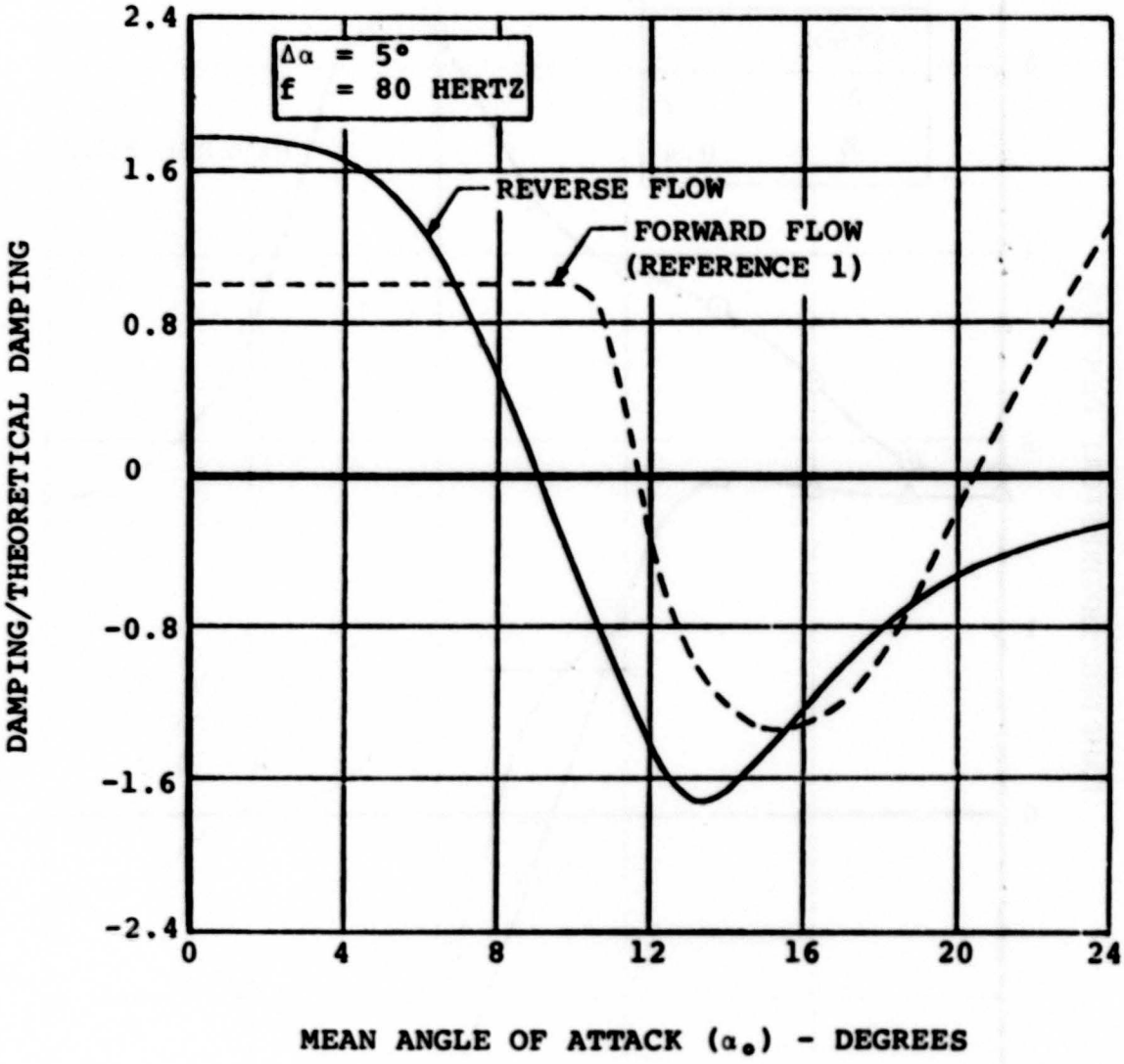

Figure 33. Comparison of Aerodynamic Pitch Damping for Forward and Reverse Flow at M = 0.4.

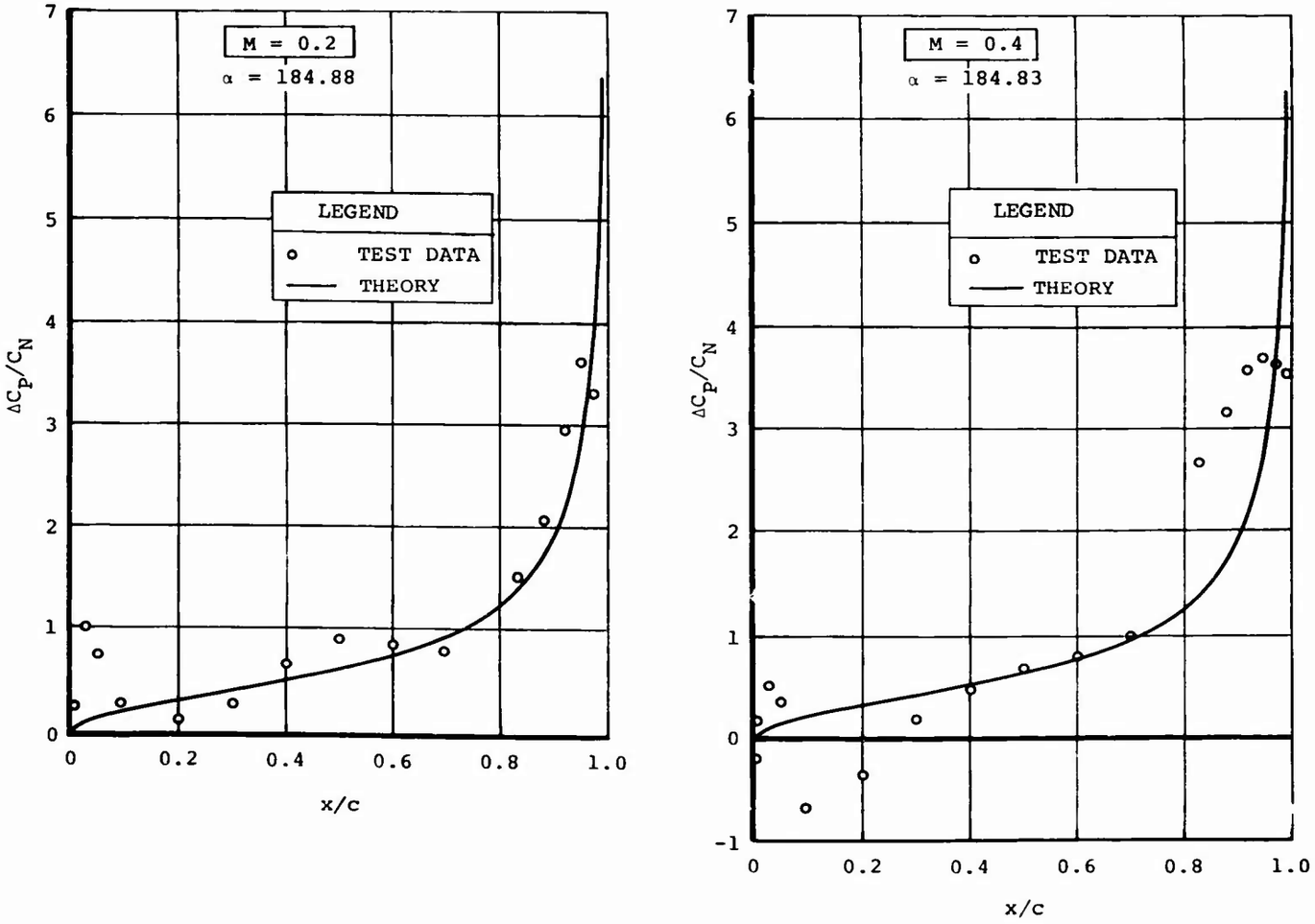

Figure 34. Comparison of Test and Theoretical Flat Plate Static Load Distributions in Reverse Flow for M = 0.2 and M = 0.4

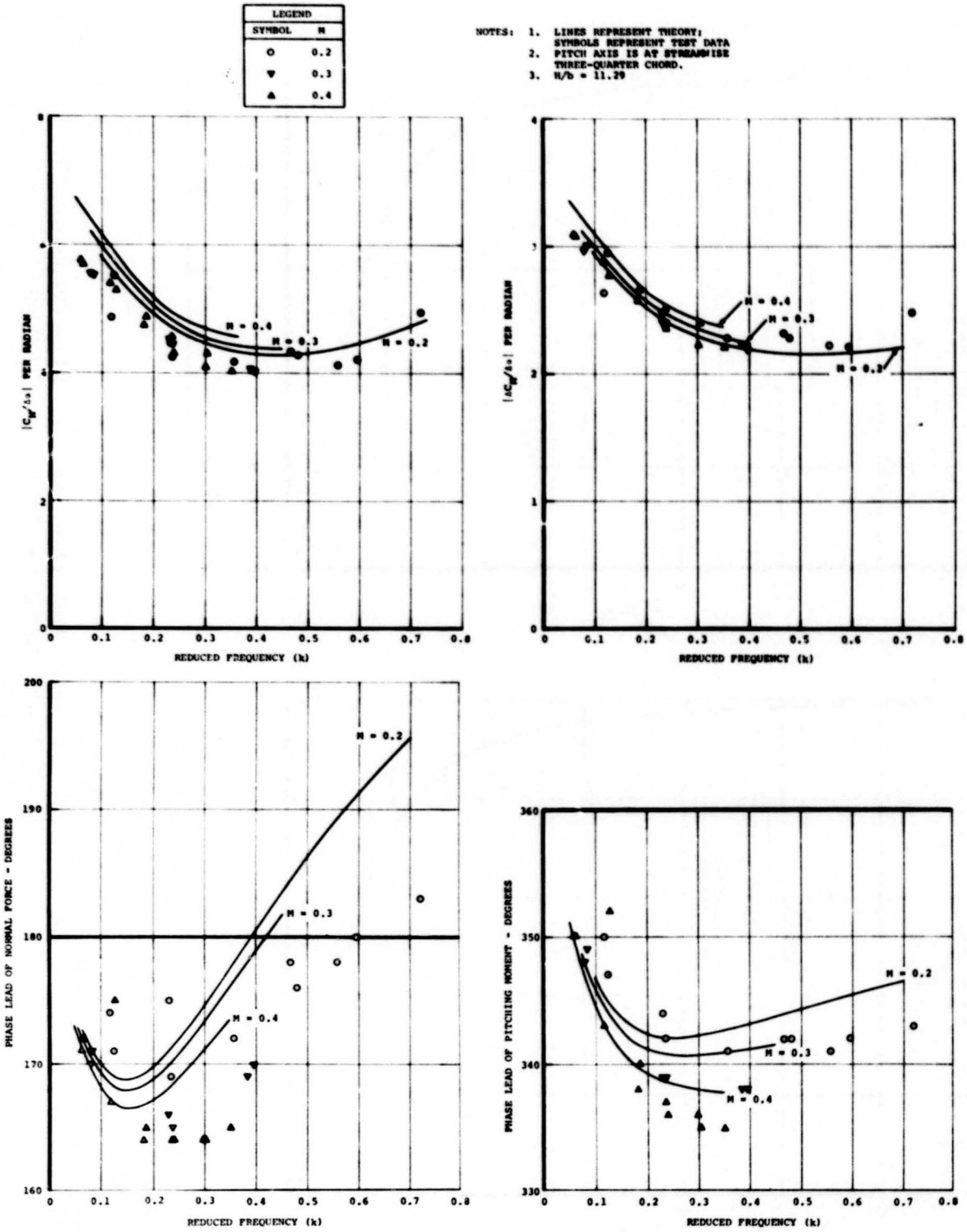

Figure 35. Comparison of Pitch Oscillation Test Data With Theory.

LITERATURE CITED

1. Liiva, J., Davenport, F.J., Gray, L., and Walton, I., TWO-DIMENSIONAL TESTS OF AIRFOILS OSCILLATING NEAR STALL, USAAVLABS Technical Report 68-13, Volumes I and II, U.S. Army Aviation Materiel Laboratories, Fort Eustis, Virginia, April 1968, AD670957 and AD670958.

2. Gray, L., Liiva, J., Davenport, F.J., WIND TUNNEL TESTS OF THIN AIRFOILS OSCILLATING NEAR STALL, USAAVLABS Technical Report 68-89, Volumes I and II, U.S. Army Aviation Materiel Laboratories, Fort Eustis, Virginia, January 1969, AD684323 and AD684324.

3. McCullough, G.B., and Gault, D.E., EXAMPLES OF THREE REPRESENTATIVE TYPES OF AIRFOIL-SECTION STALL AT LOW SPEED, NACA TN2502, September 1951.

4. Bisplinghoff, Raymond L., Ashley, Holt, and Halfman, Robert L., AEROELASTICITY, Addison-Wesley Publishing Company, Inc., Reading, Massachusetts, 1955.

5. Harris, Franklin D., and Pruyn, Richard R., BLADE STALL - HALF FACT, HALF FICTION, American Helicopter Society, Inc., 23rd Annual National Forum Proceedings, No. 101, May 1967.

6. Carta, Franklin O., and Ham, Norman D., AN ANALYSIS OF THE STALL FLUTTER INSTABILITY OF HELICOPTER ROTOR BLADES, American Helicopter Society, 23rd Annual National Forum Proceedings, No.130, May 1967.

7. Gross, David W., and Harris, Franklin D., PREDICTION OF INFLIGHT STALLED AIRLOADS FROM OSCILLATING AIRFOIL DATA, American Helicopter Society, Inc., 25th Annual National Forum Proceedings, No. 322, May 1969.

8. Davenport, F.J., SINGULARITY SOLUTIONS TO GENERAL POTENTIAL-FLOW AIRFOIL PROBLEMS, The Boeing Company, Document D6-7202, Revised May 1963.

9. Runyan, Harry L., and Watkins, Charles E., CONSIDERATIONS ON THE EFFECT OF WIND-TUNNEL WALLS ON OSCILLATING AIR FORCES FOR TWO-DIMENSIONAL SUBSONIC COMPRESSIBLE FLOW, Langley Aeronautical Laboratory, TN2552, National Advisory Committee for Aeronautics, Washington, D.C., December 1951.

10. Runyan, Harry L., Woolston, Donald S., and Rainey, A. Gerald, THEORETICAL AND EXPERIMENTAL INVESTIGATION OF THE EFFECT OF TUNNEL WALLS ON THE FORCES ON AN OSCILLATING AIRFOIL IN TWO-DIMENSIONAL SUBSONIC COMPRESSIBLE FLOW, Langley Aeronautical Laboratory, TN3416, National Advisory Committee for Aeronautics, Washington, D.C., June 1955.

11. MANUAL ON AEROELASTICITY, PART IV, North Atlantic Treaty Organization Advisory Group for Aeronautical Research and Development, NASA N63-17815, August 1965.

APPENDIX I
STATIC (NONOSCILLATORY) TESTS

The Vertol 23010-1.58 airfoil was tested under the steady-angle-of-attack condition in reverse flow over the full range of angle of attack and Mach number for which dynamic data were obtained. The effects of trailing-edge tab deflection were also measured.

Figure 36 presents steady C_N and C_M versus angle of attack for the basic airfoil (with neutral trailing-edge tab position) at each test Mach number. The sign conventions defined in Figure 4 produce what initially appears to be abnormal C_N and C_M behavior. Since pitching moment is measured about the normal 1/4-chord location defined for forward flow, it corresponds to the 3/4-chord position measured from the upstream edge in reverse flow. However, the airfoil center of pressure, measured relative to the flow direction, is not radically altered by leading- or trailing-edge contour variations, and thus, the pitching moment coefficient in reverse flow approximates half of the normal force coefficient magnitude. Measurements of the aerodynamic center in reverse flow show it to be slightly upstream of the 3/4-chord location at all test Mach members.

Stall behavior under reverse-flow conditions is characteristic of thin airfoils[3]. The sharp "leading edge" precipitates the early formation of a leading-edge separation bubble which leads to a gradual C_N and C_M transition at stall without any large or abrupt changes. Throughout the range of angles of attack shown, the C_N and C_M behaviors at $M = 0.2$ and 0.3 are quite similar except for the earlier stall at $M = 0.3$ for angles of attack greater than 180 degrees. Note that the peak value of C_M at stall occurs before that of C_N. This characteristic is indicative of the gradual downstream movement of the airfoil center of pressure during stall. At $M = 0.4$, the C_N and C_M show a negligible drop at stall followed by a rapid recovery to a reduced rate of increase. This behavior is typical of transonic flow effects and is widely reported for most types of airfoil.

Figures 37 through 39 present the effect of trailing-edge tab angle deflection on the steady C_N and C_M versus angle-of-attack behavior for each test Mach number. Tab angle changes between +3 and -3 degrees produce only minor changes in C_N, C_M, and angle of attack for stall. Although the test measurements show some inconsistency, they usually agree with expected trends. Thus, a positive tab angle movement should show a slight positive increment in C_N with a small shift of angle of attack for both stall points. Inconsistencies in the data are attributed to both measurement inaccuracies and pressure distribution changes associated with movement of the downstream

flow separation points close to the airfoil nose. These points are determined by the boundary layer profile characteristics and adverse pressure gradients which are sensitive to the high surface curvatures in this region.

Static C_D versus angle-of-attack behavior at all three test Mach numbers is shown in Figure 40 for the angle-of-attack range greater than 180 degrees. Close to 180 degrees, the C_D level is substantially above that experienced in forward flow as a result of the wide wake induced by the bluff-body trailing edge. The drag rise associated with stall starts well before $C_{N_{MAX}}$ is reached and is similar for all Mach numbers.

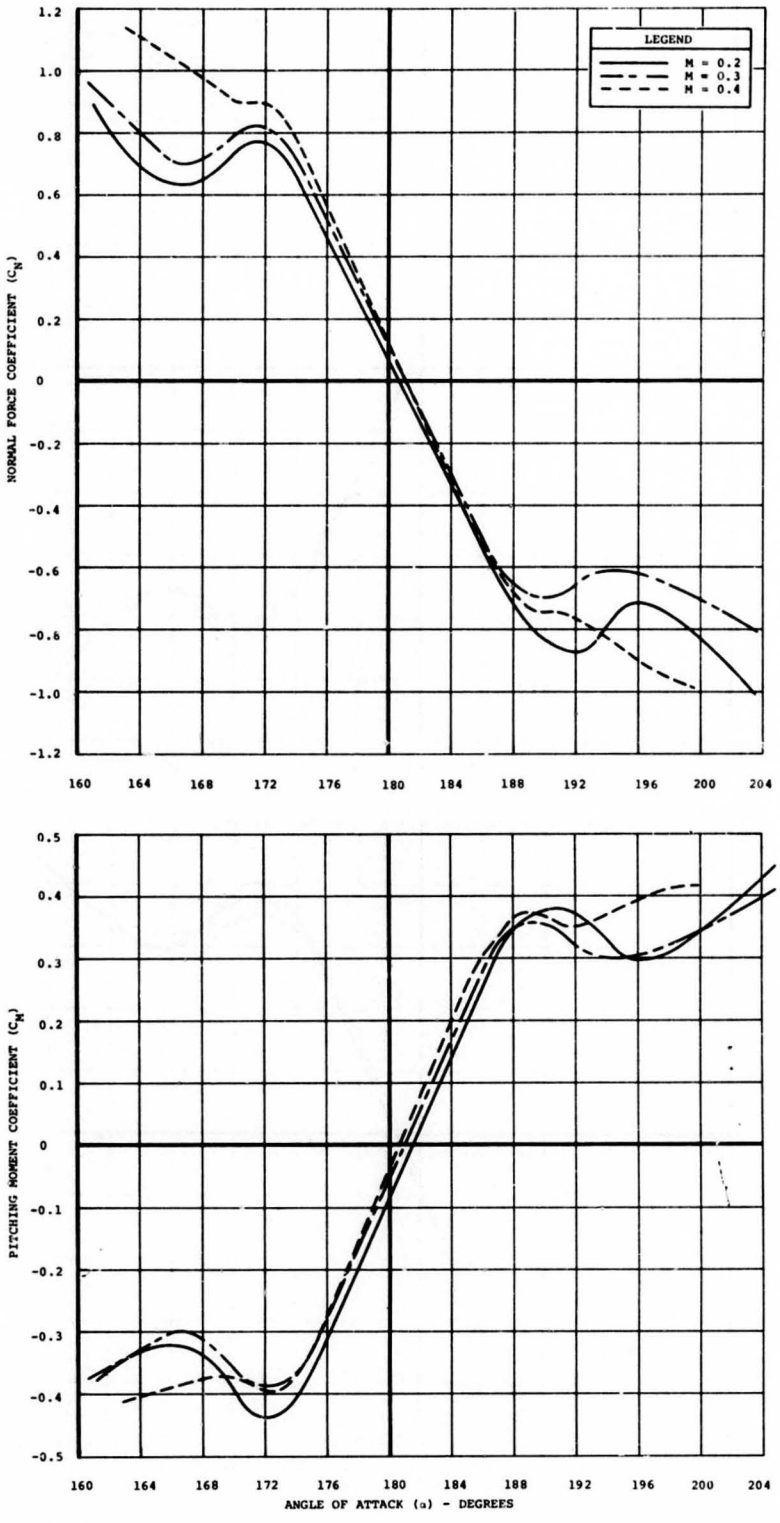

Figure 36. Static C_N and C_M Versus α in Reverse Flow for the Vertol 23010-1.58 Airfoil With the Trailing-Edge Tab in the Neutral Position.

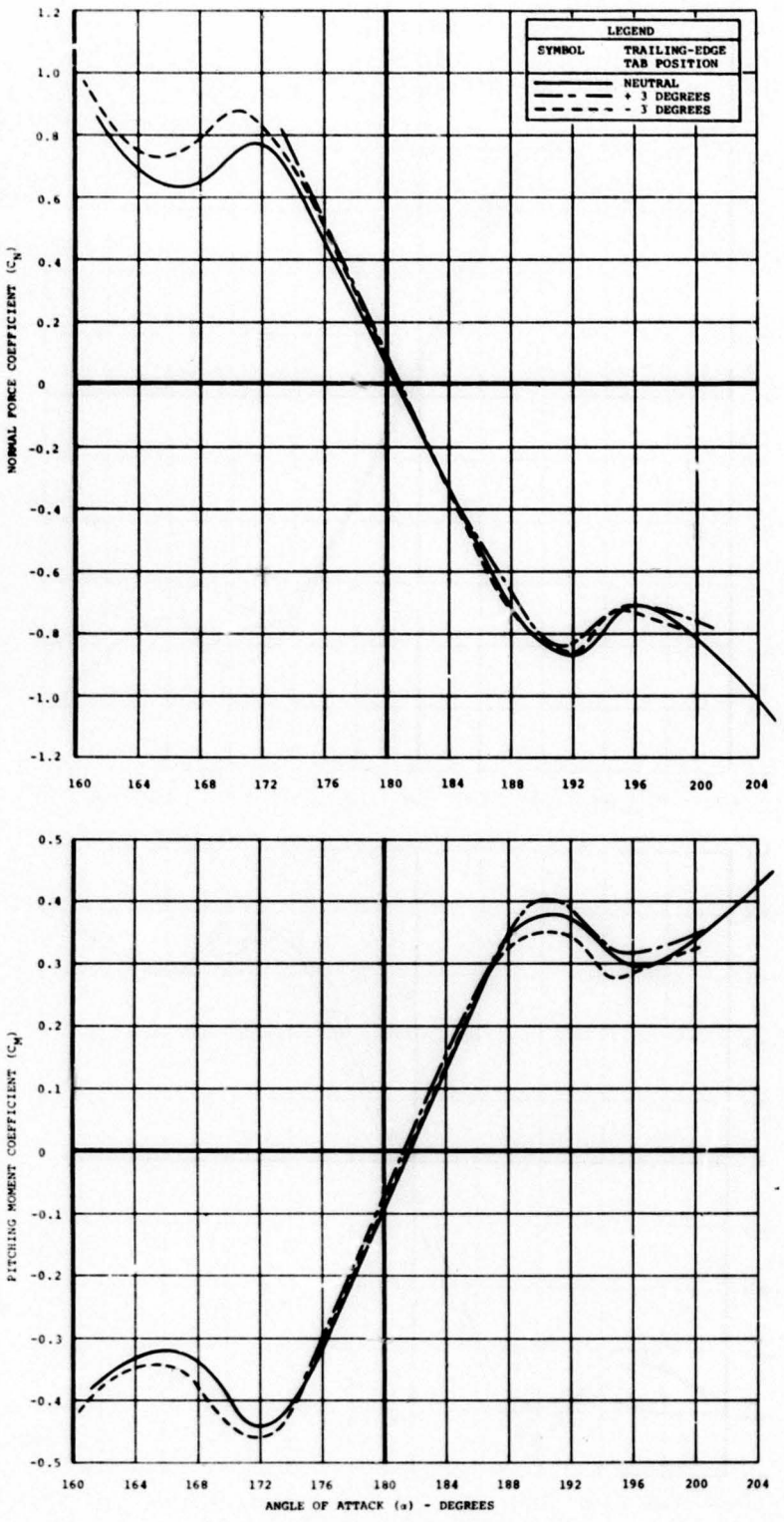

Figure 37. **Effect of Trailing-Edge Tab Deflection on Static C_N and C_M Versus α for the Vertol 23010-1.58 Airfoil in Reverse Flow at M = 0.2**

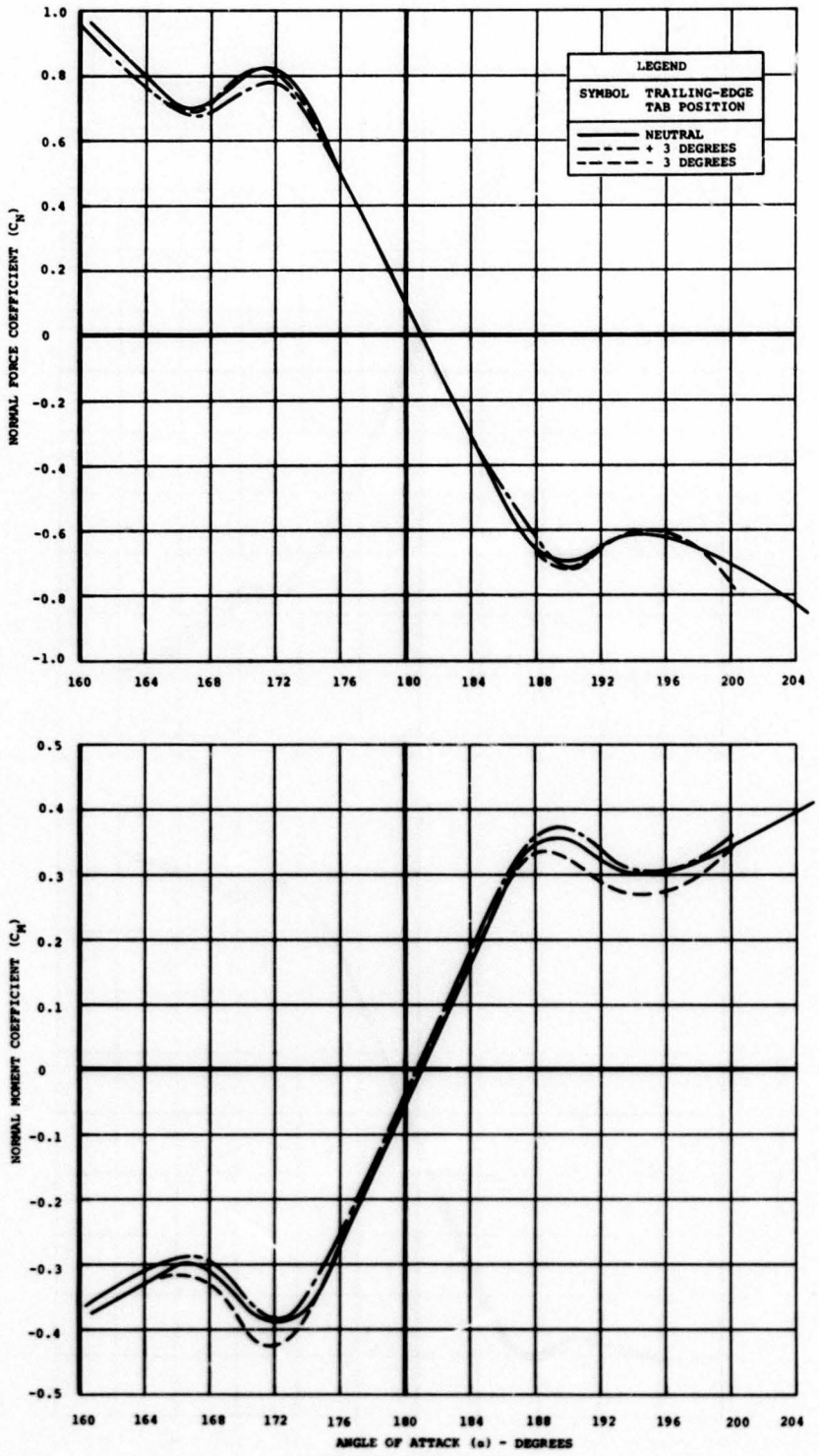

Figure 38. Effect of Trailing-Edge Tab Deflection on Static C_N and C_M Versus α for the Vertol 23010-1.58 Airfoil in Reverse Flow at M = 0.3.

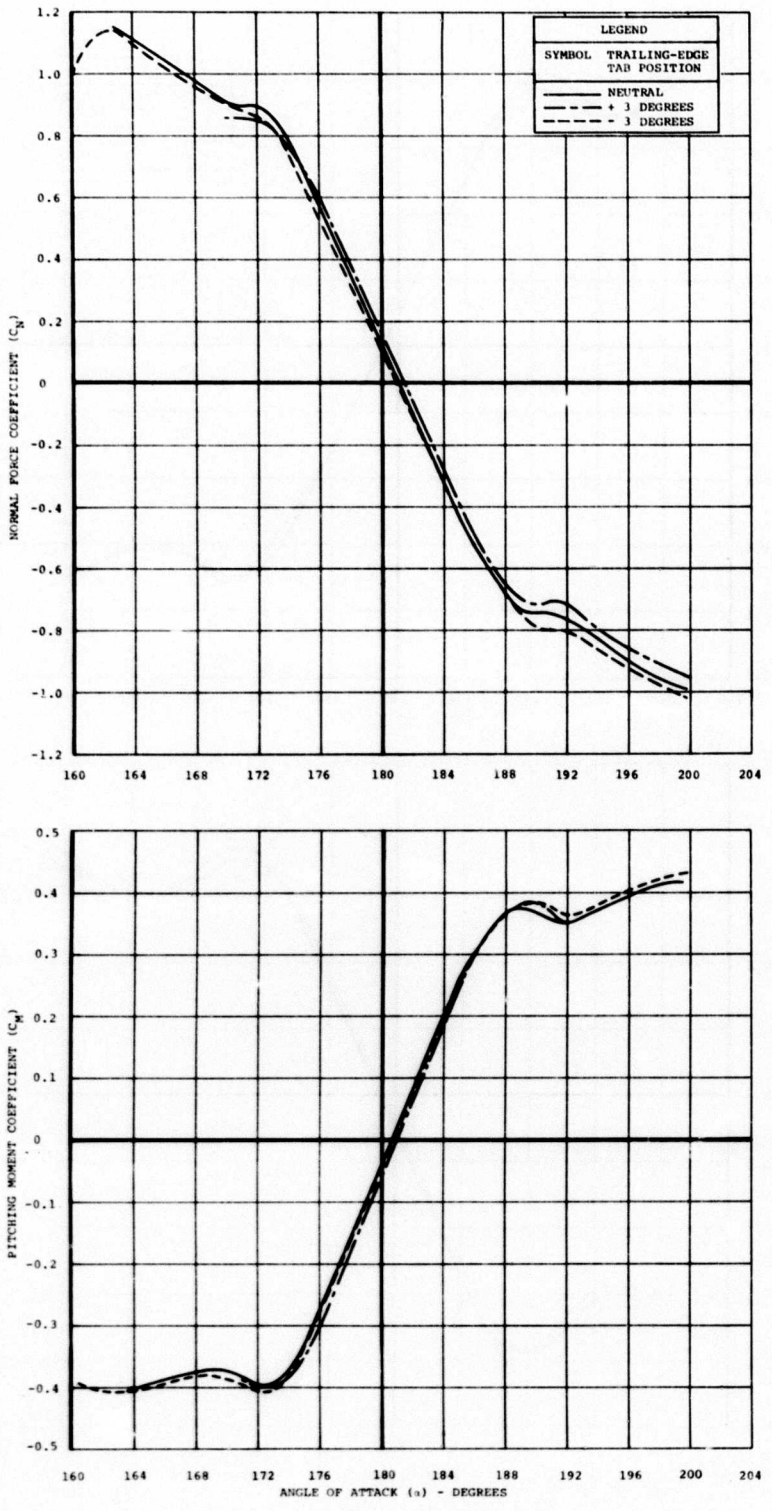

Figure 39. Effect of Trailing-Edge Tab Deflection on Static C_N and C_M Versus α for the Vertol 23010-1.58 Airfoil in Reverse Flow at M = 0.4.

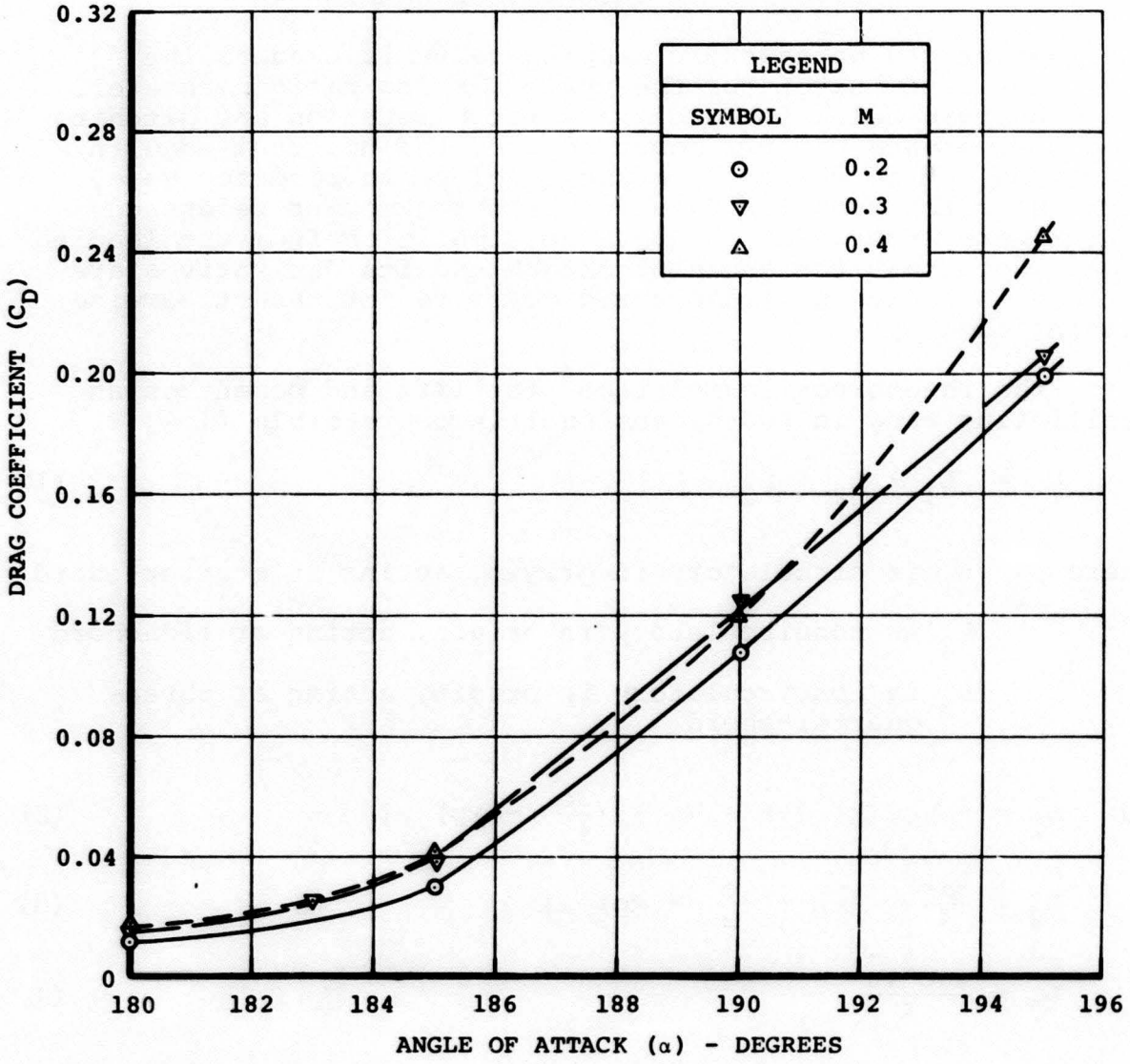

Figure 40. Static C_D Versus α in Reverse Flow for the Vertol 23010-1.58 Airfoil With the Trailing-Edge Tab in the Neutral Position.

APPENDIX II
DERIVATION OF THEORETICAL DAMPING

The theoretical aerodynamic damping value is used as the reference denominator for the cycle damping ratio parameter. It is derived below for arbitrary pitch rotation and pitching moment reference centers measured from the upstream edge in fractions of the chord. For the model tests reported here, both the pitch rotation axis and pitching moment reference center were located at the 3/4-chord position from the leading edge. Note that the angle of attack and its derivatives are defined in radian units measured positive for the streamwise leading edge up.

Using the Theodorsen formulation[4] for lift and moment on an oscillating wing in two-dimensional incompressible flow,

$$L = L_1 + L_2 + L_3 \tag{1}$$

where L_1 is circulatory in origin, acting at quarter-chord

L_2 is noncirculatory in origin, acting at mid-chord

L_3 is noncirculatory in origin, acting at three-quarter-chord

nd $$L_1 = \pi\rho VcC(k)\ [-\dot{h} + V\alpha + (\frac{3c}{4} - xp)\ \dot{\alpha}] \tag{2}$$

$$L_2 = \frac{\pi\rho c^2}{4}\ [-\ddot{h} + (\frac{c}{2} - xp)\ \ddot{\alpha}] \tag{3}$$

$$L_3 = \frac{\pi\rho c^2 V\dot{\alpha}}{4} \tag{4}$$

Note that the Theodorsen function C(k) is complex. Thus, C(k) may be written as A(k) + j B(k).

Reduction of the lift expressions to coefficient form by dividing by $\rho V^2 c/2$ per unit span assumes V to be constant.

Thus, $$C_{L_1} = 2\pi\ C(k)\ [\ -\frac{\dot{h}}{V} + \alpha + (\frac{3}{4} - \frac{xp}{c})\ \frac{c\dot{\alpha}}{V}] \tag{5}$$

$$C_{L_2} = \frac{\pi c}{2V^2} \left[-\ddot{h} + \left(\frac{1}{2} - \frac{xp}{c}\right) c\ddot{\alpha}\right] \tag{6}$$

$$C_{L_3} = \frac{\pi c \dot{\alpha}}{2V} \tag{7}$$

The pitching moment coefficient may be similarly derived, as follows:

$$C_M = \left(\frac{xm}{c} - \frac{1}{4}\right) C_{L_1} + \left(\frac{xm}{c} - \frac{1}{2}\right) C_{L_2}$$

$$+ \left(\frac{xm}{c} - \frac{3}{4}\right) C_{L_3} - \frac{\pi c^2 \alpha}{64V^2} \tag{8}$$

In pitching oscillation, the theoretical aerodynamic damping may be defined as

$$TD = \frac{1}{2\pi^2 f(\Delta\alpha)^2} \oint C_M \, d\alpha = \frac{1}{2\pi^2 f(\Delta\alpha)^2} \int_0^{2\pi} C_M(\theta) \frac{d\alpha}{d\theta} \cdot d\theta \tag{9}$$

where this integral is complex.

If pure sinusoidal pitch oscillation is assumed, then the following equations of airfoil motion apply:

$$h = \dot{h} = \ddot{h} = 0. \text{ (Airfoil in pure pitch)} \tag{10}$$

$$\alpha = \Delta\alpha \, (\cos\theta + j. \sin\theta) \tag{11}$$

$$\equiv \Delta\alpha \; e^{j\theta}$$

Hence, $$\dot{\alpha} = \dot{\theta} \Delta\alpha \; j \; e^{j\theta} \tag{12}$$

and $$\ddot{\alpha} = -\dot{\theta}^2 \Delta\alpha \; e^{j\theta} \tag{13}$$

where $$\dot{\theta} = 2\pi f \tag{14}$$

Substitution of the equations of motion into the kernel function of the aerodynamic damping integral leads to the complex expression

$$\left\{2\left(\frac{xm}{c}-\frac{1}{4}\right)\left[B(k)+\left(\frac{3}{4}-\frac{xp}{c}\right)2k\,A(k)\right]\right.$$

$$\left.+\left(\frac{xm}{c}-\frac{3}{4}\right)k\right\}.\ -\pi(\Delta\alpha)^2\,e^{j2\theta}$$

$$+\left\{2\left(\frac{xm}{c}-\frac{1}{4}\right)\left[A(k)-\left(\frac{3}{4}-\frac{xp}{c}\right)2k\,B(k)\right]\right.$$

$$\left.+\left(\frac{xm}{c}-\frac{1}{2}\right)\left(\frac{xp}{c}-\frac{1}{2}\right)2k^2-\frac{k^2}{16}\right\}.\ j\pi(\Delta\alpha)^2\,e^{j2\theta} \qquad (15)$$

Since the sinusoidal angle-of-attack variation is represented by the imaginary part of the motion equations, only the imaginary part of the integral solution is required to give the damping expression. This results from the first part of the kernel function, and the theoretical damping becomes

$$TD=\frac{1}{2\pi^2 f(\Delta\alpha)^2}\left\{2\left(\frac{xm}{c}-\frac{1}{4}\right)\left[B(k)+\left(\frac{3}{4}-\frac{xp}{c}\right)2k\,A(k)\right]\right.$$

$$\left.+\left(\frac{xm}{c}-\frac{3}{4}\right)k\right\}.\ -\pi^2(\Delta\alpha)^2 \qquad (16)$$

Simplifying, this reduces to

$$TD=\frac{k}{2f}\left[\left(\frac{xm}{c}-\frac{3}{4}\right)+4\left(\frac{xm}{c}-\frac{1}{4}\right)\left(\frac{3}{4}-\frac{xp}{c}\right)A(k)\right]$$

$$+\frac{B(k)}{f}\cdot\left(\frac{xm}{c}-\frac{1}{4}\right) \qquad (17)$$

For the present tests in reverse flow, $\frac{xm}{c}=\frac{xp}{c}=\frac{3}{4}$. (18)

Hence, $TD=\frac{B(k)}{2f}$ (19)

Values of the theoretical damping were computed in the data reduction computer program by using the approximate expression given in Reference 11, as follows:

$$B(k)=-\frac{0.001995+0.327214(k)+0.122397(k)^2+0.000146(k)^3}{0.089318+0.934530(k)+2.481481(k)^2+(k)^3}$$

APPENDIX III
WIND TUNNEL WALL CORRECTIONS

Wind tunnel boundary corrections were developed by using a computer program provided by NASA (based on the formulation in References 9 and 10) to calculate the magnitude and phase of C_N and C_M for an airfoil oscillating in a wind tunnel. Comparative free-air values were obtained from the data tables in Reference 11. The theoretical values were based on compressible thin airfoil theory, with the method of images used to simulate the tunnel walls.

Ratios of the amplitude of C_N and C_M in free air to the tunnel values, as well as phase differences, are presented in Figure 41. The magnitude corrections are seen to be greatest at low values of reduced frequency and high Mach number but are always less than 9 percent for the range of test conditions studied. The corresponding phase angle corrections, which increase with Mach number, are all less than 4 degrees.

The corrections calculated here are small in comparison with the large changes in magnitude and phase experienced during stall. Therefore, they have been omitted from the wind tunnel results.

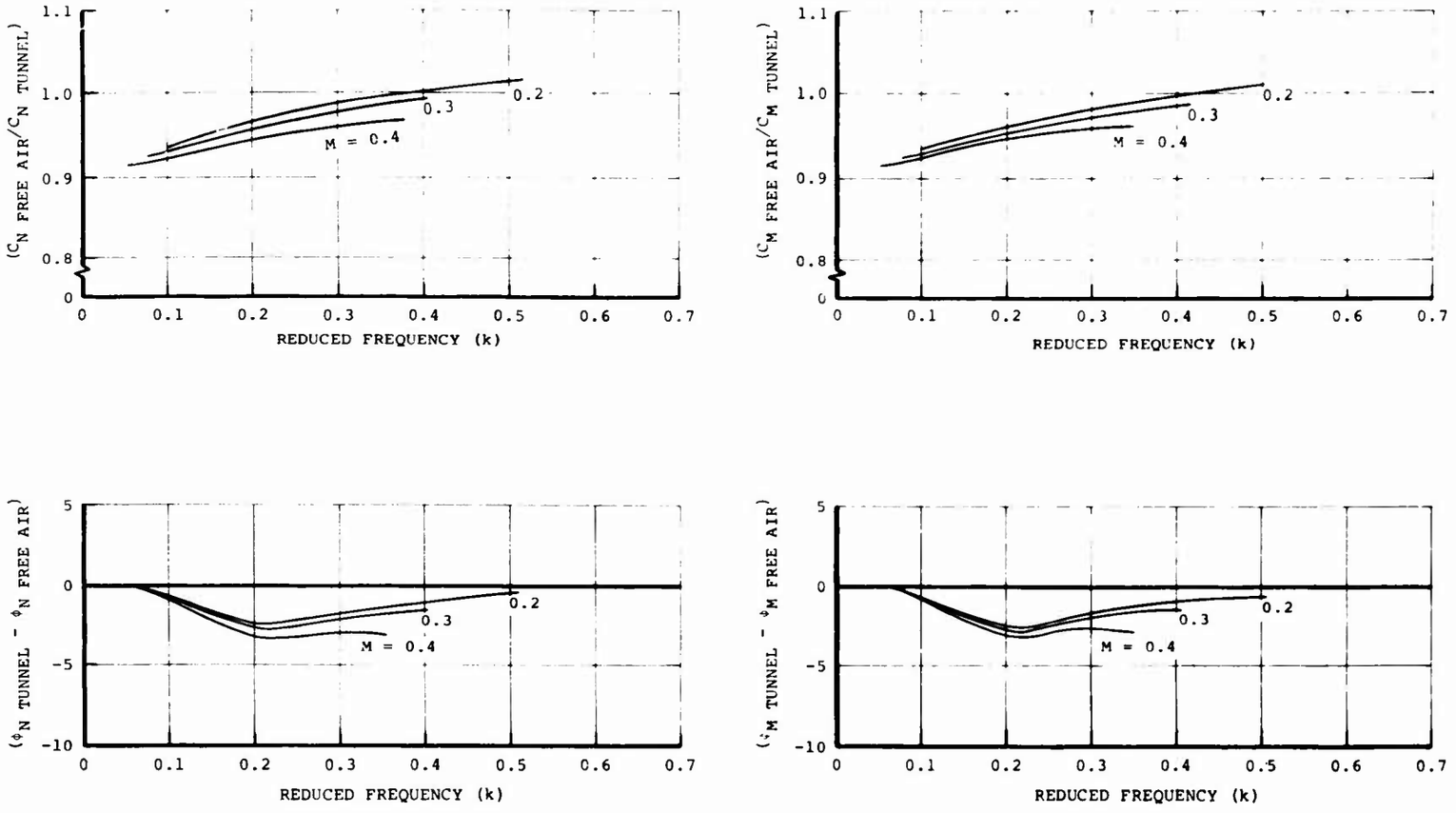

Figure 41. Wind Tunnel Wall Corrections for Pitching Oscillation.

UNCLASSIFIED

Security Classification

DOCUMENT CONTROL DATA - R & D

(Security classification of title, body of abstract and indexing annotation must be entered when the overall report is classified)

1. ORIGINATING ACTIVITY (Corporate author) The Boeing Company Vertol Division - Boeing Center Philadelphia, Pennsylvania	2a. REPORT SECURITY CLASSIFICATION Unclassified 2b. GROUP

3. REPORT TITLE

WIND TUNNEL INVESTIGATION OF AIRFOILS OSCILLATING IN REVERSE FLOW

VOLUME I, SUMMARY AND EVALUATION OF RESULTS

4. DESCRIPTIVE NOTES (Type of report and inclusive dates)

Final Report

5. AUTHOR(S) (First name, middle initial, last name)

Lewis Gray
Richard F. Child
Leo U. Dadone
David W. Gross

6. REPORT DATE	7a. TOTAL NO. OF PAGES	7b. NO. OF REFS
March 1970	90	11

8a. CONTRACT OR GRANT NO.	9a. ORIGINATOR'S REPORT NUMBER(S)
DAAJ02-68-C-0064 b. PROJECT NO. Task 1F162204A14231 c. d.	USAAVLABS Technical Report 70-4A 9b. OTHER REPORT NO(S) (Any other numbers that may be assigned this report) D8-2474-1

10. DISTRIBUTION STATEMENT

This document is subject to special export controls, and each transmittal to foreign governments or foreign nationals may be made only with prior approval of U. S. Army Aviation Materiel Laboratories, Fort Eustis, Virginia 23604.

11. SUPPLEMENTARY NOTES	12. SPONSORING MILITARY ACTIVITY
Volume I of a 2-volume report	U.S. Army Aviation Materiel Laboratories Fort Eustis, Virginia

13. ABSTRACT

This report presents the results of an experimental investigation of the dynamic airloads on an airfoil (Vertol 23010-1.58) immersed in reverse flow such as occurs on the retreating side of a helicopter rotor disc in forward flight. Forces and moments in two-dimensional flow were determined from airfoil differential pressures measured during pitching oscillation. Mach number, Reynolds number, and mean angle-of-attack ranges corresponded to those typically encountered under full-scale flight conditions. Frequencies of oscillation were varied between values corresponding to the 1/rev and typical first elastic torsional frequency of rotor blades.

Pitching oscillation was shown to postpone normal force and pitching moment stall to angles of attack well beyond static values. Large increases in dynamic C_N and C_M maxima due to reduced frequency and pitch rate effects were observed, while variations due to Mach number were found to be relatively small.

For this airfoil, the dynamic $C_{N_{MAX}}$ values achieved in reverse flow are considerably less than those achieved in forward flight for oscillation at a frequency corresponding to the rotor 1/rev rate.

DD FORM 1 NOV 68 1473 REPLACES DD FORM 1473, 1 JAN 64, WHICH IS OBSOLETE FOR ARMY USE.

UNCLASSIFIED

Security Classification

14. KEY WORDS	LINK A		LINK B		LINK C	
	ROLE	WT	ROLE	WT	ROLE	WT
Two-dimensional flow Pitch oscillation near stall Vertol 23010-1.58 airfoil Negative aerodynamic damping Dynamic stall Reverse flow						